Graduate Theses and Dissertations

8-2022

Performance and Fouling during Bioreactor Harvesting

Da Zhang
University of Arkansas, Fayetteville

Citation

Performance and Fouling during Bioreactor Harvesting

A dissertation submitted in partial fulfillment
of the requirements for the degree of
Doctor of Philosophy in Engineering

by

Da Zhang
Shenyang University of Chemical Technology
Bachelor of Science in Biochemical Engineering, 2012
Hebei University of Technology
Master of Science in Biochemical Engineering, 2015

August 2022
University of Arkansas

This dissertation is approved for recommendation to the Graduate Council.

_____
Ranil Wickramasinghe, Ph.D.
Dissertation Director

_____
Xianghong Qian, Ph.D.
Dissertation Co-director

_____
Bob Beitle, Ph.D.
Committee Member

_____
Daniel Strauss, Ph.D.
Committee Member

_____
Mathias Ulbricht, Ph.D.
Committee Member

Abstract

Tangential flow filtration has many advantages for bioreactor harvesting as the permeate could be introduced directly to the subsequent capture step, the process is easy to scale up, and fouling of the filter is limited by the cross flow. However, membrane fouling has limited its widespread use. This is particularly problematic given the high cell densities encountered today. Here a reverse asymmetric commercial membrane, BioOptimal™ MF-SL(Asahi Kasei), where the more open surface faces the feed stream, and the tighter barrier layer faces the permeate stream, has been investigated for bioreactor harvesting. The open surface contains pores up to 40 µm in diameter, while the tighter barrier layer has an average pore size of 0.4 µm.

The filtration performance, including fouling analysis conducted in this dissertation, involves using different feed streams, comparison of the filter performance with other filters possessing different membrane structures, mathematical modeling to predict the flux and fouling, fouling visualization using confocal laser scanning microscopy, and fouling identification using liquid chromatography-mass spectrometry.

For the feed streams studies, filtration of yeast suspensions and Chinese hamster ovary cell culture has been conducted under various conditions. The yeast cells are trapped in the open pore structure, while CHO cells are more externally deposited. The membrane stabilizes an internal porous cake that acts as a depth filter. This stabilized cake layer removes particulate matter that fouls the barrier layer, protecting the fine pores from the large aggregates. As filtration continues, a cake layer forms on the membrane surface.

Resistance-in-series model has been developed to describe the permeate flux during tangential flow filtration. The model contains three fitted parameters, which can easily be determined from constant pressure normal flow filtration experiments and total recycle constant

flux tangential flow filtration experiments. The model can be used to estimate the filter's capacity for a given feed stream. Our results suggest that using a reverse asymmetric membrane could avoid severe flux decline associated with fouling of the barrier during bioreactor harvesting.

Laser scanning confocal microscopy is used to observe the location of particle entrapment. The throughput of the reverse asymmetric membrane is significantly greater than the symmetric membranes. The membrane stabilizes an internal high permeability cake that acts as a depth filter. Confocal imaging helps visualize the secondary membrane directly by staining the DNA and membrane proteins using fluorescent dyes.

Host cell proteins are the most challenging impurities for downstream purification processes. In order to investigate the fouling during cell clarification, HCPs in the bioreactor, harvest, and backwash are identified and quantified using different methods. A dataset is established using the identified HCPs and used to train the deep learning model. The model predicts unknown HCPs on fouling potential with an accuracy of 76%. The dataset of identified HCPs in this study provides insights into the characterization of membrane fouling, membrane selection, and process development. This approach could be used to screen cell lines or hosts to select those with reduced HCP profiles or identify HCPs that are problematic and difficult to remove.

Acknowledgement

First and foremost, I would like to express my overwhelming and sincerest appreciation to my advisors for their incredible and constant support throughout my Ph.D. studies. Their collective knowledge, insights, and unending patience have been a source of security that has aided my growth as a research scientist. It has been a privilege and pleasure to have them as my advisors. I would like to express my sincere gratitude to my supervisor, Dr. Ranil Wickramasinghe, for his guidance, understanding, and patience. Most importantly, he has provided positive encouragement and a warm spirit to finish this dissertation. It has been a great pleasure and honor to have him as my supervisor. Thanks to my co-advisor, Dr. Xianghong Qian. Her invaluable help of constructive comments and suggestions throughout the experimental and dissertation works have contributed to the success of this research.

I want to extend my thanks to my doctoral committee members Dr. Bob Beitle, Dr. Daniel Strauss, and Dr. Mathias Ulbricht, for taking the time to serve on my committee. Their suggestions and ideas broaden and deepen my research from many perspectives.

Thank The Membrane Science Engineering and Technology (MAST) and Asahi Kasei Bioprocess America, Inc, Amgen Inc, Biogen Inc, MilliporeSigma for providing the materials, funding and various support.

A special thanks to Dr. Yu-Hsuan Chiao, Dr. Shu-Ting Chen, Dr. Rong Fan, Dr. Anh Vu, Dr. Tonmoy Patra for their accompany in my spare time. Without them, I could not have had a colorful life both in and out of the lab.

I also want to express my sincerest gratitude to the staff and faculty of the entire Ralph E. Martin Department of Chemical Engineering for providing the facilities, education, and support. I felt lucky that I chose here to pursue my Ph.D. degree. Finally, I would like to thank my family

and friends for being supportive, persistent, and patient during these years. Thank you for being

my constant cheerleaders.

Table of Contents

List of Tables

List of Figures

List of Published Papers

[1]   Zhang D, Patel P, Strauss D, Qian X, Wickramasinghe SR. Modeling flux in tangential flow filtration using a reverse asymmetric membrane for Chinese hamster ovary cell clarification. Biotechnology Progress. 2021 May;37(3):e3115.

[2]   Zhang D, Patel P, Strauss D, Qian X, Ranil Wickramasinghe S. Modeling tangential flow filtration using reverse asymmetric membranes for bioreactor harvesting. Biotechnology Progress. 2021 Jan;37(1):e3084.

[3]   Namila FN, Zhang D, Traylor S, Nguyen T, Singh N, Wickramasinghe R, Qian X. The effects of buffer condition on the fouling behavior of MVM virus filtration of an Fc-fusion protein. Biotechnology and bioengineering. 2019 Oct;116(10):2621-31.

Nomenclature

List of Symbols

A	Membrane area (m^2)
A_{vavle}	Cross-section area of the valve (m^2)
c	Concentration of the feed (kg/m^3)
c_0	Initial concentration of the feed (kg/m^3)
f'	Fraction of particulate matter that contributes to cake growth, taken as 1.0.
J	Permeate flux $(m^{-1}\,s)$
J_o	Initial Permeate flux $(m\,s^{-1})$
K	Unsteady state attrition factor $(1/m^3)$
m	Mass of the cake (kg)
n	Compressibility index of the cake
P_F	The pressure of feed port (Pa)
P_R	The pressure of retentate port (Pa)
P_P	The pressure of permeate port (Pa)
Q_F	Feed flux (m^3/s)
Q_P	Permeate flow rate (m^3/s)
Q_R	Retentate flow rate (m^3/s)
R	Radius of lumen (m)
R_c	Cake resistance (m^{-1})
R_m	Membrane resistance (m^{-1})
R_{valve}	Resistance of the valve (m^{-1})
t_c	Time at which a particular region was first covered or blocked by cells (s)
TMP	Total trans membrane pressure (Pa)
TMP_c	Trans membrane pressure drop cross cake (Pa)

TMP$_m$	Trans membrane pressure drop cross membrane (Pa)
V	Permeate volume (m^3)
v$_0$	Initial feed volume (m^3)
x	A parameter from various back migration transport mechanism
y	A parameter from various back migration transport mechanism

Greek letters

α	Resistance coefficient of the cake (m kg^{-1})
α$_0$	Specific resistance of the cake (m kg^{-1} Pa^{-n})
ΔP	Pressure drop in normal flow filtration (Pa)
η	Constant in predicting back migration.
γ	Shear rate (s^{-1})
μ	Viscosity of the feed (Pa s)

Abbreviation

2-dimensional electrophoresis (2DE)

4',6'-Diamidino-2-phenylindole dihydrochloride (DAPI)

Alternative tangential flow(ATF)

Carboxymethyl Dextran Sulfate (CMD)

Cell culture fluid (CCF)

Cell-specific perfusion rate (CSPR)

Chinese hamster ovary (CHO)

Confocal laser scanning microscopy (CLSM)

Continuous stirred tank reactor (CSTR)

Critical micelle concentration (CMC)

Disc stack centrifuges (DSC)

Dithiothreitol (DTT)

Elastin-like polypeptides (ELP)

Enzyme-linked immunosorbent assays (ELISA)

Fourier transform mid-infrared spectroscopy (FT-MIR)

Gas chromatography/mass spectrometry (GC/MS)

Gene ontology(GO)

Good manufacturing practice (GMP)

Grand average of hydropathy (GRAVY)

Host cell proteins(HCPs)

Hydrophobic interaction chromatography (HIC)

Hydrophobic interaction chromatography(HIC)

Immobilized pH gradient (IPG)

Iodoacetamide (IAA)

Ion exchange chromatography (IEX)

Isoelectric focusing (IEF)

Isoelectric point (pI)

Liquid chromatography/mass spectrometry (LC/MS)

Molecular weight (MW)

Octanoic acid (OA)

Poly (ethylene glycol) (PEG)

Poly-(Diallyldimethylammonium Chloride) (pDADMAC)

Polyacrylic Acid (PAA)

Polyvinyl Sulfonic Acid (PVS)

Reversed Phase Liquid Chromatography (RPLC)

Sodium dodecyl sulfate-polyacrylamide gel electrophoresis (SDS PAGE)

Staphylococcal Protein A(SPA)

Tangential flow depth filtration (TFDF)

Tangential flow filtration(TFF)

Tangential flow filtration(TFF)

Ultrafiltration/diafiltration (UF/DF)

Vessel volumes of media per bioreactor volume per day (vvd)

Chapter 1.   Introduction

1.1   What is the membrane fouling

Membrane-based separation has gained popularity over the past few decades, particularly in water treatment and biotechnology[1]. Membrane fouling refers to the deposition and accumulation of undesired materials on the surface of or inside of the membrane barrier. The fouling process varies depending on the membrane materials, feed stream and operation conditions. However, it is always reflected by an increase in TMP to maintain a particular flux or the flux decay during a constant pressure filtration. The mechanisms for membrane fouling can be different if different feed streams are used and also depend on the feed and operation conditions. Fouling is critical because, firstly, a layer of foulants is deposited onto the surface of the filter medium, called the cake layer. The additional cake layer on the membrane adds resistance to the filtration process. Therefore the required power for the operation increases. Secondly, the cake fouling layer narrows the pore size and decreases the product's sieving. Thirdly, the foulants on the membrane may have detrimental interactions with target molecules which causes product degradation. A thorough understanding of the fouling enables choosing the optimal filter materials, size of the filter, operations condition, and, therefore, obtaining a higher product quality in the shortest time frame. Although the concentration polarization has successfully explained the fouling in microfiltration and ultrafiltration, the fouling in a complex system, where intramolecular interaction prevails, and the fouling analysis in novel membrane structures are still "white areas".

1.2   Introduction of protein-based pharmaceuticals and their purification

Bioreaction utilizes expression systems to secret target recombinant proteins. Commonly used expression systems in bioreactions are bacteria, yeast, insect, and mammalian cells. The

most popular bacterial strain is E. coli, featuring its fast growth, high cell density, high secretion efficiency, and well-known genome. However, many proteins expressed as inclusion bodies are generally not in their native conformation. The refolding of such inclusion bodies reduces productivity and reproducibility. Yeast is the simplest eukaryote which combines the advantages of both prokaryotic and eukaryotic expression systems. Its advantages include the ability to accomplish proper posttranslational modifications, fast growth, simple genetic manipulation, scalable fermentation, high biomass concentrations, and safe pathogen-free production[2]. However, the product cannot meet the strict glycosylation of structural requirements, and especially the glycosylation pattern is dissimilar to humans. Insect expression systems are among the most used techniques to express mammalian proteins. Baculovirus vectors are used to insert the desired gene and transfected into cultured insect cells, such as from Spodoptera fugiperda (Sf9). The drawbacks are that baculovirus infection ultimately results in cell death, and insect cell glycosylation differs from mammalian cells. Although easy to handle, insect cell systems have not been licensed for the industrial production of biopharmaceutical proteins[3]. The mammalian cell has complete post-translational modifications and proper protein folding among the express systems. Therefore, it is an ideal choice for therapeutic proteins and vaccines.

The production of therapeutic macromolecules differs from chemically synthesized small molecule drugs. There are plenty of uncertainties and variations during the productions. Production of biopharmaceuticals consists of upstream and downstream. The upstream includes the process from vial to full-scale bioreactor production. The downstream processes are a series of unit operations for product purification and formulation. The downstream processing costs about 70% of the total production cost of a particular biopharmaceutical[4], largely contributed by disposable membrane module, the large volume of buffer, and expensive chromatographic

runs such as affinity, hydrophobic interaction, ionic exchange, and size exclusion[4]. The template of monoclonal antibodies(mAbs) purification begins with cell clarification, where the cells and cell debris are removed. The supernatant which contains the product of interest is delivered to the protein A capture, also known as product recovery, where the mAbs are specifically bound and eluted. The elution of protein A column is kept at low pH for virus inactivation. The next step is the polishing, consisting of two or three chromatography steps. Ion exchange chromatography (IEX) and hydrophobic interaction chromatography (HIC) are the most used polishing methods. Before the buffer is exchanged for the final storage formula in UF/DF, an additional virus filtration step is adopted to meet the overall safety margin[5]. The downstream platform for antibody purification is illustrated in Figure 1.1. Membrane-based separation is widely used in cell clarification, virus filtration, and buffer exchange due to its easy operation, high throughput, and excellent sieving performance. However, major drawbacks of membrane-based separation in clarification, TFF and virus filtration encounter membrane fouling and product rejection leading to unacceptably low product recoveries[6]. Therefore, it is crucial to understand the mechanism of fouling.

Monoclonal antibody(mAb) purification template

Bioreactor	Disc stack centrifuge/Depth filter	Protein A chromatography
Cell culture	Primary recovery	Product capture
Liquid holding tank	AEX/CEX/HIC resin	Virus filter	Tangential Flow Filter
Viral Inactivation	Polishing	Virus filtration	UF/DF
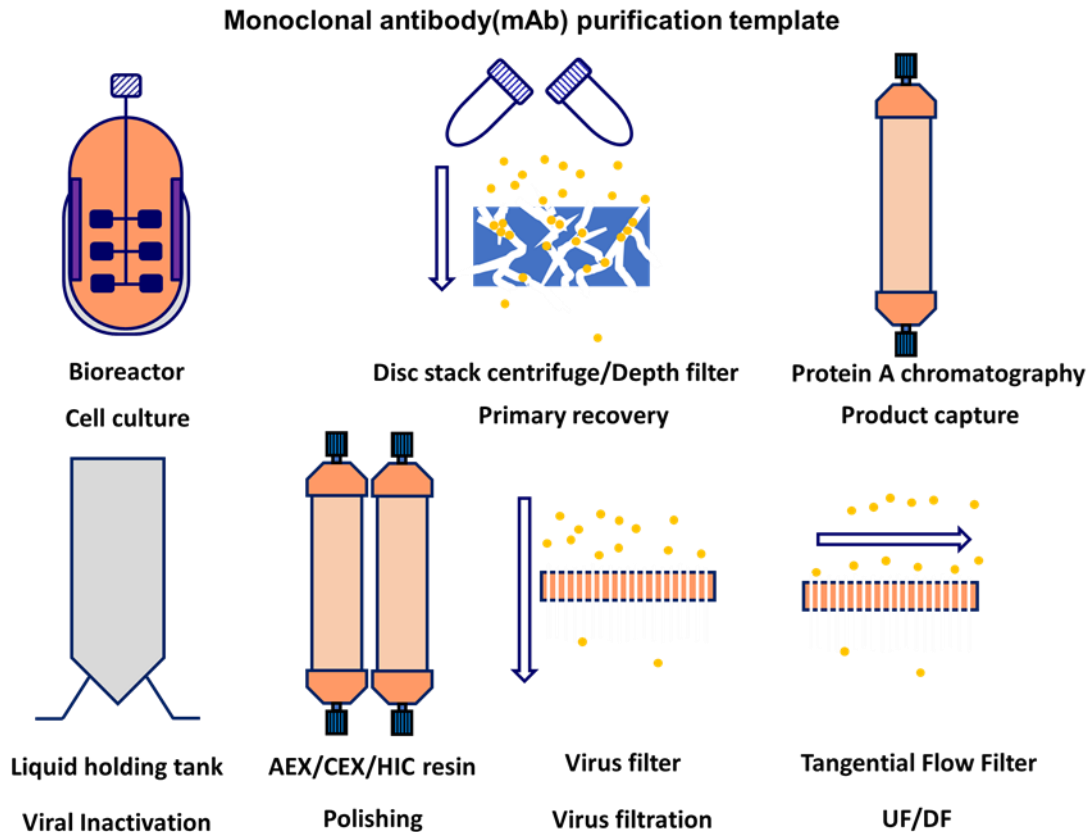
Figure 1.1 Illustration of monoclonal antibodies purification template

1.3 Cell clarification

Increases in product titer during cell culture operations have led to significant challenges during the downstream purification of biopharmaceutical products. In the case of the bioreactor harvesting step, a high product titer is accompanied by a rather high cell density which places a significant burden on traditional clarification operations. Harvesting operations, in terms of capital cost and energy consumption, can account for up to 25% of the cost of the entire downstream process[7]. Therefore, selection and understanding of the cell clarification approach are crucial. Typical cell clarification method includes precipitation technologies (acidification, affinity precipitation, flocculation)[8], centrifugation[9], settling[10], expanded bed adsorption[11], and depth filtration.

1.3.1 Disc stack centrifuges (DSC)

Disc stack centrifuges (DSC) is the predominant design used at the industrial scale for E.coli, and microalgae harvest[12, 13]. The designs of DSC used in the mammalian cell have been less popular in the past 20 years[14, 15] because both E.coli and microalgae have cell walls that can protect them from the shear stress during the DSC. However, the DSC may help cell lysis in viral vaccine production and adenovirus for gene therapy because the lysis is required to release the viral vector from the host cell[16]. DSC is primarily fabricated from stainless steel and designed with angled conical discs stacked coaxially around the vertical axis of rotation. The feed enters through a vertical intake pipe that runs along the axis of rotation and flows to the bottom of the rotor. Then the stream is redirected towards the outer edge of the separation chamber through the distributor. The distributor is designed with guiding fins accelerating the fluid entering the bowl. The rotation of the rotor imparts a centrifugal force on the cell culture material, causing solids to separate and build up along the outermost radius of the rotor. The accumulated solids are discharged after a certain time intervals. The clarifying culture material flows radially inward between the conical discs, continuing to be clarified along the way. Finally, the effluent fluid, now depleted of solids, exits the rotor from the top of the DSC and continues to the next unit operation or hold tank[9].

The clarification efficiency of the centrifugation process is affected by harvest parameters such as centrifuge feed rate, G-force, bowl geometry, operating pressures, discharge frequency, and ancillary equipment used to transfer cell culture fluid to the centrifuge. Optimizing the centrifugation process involves selecting the feed rate and bowl rotational speed using the feed rate (Q) scaling factors and equivalent settling area (Σ) in the centrifuge. The settling area can be

calculated based on the centrifuge geometry, the number of discs in the stack, and rotational speed. The expression of the settling area is shown in the following equation

$$\Sigma = \frac{2\,\pi\,n\,\omega^2(r_2^3 - r_1^3)}{3g\,tan\theta}$$

In that equation, n is the number of discs, θ is the disc's half-cone angle (degrees), r1 and r2 (meters) are the respective inner and outer radii of the discs, and ω (radians/second) is the angular rotation frequency of the disc-stack centrifuge.

As a general rule, the lower the value of Q/Σ, the better the clarification that will be achieved[17]. However, lower Q/Σ gives less throughput of the crude materials.

The drawback of DSC is that for a culture broth containing fragile or dead cells, increased rotational speed or increased residence times through the inlet zone may negatively impact shear force and cell lysis, generating submicron particles that are difficult to be removed through centrifugation. The second issue is the turbidity of effluent is about 100 NTU which is 10 times higher than depth filtration[18]. In this case, secondary depth or tangential flow filtration may be necessary.

1.3.2 Depth filtration

Depth filters consist of a thick, porous bed that can trap particles within the filter compared to screen-type filters that largely reject particulate matter based on surface exclusion. On the other hand, tangential flow filtration(TFF) utilizes its perpendicular flow relative to the membrane surface to suppress cake growth. Therefore the main difference between depth filter and TFF filter is the membrane structure. There are usually different filtration zones in a gradient density depth filter: the pre-filtration zone, the primary filtration zone, and the polishing zone that efficiently capture particles with a broad particle size distribution. A broad and efficient gradient density structure enables the filter to retain the particles instead of forming a deposit that

plugs rapidly[8]. Depth filter is typically performed better in complex feed streams compared to TFF.

The impurities in the cell culture can be divided into process-related impurities and adventitious agents [3]. Process-related impurities are essential for the production or introduced into the purification process to enhance the separation process, for example, cell, cell debris, product aggregates, host cell DNA, host cell proteins(HCPs), endotoxin, ligands from membrane or chromatography. In contrast, the adventitious agent is the potentially infectious impurities that have not been added intentionally and are not essential to the process but are typically extremely hazardous, such as bacteria and viruses. Those presenting impurities consist of the potential foulants for membrane separation. The concentration of those impurities is shown in Table 1.1

Table 1.1 The concentration of process-related impurities in the literature.

Impurities	Concentration	Reference
DNA (ppm)	6-30	[19]
	15-68	[20]
HCP (ppm)	6000-10000	[19]
	300	[21, 22]
	150	[23]
	200-900	[24]
Poloxamer(w/v)	0.1%	[25]
	0.05-0.25%	[26]
Antifoam(w/v)	0.01 and 0.07%	[25]
	1%	[27]

Depth filtration is the typical method for cell clarification. Due to the complex composition and multiple mechanisms, the fouling analysis during the cell clarification process

7

could be tedious. The depth filters trap particles by two mechanisms (i) particle entrapment by interception and sieving (ii) adsorptive binding via charged and hydrophobic moieties[28].

Researchers design the experiment regarding the different choices of filters and focus on the clearance of those impurities. The fouling studies on cell clarification are listed in Table 1.2.

Table 1.2. Research on the fouling of depth filters in the literature

Membrane	Conclusion	Reference
Millipore Millistak+ D0HC/ X0HC	Characterization of HCP and DNA breakthrough using Confocal laser scanning microscopy	[19]
3M Zeta Plus™ polishing grade depth filter(90ZB08)	Comparison of HCP and DNA clearance between depth filter and flow through anion exchanger	[29]
Clarisolve® 20MS, 40MS, 60HX, XoHC, DOHC	Reduction of minimal filter area by more than 4-fold compared to the 'classical' two-stage depth filtration	[30]
Millistak+ A1HC, Cuno 90ZA depth filters	Evaluation of the absorption ability of depth filter for soluble impurities clearance	[31]

1.3.3 Precipitation

The precipitation technique is simple and initiated by contacting a precipitation agent with a protein solution of interest, such as cell culture. Subsequently, a mixing step is performed

8

to achieve homogeneity and solid-liquid separation (such as filtration or centrifugation) to isolate the precipitated protein.

The mechanism of precipitation is varied based on the precipitation reagent. If an acidification reagent was used in precipitation, the relevant mechanism is to adjust pH to the isoelectric point (pI) of the target protein. Therefore it is possible to perform selective precipitation of process-related impurities such as HCPs and DNA in aqueous solutions leaving the target protein in the solution[32].

Surfactant is also a common precipitation agent, where the surfactant is directly added to a complex solution containing the protein of interest. The final surfactant concentration is maintained below its critical micelle concentration (CMC) in order to allow for electrostatic and hydrophobic interactions between the surfactant and the target protein. An insoluble protein-surfactant complex is formed, and back extraction of the target protein from the precipitate into a new aqueous phase is then carried out using either solvent extraction or the addition of a counter-ionic surfactant[33]. In addition to the protein-surfactant complex, other reagents can also form the complex with protein, resulting in protein precipitation. For example, At low pH, the hydrophobicity of the octyl moiety of octanoic acid (OA) dominates, and acidic proteins such as HCP tend to precipitate along with OA. Antibodies with relatively basic pI have sufficient charge to counteract that hydrophobicity and remain in solution[34]. Larger protein complexes such as HMWs precipitate more readily in the presence of polar uncharged polymers like PEG due to the larger exposed surface being destabilized by competition with the PEG for binding of water molecules and the exclusion of the PEG from the protein surface. Therefore the precipitation mechanism of PEG is based on steric exclusion, which provides specificity based on size[35].

Organic solvents can be used as precipitation reagents due to decreased solubility of proteins in the presence of organic solvents resulting in selective precipitation. However, organic solvents are protein destabilizers and can denature proteins at high concentrations or temperatures due to their favorable interactions with hydrophobic groups [36].

Affinity-based precipitation has been demonstrated to be useful in laboratory and medium-scale purification. This tag-based precipitation needs more evaluation in terms of cost and robustness at large-scale preparative processes. Elastin-like polypeptides (ELP)-Protein A fusion has been used as an affinity precipitating agent for mAbs. Following precipitation, the ELP-Protein A-antibody complex is re-solubilized, dissociated by low pH treatment, and the ELP-Protein A fusion is re-precipitated, leaving the mAb in solution[37].

1.3.4 Flocculation

Flocculation is widely implemented in wastewater treatment, food, beverage, and cosmetics [38, 39]. However, it has been recently explored in antibody manufacturing [40, 41]. The principle of flocculation is simply based on ionic interactions. Flocs formed by bridging the oppositely charged particles produce larger and less stable agglomerates, resulting in the neutralized particle falling out of the solution. When the solution pH is less than the pI of a particular protein, the protein carries a net positive charge. Under these conditions, a cationic polyelectrolyte may precipitate impurities and leave the protein of interest in solution. Conversely, an anionic polyelectrolyte may precipitate the protein of interest forming a protein-polyelectrolyte precipitate, leaving impurities in solution. The efficacy of flocculation for any given process depends on the nature and the amount of insoluble particulates in the feed stream, the concentration, charge density and molecular weight of the flocculant, the shear rate, duration of flocculation, properties of the feed stream and the properties of the target products. Poly-

(Diallyldimethylammonium Chloride) (pDADMAC)[42], and polyamines are commonly used

for cationic flocculation[43]. In contrast, Polyvinyl Sulfonic Acid (PVS), Polyacrylic Acid

(PAA), and carboxymethyl Dextran Sulfate (CMD) are commonly used for anionic

flocculation[8].

1.4 Affinity Chromatography

1.4.1 Separation mechanism of Protein A

Staphylococcal Protein A(SPA) is a 42 kDa single-chain polypeptide located on the outer

surface of Staphylococcus aureus[44]. Protein A has a high affinity to bind immunoglobulins

from various species, such as humans, rabbits, and guinea pigs, but only weak interaction with

bovine and mice. SPA consists of three different regions, as shown in the Figure 1.2; S, being the

signal sequence that is processed during secretion, five homologous IgG binding domains E, D,

A, B, and C, and a cell-wall anchoring region XM[45]. The three α-helical in binding domains

form a hydrophobic core that can specifically interact with helix structure in the FC part of the

antibody.
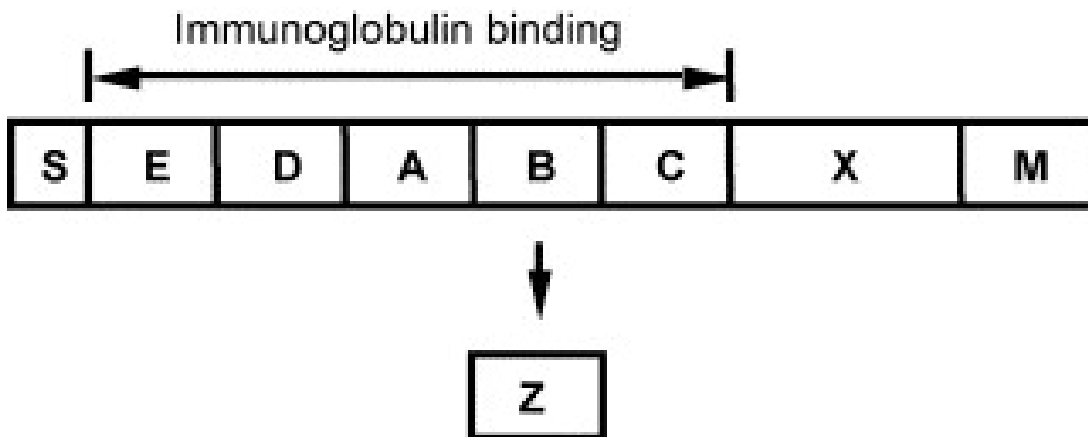
Figure 1.2 Different domains in the Staphylococcal Protein A.

1.4.2 Properties of Protein A resin

The basic properties of Protein A column include base matrix, protein A ligand

progenitor domain, and particle diameter. The base matrix has two functions: support SPA ligand

and control flow pattern, which determine the latter two properties. Except for the low non-specific binding, a better matrix should be easy to link with SPA and maintain a constant pressure-flow relationship. Agarose is the widely used matrix; polymethacrylate, cellulose, and polyvinyl ether are also found in different manufacturers. Because E, D, A, B, and C domain has the independent ability to bind with antibody, not all binding domains are required in a ligand. Protein A ligand progenitor domain normally uses B or C domain with 4-6 repeats. The common properties of protein A matrix is shown in the table below.

Table 1.3 Properties of protein A stationary phase

Base matrix	Agarose, polymethacrylate, cellulose, and polyvinyl ether
Ligand	use B or C domain with 4-6 repeats
Beads Particle size(μm)	45-90
r_{pore}(nm)	30-60
ε	0.3-0.4
ε_p	0.5-0.9
EBC (mg/mL)	30-90
DBC (mg/mL)	30-50
q_m(mg/mL)	90-130
Lifetime (cycles)	100-300

1.4.3   Operation of Protein A column

Affinity chromatography is one of the most effective ways to purify monoclonal antibodies. Protein A affinity chromatography columns absorb the IgG molecules onto the affinity resins, which contain immobilized protein A ligand. Then, the remaining impurities and

byproducts from the bioreaction can be removed. The phosphate buffer in pH 7 can be used as binding and washing buffer, and citrate acid buffer around pH 3 is used for elution. In theory, the protein A column removes any impurities other than IgG; however, due to the complex structure of the protein, some HCPs will bind, react, or aggregate with IgG. Therefore those HCPs may break through the protein A.

1.4.4 Advanced development of Protein A stationary phase

In order to improve the stability of Protein A resins, different attempts have been carried out. For instance, Linhult et al. [46] replaced asparagine 23 residues for a threonine, causing higher stability toward 0.5 M NaOH. This improvement avoided deamidation, which causes protein instability at alkaline pH. The protein A has shown non-specific binding with impurities in the cell culture media, including yeast extract and fetal bovine. Data have shown that the ligand accounted for this binding instead of the base matrix. González-Valdez et al.[47] modified the ligands with 5 and 20.7 kDa poly (ethylene glycol) (PEG). It was observed that static binding affinity was preserved after PEGylation. DBC was reduced due to a decrease in IgG effective pore diffusion and slower IgG association kinetics for the PEGylated ligands. Despite this, the mass of media-associated contaminants was reduced by a factor of $\geq$2. Finally, an increase of 15% in the recovery of IgG was observed on elution after PEGylation.

To address the loss of Protein A activity from repeated binding, elution, and sanitization cycles, Protein A mimetic ligands have been proposed[48]. For instance, peptide ligands from combinatorial solid-phase hexapeptide libraries, such as HWRGWV, HYFKFD, and HFRRHL have been developed. These ligands have demonstrated their affinity towards the Fc fragment of human IgG, and their performance has been tested. The antibody-binding sequence HWRGWV was used as a ligand to purify the chimeric mAb of the IgG1 subclass. On the other hand,

HWRGWV, HYFKFD, and HFRRHL ligands were used to purify the humanized mAb of the IgG4 subclass. The purification yields for IgG1 and IgG4 were higher than 94 and 85%, respectively. However, DBC of the three peptide resins was about 20 g/L.

1.5 Ion-exchange(IEX) chromatography

1.5.1 Separation mechanism of IEX stationary phase

IEX separates proteins based on differences in the molecules' surface charge, with separation dictated by the protein interactions with the stationary phase[49]. Ion exchange chromatography could be deliberately synthesized resins containing positive ions (cation exchangers), called anion exchange chromatography, or negative ions (anion exchangers), called cation exchange chromatography. The separation is based on the formation of ionic bonds between the charged groups of biomolecules and an ion-exchange gel/support carrying the opposite charge.

1.5.2 Properties of IEX resin

The selection of a suitable ion-exchange matrix probably is the most important in ion-exchange protocol. It is based on various factors such as ion exchanger charge/strength, linear flow rate/sample volume, and sample properties. Stationary phases are comprised of two structural elements; the charged groups involved in the exchange process and the matrix on which the charged groups are fixed. Matrix materials include cellulose, dextran, agarose, polyacrylamide, acrylate-copolymer, and silica[50]. Both exchangers can be further classified as strong and weak types. The terms weak and strong are not related to the binding strength of a protein to the ion exchanger but describe the degree of its ionization as a function of pH. Strong ion exchangers are completely ionized over a wide pH range, while weak ion exchangers are only partially ionized in a narrow pH range. Therefore, with strong ion exchangers, proteins can

adsorb several exchanger sites. For this reason, strong ion exchangers are generally used for the initial development and optimization of purification protocols. On the other hand, weak ion exchangers are more flexible in terms of selectivity. They are a more general option for the separation of proteins that retain their functionality over the pH 6-9 range as well as for unstable proteins that may require mild elution conditions. An example of a strong cation ligand is sulfonic acid, working in the pH range of 4-13; Weak cation is Carboxylic acid, working in the pH range of 6-10; strong anion is a quaternary amine, working in the pH range of 2-12; Weak anion are primary amine, secondary amine, and tertiary amine, working in the pH range of 2-9.

The basic information of the IEX stationary phase is shown in the table below.

Table 1.4 Properties of IEX stationary phase

Base matrix	cellulose, dextran, agarose, polyacrylamide, acrylate-copolymer, silica	
ligands	Strong cation ligand: sulfonic acid	Strong anion: quaternary amine
	Weak cation: carboxylic acid	Weak anion: 1 °, 2 °, and 3 °amine
Particle size (μm)	2 (analytical purposes)-200 (preparative applications)	
Pore size (nm)	10-100	
Mean surface area(m2/mL)	5-100	

1.5.3 Operation of IEX column

Charge-based purification is frequently employed in the form of ion-exchange chromatography as polishing steps. Therefore, IEX is influenced by salt concentration. As a loading pH of 1-3 units away from the isoelectric point of the target molecule is typically

recommended for the use of ion-exchange resins in the bind and elute mode, it is important to

consider the isoelectric point (pI) of the target molecule before selecting the appropriate buffer

pH due to the potentially huge variability of pI across different mAb formats. The IEX columns

are normally used to remove the host cell DNA and host cell protein from the IgG

1.5.4 Advanced progress of IEX stationary phase

To improve the sensitivity of protein variants determination or handle very small amounts

of samples, the use of capillary columns in IEX appears to be a promising approach. However,

several key modifications to a commercially available liquid chromatography system are

required to reduce the system volume and associated extra-column band broadening, which

could be critical for capillary IEX operation. Until now, the number of applications in this field is

rather limited, but a 0.32 mm I.D. IEX capillary column was successfully applied in the pH-

gradient mode as the first dimension in a 2D separation of standard protein mixtures[51].

Another multidimensional method has been applied by Zheng et al.[52] for the separation

and comparison of E. coli bacteria lysates using pH gradient-based IEX coupled with Reversed

Phase Liquid Chromatography (RPLC). The method provided a 2D map of protein expression

with proteins categorized by both pI and hydrophobicity. This 2D method offered significantly

higher loadability than conventional techniques while maintaining a high degree of resolution.

1.6 Hydrophobic interaction chromatography(HIC)

1.6.1 Separation mechanism of HIC

HIC is the preferred technique for determining the relative hydrophobicity of mAbs and

removing hydrophobic impurities in the downstream purification of mAbs. The hydrophobic

effect is the observed tendency of nonpolar substances to aggregate in an aqueous solution and

exclude water molecules. The separation mechanism in hydrophobic interaction chromatography can be explained by the salting-out effect and formation of a cavity[53].

1.6.1.1 Salting-out effect

The salting-out effect indicates the normal dissolved protein has its hydrophilic group exposed to the bulk solution, while the hydrophobic core was hidden inside the protein 3D structure. With adding the salt, proteins started to unfold. When the exposed hydrophobic surface is large enough, water molecules will solvate predominantly salt ions. Therefore, the number of water molecules available to interact with the hydrophilic part (charged) of the protein will decrease. Under these conditions, the protein-protein intermolecular interactions become stronger due to the decreased amount of surrounding water molecules. In the end, the protein molecules can associate by forming hydrophobic interactions with each other.

1.6.1.2 Formation of cavity

The structure of water is highly ordered and stabilized by a hydrogen bond. The energy in this form is the lowest. When protein is added to the water, hydrophobic moieties of a protein are dissolved in an aqueous system, and the neighboring water molecules have to be separated from each other in order to form a cavity for the protein. This requires energy investment, which corresponds to the surface of the cavity multiplied by the surface tension. In order to minimize the energy, the hydrophobic protein is attached, decreasing the surface of the cavity. As a result, hydrophobic molecules in aqueous solutions occur spontaneously and are mainly driven by the entropy change.

1.6.2   Properties of HIC

In HIC, mildly hydrophobic stationary phases are used in most cases (much less hydrophobic than in RPLC). Most common ligands include relatively short n-alkyls (butyl,

hexyl, octyl), phenyl, or ether, which are linked to the silica or polymeric material through several coupling approaches. The hydrophobicity of the stationary phase increases with the length of the alkyl-chain, but the loading capacity may decrease. The strength of hydrophobic interactions between the protein and stationary phase ligand can be easily controlled by the ligand density. The basic information of the HIC stationary phase is shown in the table below

Table 1.5 Properties of HIC stationary phase

Base matrix	silica or polymeric material
Ligand	short n-alkyls (butyl, hexyl, octyl), phenyl, or ether
Particle size (µm)	5-90
Pore size (Å)	300-1000
Surface area (m²/g)	20-100

1.6.3 Operation of HIC

Kosmotropic salt such as ammonium sulfate is typically used at high concentrations during the loading step to facilitate reversible interaction between the surface-exposed non-polar residues on the mAb to the resin, with elution performed at a lower salt concentration. It has also been reported that employing too high salt concentrations may lead to the formation of irreversible hydrophobic interactions between the resin and target, resulting in overall low yields. In order to overcome potential difficulties in eluting hydrophobic proteins from the resin, mobile phase additives of up to 5% hexylene glycol and 1M arginine have been proposed to be effective in facilitating mAb elution.

1.6.4 Advanced development of HIC stationary phase

Applying columns packed with sub 3 μm particles opened a new level of performance in HIC. Decreasing the particle diameters provided higher surface area and separation efficiency. From a commercial point of view, the smallest particle size in HIC currently available is 2.5 μm. Another development of HIC is column coupling. The HIC could be coupled with another HIC, resulting in a higher length. The resolution between the hydrophobic species can be increased from 1.14 to 1.55 and 1.95 by increasing the column length from 10 cm to 20 and 30 cm, respectively. The HIC could also work with a mass spectrum to form an online analytics platform.

Recent progress in top-down protein analysis has led to the demand for MS-compatible chromatographic techniques to separate intact proteins using volatile mobile phases. Conventional HIC provides a "high-resolution" separation of proteins under non-denaturing conditions but requires high concentrations of nonvolatile salts. A recent study proposed a new series of more hydrophobic HIC materials that can retain proteins using MS-compatible concentrations of ammonium acetate and 50% acetonitrile as the organic modifier. These new HIC materials appeared to work as a hybrid form of conventional HIC and RP chromatography. Online HIC-MS was feasible for both qualitative and quantitative analysis[54].

1.7 Modeling of the cell clarification

A mathematical model is an alternative way to understand and develop a process. For a given complex process, the model simplifies the process into parameters, reduces the dimensions of the analysis, and provides valuable insights into cell clarifications.

1.7.1   Fick's first law

Several models have been used in the cell clarification process. The models are divided

into two categories. The first category is based on Fick's first law, where diffusion is the major

resistance. The general equation is shown in [1.1].

$$J = -D \frac{d\varphi}{dx} \qquad [1.1]$$

where J is the diffusion flux, of which the dimension is the amount of substance per unit area per

unit time ($kg\ m^{-1}s^{-1}$). J measures the amount of substance flowing through a unit area during a

unit time interval. D is the diffusion coefficient or diffusivity. Its dimension is area per unit time

(m^2s^{-1}). φ (for ideal mixtures) is the concentration, of which the dimension is the amount of

substance per unit volume ($kg\ m^{-3}$). x is position, the dimension of which is length (m).

Fick's first law is adjusted to fit filtration, shown in Figure 1.3 and equation [1.2]

where c_x is the solute concentration at a distance, x, from the membrane, and c_p is the solute

concentration in the permeate. D is the diffusion coefficient. Assuming D is constant, and solute

is complete rejected ($c_p = 0$), this expression can be re-arranged to give

$$J = \frac{D}{\delta} ln \frac{c_w}{c} = k ln \frac{c_w}{c} \qquad [1.2]$$

D/δ term is a mass transfer coefficient, typically denoted k.
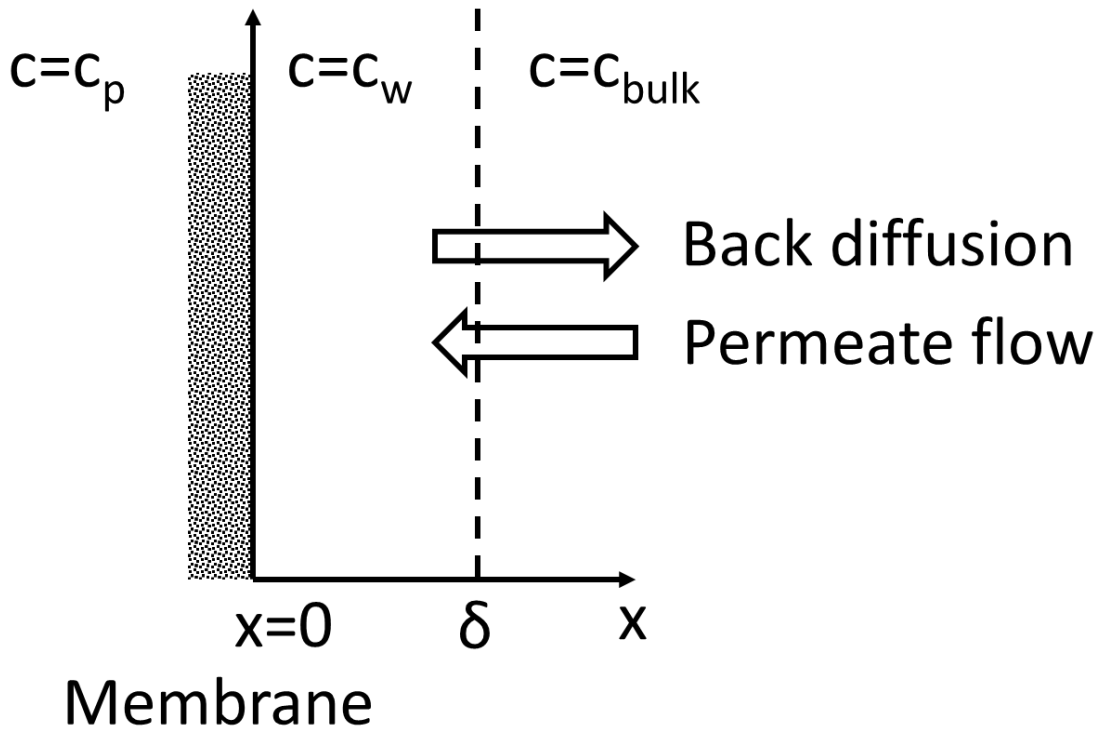
Figure 1.3 Diagram of Fick's first law in filtration.

1.7.2 Darcy's law

The second modeling category is based on Darcy's law, where convection prevails. The general equation of Darcy's law is

$$q = -\frac{k}{\mu}\nabla p \qquad [1.3]$$

where the instantaneous q (m³ /s) / m² through a porous medium, k is the medium's permeability, μ is the dynamic viscosity of the fluid, and ∇p is the pressure drop over a given distance. The equation can be simplified into a linear integral form

$$Q = -\frac{kA}{\mu L}\Delta p \qquad [1.4]$$

where A is the cross-sectional area (m²), L is the length of the sample in units (m).

Darcy's law was adjusted to fit in filtration as the Figure 1.4, following

$$\frac{Q}{A} = -\frac{\Delta p}{\mu R} \qquad [1.5]$$

where R is the resistance of the fouling.

Cake layer R_c

Concentration
polarization layer R_p

Membrane R_m

R_a
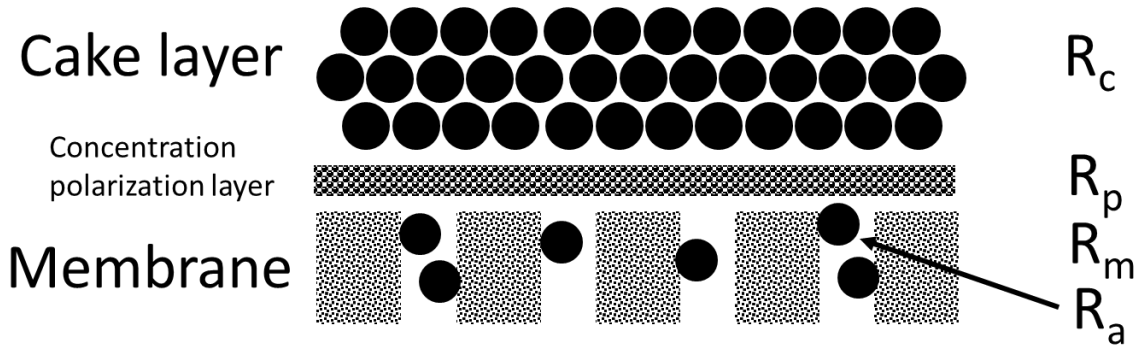
Figure 1.4 Diagram of Darcy's law in filtration

Based on Darcy's derived equation, Hermia proposed a blocking filtration model in

constant pressure, which is considered the classic fouling analysis method [55].

$$\frac{d^2t}{dv^2} = k\left(\frac{dt}{dv}\right)^n \qquad [1.6]$$

The fouling index n is determined by the best fitting of the filtrate volume with filtration

time. Based on the value of n, fouling can be classified into 4 different types, as shown in Table

1.6. The first fouling type is standard blocking, where the foulants are adsorbed on the pore's

inner channel, causing the channel's shrink. Therefore, the flux decays. The correlation between

pore diameter and flux is described in Poiseuille's equation
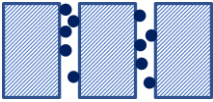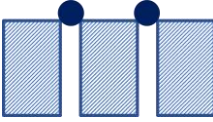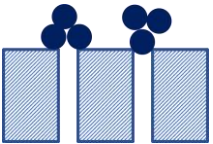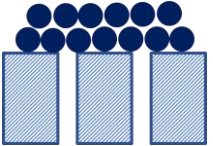
$$Q = N \times \left(\frac{\pi\, r^4\, P}{8\, \mu\, L}\right) \qquad [1.7]$$

In this type, the foulant type is always smaller than the pore size, so it could let the

foulant go inside the channel. Therefore, standard blocking is often found in diafiltration. And

the n is equal to 1.5.

The second class is competed blocking, where the foulant is larger than the pore size. The

fouling pattern is called intermediate blocking if the following foulant can deposit on top of

existing ones. The flux decays in competed blocking or intermediate blocking because the

available filtrate area decreases. Therefore the competed blocking or intermediate blocking

always occurs at the beginning of the filtration. n is equal to 2 for competed blocking and 1 for

intermediate blocking.

22

The last type is called cake blocking, in which all the foulants are deposited on the top of the membrane surface layer by layer. The n is 0. By fitting the dominating equation, the type of fouling can be determined. The issue here is that the blocking index, n, is not always an integer in most cases. Secondly, the model is only for dead-end filtration. Thirdly, foulants are not compressible.

Table 1.6 Classifications of fouling types based on Hermia's blocking filtration model

Type	Diagram	Foulant size	Results	Application	Blocking index, n
Standard blocking		< pore size	Pore diameter decreases	Diafiltration	1.5
Complete blocking		> pore size	Filtration area decreases	Beginning of the filtration	2
Intermediate blocking					1
Cake blocking		> pore size	Hydraulic resistance increases	Cell harvest	0

Ho et al. proposed a pore blockage and cake filtration model[56]. Sequentially, the model assumes the membrane is fouled by pore blockage and cake filtration. At the beginning of the filtration, foulants first block the open area of the membrane. The decreasing rate of open area is proportional to the pore blockage parameter α, the permeate flow through the open area of the

membrane, and the feed concentration. Therefore, in the first stage, the flux decays because of the decrease of the opened membrane area.

$$\frac{dA_{open}}{dt} = -\alpha \times Q_{open} \times C \qquad [1.8]$$

Then at the blocked area, the cake builds up and grows on the surface of the membrane. The growth rate of the cake is proportional to the fraction of the proteins that contribute to the growth of the deposit, f', the flux through the blocked area, and the feed concentration.

$$\frac{dm}{dt} = f' \times J_{blocked} \times C \qquad [1.9]$$

Plugging these equations into Darcy's law, the pore blockage and cake filtration model could be solved by an equation group. Three parameters need to be determined: the pore blockage parameter α, the resistance of a single protein aggregate, R_{p0} and the specific protein layer resistance, $f'R'$.

$$Q = Q_0 \left[e^{-\frac{\alpha \Delta pc}{\mu R_m}t} + \int_0^t \frac{\alpha \Delta pc}{\mu(R_m+R_p)} \times e^{-\frac{\alpha \Delta pc}{\mu R_m}t_p} dt_p \right] \qquad [1.10]$$

$$R_p = (R_m + R_{p0})\sqrt{1 + \frac{2f'R'\Delta pc}{\mu(R_m+R_{p0})^2}(t - t_p)} - R_m \qquad [1.11]$$

Belton et al. developed combined models of membrane fouling based on the classic blocking models[57]. The model assumes two classic blocking models occur at the same time. Therefore, the models use two fitted parameters and are reduced to the individual models when one mechanism is dominated. The combined models are less physically detailed than the pore blockage and cake filtration model proposed by Ho in terms of estimation of physical parameters but more numerically simple to implement, providing two fitted parameters need to be fitted and analytical equations to calculate volume or pressure as a function of time are available.

Belton et al. proposed an additional classic model called the adsorption model[58]. The adsorption fouling model can be derived by assuming foulant deposition has zeroth-order

kinetics and is only determined by adsorption rate constant and inter-channel surface. As

filtration proceeds, the pore becomes narrowed due to the adsorption, and the inter-channel

surface also decreases. The value of blocking index n turns out to be 9/4 for the adsorption

model. Those classic blocking-based models assume the filtration of normal flow filtration,

uniform pores, only one type of foulant in the system, and incompressible foulants. Therefore,

the application is limited to bioprocess.

For the tangential flow filtration models, Davis et al. combined the continuity equations

and mass balance in the sheared concentration-polarization boundary layer [59]. The feature of

this work is the characteristic value for the particle diffusivity, which considers the effect of

shear rate instead of Brownian diffusion. Shear-induced diffusivity is proportional to the local

shear rate. Their model could predict the permeate flux and concentration profiles.

Juang et al. introduced cake compressibility index n, and the value can be determined

from dead-end filtration[60]. The higher n indicates a higher compressive of the cake.

Compressibility index n is also affected by the shape of foulant. The higher the length/diameter

ratio of the microorganisms, the greater the compressibility index that could be achieved[61].

1.7.3 Deep learning model

Recently, many information technologies, such as machine learning, the Internet of

things, data mining, and cloud computing, have been used in industrial production, resulting in

an explosive development of industrial informatics. Deep learning is a subset of machine

learning, which is essentially a neural network with three or more layers. In the past decade, deep

learning has achieved the sate-of-the-art performance for hierarchical features and

representations learning in the tasks of classification and recognition, where deep learning

attempts to mimic the human brain, enabling systems to cluster data and make predictions with

high accuracy. They use the supervised and unsupervised methods to train the parameters for extracting the multi-level features in the deep architecture. During the training process, this neural network optimizes this step to obtain the best possible abstract representation of the input data. This means that deep learning models require little to no manual effort to perform and optimize the feature extraction process.

A neural network generally consists of a collection of connected units or nodes. We call these nodes neurons. These artificial neurons loosely model the biological neurons of our brain. A neuron is simply a graphical representation of a numeric value. Any connection between two artificial neurons can be considered an axon in a biological brain. The connections between the neurons are called weights. When an artificial neural network learns, the weights between neurons change. The training aims to set weights that allow the neural network to perform the classification or prediction. The set of weights is different for every task and every data set. Therefore the values of these weights can not be set in advance. Normally 80% of the dataset is used to train the model, and 20% of the dataset is used to validate the model.

The application of deep learning to a diverse array of research problems has accelerated progress across many fields. In the chemical engineering area, the deep learning model is trained as a generative model to predict the CO2 adsorption capacity of unknown porous carbons[62]. The deep learning model also can be employed as an accurate descriptor to predict the transformation capability of CO molecules on gold catalysts[63]. Marcato et al. create a dataset of CFD simulations for the filtration process. The results of CFD simulations were the training data for the neural networks. The permeability and the filtration rate were efficiently predicted by the networks, and the prediction time by deep learning is much less than the CFD[64].

1.8   Host cell proteins in cell clarification

Host cell proteins (HCPs) are endogenous proteins derived from the host cells used for bioproduction [65]. HCPs could be generated from cell debris, secreted protein, and cell lysate. More than 6,000 HCPs have been found in the CHO cell proteome, and many HCPs are released to cell culture fluid (CCF) as the results of secretion and cell lysis caused by either normal cell death or shear stress during harvest[66]. HCPs form a major class of process-related impurities because they can potentially cause the patient's immune response. Second, HCPs consist of thousands of proteins and therefore have a range of molecular weight, isoelectric point, and hydrophobicity. The peripeties of HCPs need to be studied and determined case by case. Third, the HCPs are normally co-purified with biopharmaceutics, for example, monoclonal antibodies. Final recombinant mAb products must be clear of impurities and typical target levels of impurities are <100 ppm of HCP. Therefore, the present of HCPs cannot be ignored.

HCP level in the harvested cell culture from a particular production platform depends on the cell culture process and harvest conditions. Cell viability plays an important role at the HCP level. Low viability cell culture introduces more cell debris, cells with fewer cell diameters, and high HCPs due to lysing of the cells, applying more burden on the downstream purification steps. Removal of HCPs occurs at the beginning of the purification, i.e., cell clarification, and is expected in each unit operation.

Although HCPs are typically removed by chromatography and the primary purpose of the depth filtration step is cell removal, several studies have demonstrated that these depth filtration filters also provide significant adsorptive removal of host cell proteins[67]. The mechanism of depth filtration involves absorption, trapping, and pore blocking. Therefore, depth filtration could remove the impurities even smaller than the nominal pore size, for example, the HCPs. In

27

addition, the HCPs easily form aggregates or interact with products due to the hydrophobic interaction. The size of the resulting aggregates increase. Therefore, those aggregates may be rejected by the membrane surface. Due to the complexity of these mechanisms, the fouling of the depth filtration is difficult to determine and analyze. The classic blocking model cannot be applied in this case because the depth filters do not have well-defined pore size and cylindrical porous matrix. The feed stream for depth filtration is typically high compressible and varied shapes. Several studies investigate the HCP fouling during the downstream process. Hogwood et al. demonstrated that the selection of early downstream process steps influences the resulting HCP profile and that 2D-PAGE can be used to monitor and identify HCPs post-protein A chromatography[68]. This approach could be used to screen cell lines or hosts to select those with reduced HCP profiles or identify HCPs that are problematic and difficult to remove so that cell-engineering approaches can be applied to reduce or eliminate such HCPs. However, 2D PAGE only gives a qualitative result as a map of fouling HCPs. The following identification of the interest spot identification encounters high investment because, in each case, there are a hundred spots on the 2D-PAGE. Throughout those studies, few studies focus on identifying the HCPs, specifically on the cell clarification process using a robust, high capacity, and quantitative method. The attempt to use SDS-PAGE coupling with the LC-MS/MS method is discussed in this work. The HCPs are identified and analyzed using fouled filter from the cell clarification process. The resulting identifications are fed into a machine learning model to evaluate those HCPs' profiles and characteristics. The fouling potential of HCPs is predicted using the trained models.

1.9   Perfusion culture

The production of industrial pharmaceutics involves the cultivation of the cell intensely. The mammalian cell can grow in a different medium, for example, on the surface of the flasks or directly in the cell culture medium, forming a suspension. Although the suspension cells need to be trained, selected, or engineered, the equipment for suspension cell culture is far more complex; almost all industrial pharmaceutics are produced in suspension style. With the development and intensification of the cell culture process, the suspension of cell culture can be achieved in batch mode, fed-batch mode, and continuous mode. Batch and fed-batch are the most common type of mammalian cell culture, regardless of scale. In batch cultures, cells, media, and nutrients are delivered into a bioreactor for up to three weeks with no more nutrients or waste removal. Fed-batch culturing involves adding nutrients at varying intervals to extend the culture and improve yield. In both cases, the product is harvested at the end in one batch. In continuous cultures, the nutrients are perfused constantly, and the product is continuously delivered to the harvest unit. Perfusion cultures have serval benefits over batch culturing. First, perfusion cultures normally last for a few weeks with high cell viability and density. Therefore, it has fewer turnovers than batch culture. Second, the product is harvested with time, largely reducing the equipment footprint requirement. Third, the fresh medium is continuously fed into the bioreactor while the toxic components are stripped off. Therefore, the cells can be maintained at a very high cell density and healthy state. The productivity of the cell is reported to be 7.5 times higher than fed-batch culture[69].

The continuous operation in chemical production is referred to continuous stirred tank reactor (CSTR), where the reactants are carefully designed to be reacted properly depending on the optimal dilution rate. In continuous cell culture, unlimited discharge of the producing cells

will be expensive because the cell has the capability to secret until its apoptosis. Therefore, the

cell retention device is key in the continuous cell culture. The typical retention devices are based

on membrane separation, although other devices like gravitational settling, centrifugation, and

ultrasonic separation are reported[70]. The membrane separation device can be used in tangential

flow filtration(TFF) mode or alternative tangential flow(ATF) mode. TFF is designed to reduce

the fouling in high cell density using its perpendicular flow. However, the cells are also exposed

to the shear rate caused by this tangential flow. ATF involves less shear rate and features by its

back and forward flow during the pressurized and exhausted cycles. The commonly used

modules for cell retention are summarized in Table 1.7.

Table 1.7 The commonly used modules for cell retention in the literature

Materials	Cell line	Reference
Acoustic filter, Applikon	CHO	[71]
PES filters, Repligen	CHO	[69, 72-74]
PES filters, Spectrum Laboratories	CHO	[75, 76]
Hollow fiber filters, GE	PER.C6	[77]
PVDF filters, Asahi Kasei	CHO	[78]

Although any filters that fit the ATF controller can be used for perfusion, a specific

membrane design for the perfusion process could streamline the process and reduce the risk

brought by the complexity of the perfusion system. For example, a hollow fiber module with a

low holding volume would reduce the heat transfer from the bioreactor to the ambient, therefore,

the temperature control for the bioreactor is more stable.

A key parameter is the medium exchange rate to achieve a successful perfusion cell culture. If the exchange rate is too high, the cost of the run increases, and the product in the permeate is diluted. In contrast, if the exchange rate is too low, the nutrition presented in the bioreactor will not be sufficient to support a high cell density, and the undesired chemicals cannot be stripped off. The quantitate parameter for medium exchange rate is known as cell-specific perfusion rate (CSPR) or expressed in vessel volumes of media per bioreactor volume per day (vvd). The typical CSPR is reported to be 40-400 pL/cell/day or 1-3 vvd per day.

Shear rate is another parameter to be considered. The shear rate in perfusion could be much different from the fed-batch because of the introduction of the external cell retention device. The cell repeatedly entering the lumen and pulling back to the bioreactor could experience damage to the cell membrane, especially given the typical run for perfusion is a few weeks. However, the shear rate in TFF perfusion is higher than the ATF perfusion, and the major shear rate is introduced if a peristaltic pump is used[79].

1.10 Methods in fouling study

1.10.1 Sodium dodecyl sulfate-polyacrylamide gel electrophoresis (SDS PAGE)

The term electrophoresis refers to the movement of charged molecules in response to an electric field, resulting in their separation. In an electric field, proteins move toward the electrode of opposite charge. The rate at which they move is governed by a complex relationship between the physical characteristics of both the electrophoresis system and the proteins. Factors affecting protein electrophoresis include the strength of the electric field, the temperature of the system, the pH, ion type, and concentration of the buffer as well as the protein's size, shape, and charge of the protein [80]. The electrophoresis can be used in many other analyses. Once proteins are separated, they are available for a number of downstream applications, including enzymatic

assays, further purification, transfer to a membrane for immunological detection, and elution and digestion for mass spectrometric analysis. The acrylamide gel serves as a size-selective sieve during the separation. As proteins move through a gel in response to an electric field, the gel's pore structure allows smaller proteins to travel more rapidly than larger proteins.

Two types of buffer systems can be used in SDS-PAGE. A continuous buffer system uses the same buffer in the gel, sample, and electrode reservoirs. However, continuous systems are not common in protein separations. They are used mostly in nucleic acid analysis instead. Discontinuous buffer systems refer to the gel separated into two sections. A larger pore stacking gel is on the top of a small pore resolving gel. The buffers in the gel and electrode solutions are also different. In the discontinuous gel, the protein first migrates quickly through the large pore stacking gel and then are slowed as they enter the small pore resolving gel. The timing that proteins enter the gel is minimized. Therefore the discontinuous gel provides higher resolution.

Proteins in the sample are required to be stabilized. Protein solubilization is the process of breaking interactions involved in protein aggregation, for example, disulfide bonds, hydrogen bonds, van der Waals forces, ionic interactions, and hydrophobic interactions. If these interactions are not prevented, protein can aggregate or precipitate, resulting in artificial results. The protein can be well stabilized with the help of chaotropic agents, detergents, reducing agents, buffers, salts, and ampholytes.

1.10.2 2-Dimensional electrophoresis (2DE)

2-dimensional electrophoresis (2DE) is a biochemical method for separating complex mixtures of proteins into individual species. Proteins are firstly separated by charge using isoelectric focusing (IEF), then by size using SDS-PAGE. The spot pattern of protein spots is visualized on the final 2DE slab gel by staining or western blotting. Proteins of interest may be

identified by mass spectrometry. Various methods and specialized software programs are available for processing 2-DE images, such as MELANIE, PDQuest, Z3, Progenesis Workstation, ProteomeWeaver, ProteinMine, Delta2D, and DeCyder[81, 82]. However, due to the anomalies present in these images, a reliable, automated, and highly reproducible system for 2-DE image analysis has still not been achieved. The most common anomalies in 2-DE images include vertical and horizontal streaking, fuzzy spots, and background noise, which greatly complicate computational analysis[83].

IEF combines the use of an electric field with a pH gradient to separate proteins according to their pI. When a protein moves through a pH gradient, its net charge changes will be in response to the pH it encounters. Under an electric field's influence, a protein in a pH gradient migrates to a pH where its net charge is zero. pI values of protein usually fall in the range of pH 3-11. In practice, the common way to run IEF is to use immobilized pH gradients strips formed by covalently grafting buffering groups to a polyacrylamide gel backbone. A gradient of different buffering groups generates a stable pH gradient that can be tailored for different pH ranges and gradients. After IEF, the strip is transferred to the top of the SDS-PAGE gel. Therefore a regular SDS-PAGE can be performed as the second-dimensional separation.

The two main drawbacks are its low efficiency in the analysis of hydrophobic proteins and its high sensitivity to the dynamic range and quantitative distribution issues. The three main advantages are its robustness, parallelism, and unique ability to analyze complete proteins at high resolution[84]. In the future, an automatic platform and experiment design need to be developed to combine several steps to enhance efficiency. Novel gel materials and specific gradients should be chosen readily in order to increase the dynamic range. An IPG needs to be improved for broader analysis and in linear scale for quantitative distribution.

1.10.3 Liquid chromatography/mass spectrometry (LC/MS)

LC/MS combines the resolving power of liquid chromatography with the detection specificity of mass spectrometry. Liquid chromatography separates the sample components and then introduces them to the mass spectrometer. The MS creates and detects charged ions. The LC/MS data may be used to provide information about the molecular weight, structure, identity, and quantity of specific sample components. Compared to gas chromatography/mass spectrometry (GC/MS), LC/MS imparts little or no heat to the analyte molecules, LC and LC/MS-based methods can be applied to more widely compounds. Sample types range from small pharmaceutical compounds to large proteins.

Besides the conventional LC, which utilizes only one chromatography technique and column, the multi-dimensional chromatography uses a combination of techniques for separation. One such system is the two-dimensional LC which can achieve higher selectivity not possible with conventional LC alone. The MS system is complex, which includes an ion source that ionizes samples, an ion guide (an electrostatic lens that efficiently introduces the generated ions into the MS, a mass analyzer unit that separates the ions based on their mass-to-charge (m/z), and a detector unit that detects the separated ions.

Based on Newton's second law of motion and momentum, a mass spectrometer uses this property of matter to plot ions of varying masses on a mass spectrum. From the law, we infer how much mass is relevant to the inertia and acceleration of a body. This principle is applied to the aspect where ions with different mass to charge ratios are deflected by different angles in an electric or magnetic field. Firstly, the sample is bombarded by electrons to ionize it. The bombarding of the sample is done by the electrons. These electrons move between cathode and anode. When the sample passes through the electron stream between the cathode and anode,

electrons with high energy knock electrons out of the sample and form ions. The second step is acceleration. The ions placed between a set of charged parallel plates get attracted to one plate and repel from the other plate. The acceleration speed can be controlled by adjusting the charge on the plates. Then the ions went through the deflector. A magnetic field deflects ions based on its charge and mass. If an ion is heavy or has two or more positive charges, then it is least deflected. If an ion is light or has one positive charge, then it is deflected the most. Finally, the ions arrived detector. When ions with correct charge and mass move to the detector, the ratio of mass to charge is analyzed through the ion that hits the detector. Based on the mass spectrum produced by the charged ions, we can identify the atoms or molecules constituting the sample by comparing them with known masses or through a characteristic fragmentation pattern.

1.10.4 MALDI-MS

Matrix-assisted laser desorption/ionization (MALDI) is a key technique in mass spectrometry (MS)-based proteomics. MALDI MS is extremely sensitive, easy to apply, and relatively tolerant to contaminants[85]. The sample for analysis by MALDI MS is prepared by mixing or coating with a solution of an energy-absorbent, organic compound called matrix[86]. When the matrix crystallizes on drying, the sample entrapped within the matrix also co-crystallizes. When a laser beam is irradiated to the targeted spot, where the sample is mounted, a laser pulse with the aim of the matrix (and ionizing agent in some cases) desorbs and ionizes the analyte of interest in an indirect manner. Normally, The matrix absorbs ultraviolet light and converts it to heat energy. A small part of the matrix heats rapidly and is vaporized, together with the sample. Desorption and ionization with the laser beam generate singly protonated ions from analytes in the sample.

The protonated ions are then accelerated at a fixed potential, where these separate from each other on the basis of their mass-to-charge ratio (m/z). As a result, a high-mass ion can be produced by this technique. The charged analytes are then detected and measured using different types of mass analyzers like quadrupole mass analyzers, ion trap analyzers, time of flight (TOF) analyzers, etc. For microbiological applications, mainly TOF mass analyzers are used. During MALDI-TOF analysis, the m/z ratio of an ion is measured by determining the time required for it to travel the length of the flight tube. Based on the TOF information, identification of microbes by MALDI-TOF MS is done by either comparing an unknown organism with the database or matching the masses of biomarkers of an unknown organism with the proteome database.

The principle of MALDI-TOF MS is based on the charged ions of various sizes generated on the sample slide. After the matrix is irradiated, generated ions that can be matrix ions, analyte ions, or possibly ionized fragments of the analyte molecules are accelerated and led towards the drift zone. The law of conservation of energy determines the velocity of the attracted ions. As the potential difference is constant with respect to all ions, ions with a smaller mass-to-charge ratio(m/z) value and more highly charged ions move faster through the drift space until they reach the detector. At the end of the flight path, the ion detector is located that can register the flight time and the intensity of the individual ions that arrive at the ion detector. As expected, heavier analyte ions take longer to reach the detector while lighter ions travel the same distance in a shorter period [87]. Consequently, the time of ion flight differs according to the mass-to-charge ratio value of the ion.

1.10.5 Confocal spectroscopy

Confocal microscopy offers several advantages over conventional widefield optical microscopy, including the ability to control depth of field, elimination or reduction of

background information away from the focal plane (that leads to image degradation), and the capability to collect serial optical sections from thick specimens.

Illumination from a point light source is reflected by a dichroic mirror into the back aperture of a microscope objective. The objective lens focuses the light on a diffraction-limited spot within the specimen. Fluorophores at the focal spot and within the cones of illumination above and below it are excited, emitting fluorescence in all directions. The fluorescence captured by the objective passes through the dichroic mirror because the fluorescence is at a longer wavelength than the excitation. The confocal pinhole allows fluorescence from the focal spot to reach the photodetector and blocks fluorescence from out-of-focus areas. Therefore the pinhole reduces background information away from the focal plane. Adjusting the pinhole to a diameter slightly less than the diameter of the central region of the Airy disk allows most of the light from the focal point to reach the detector. It reduces the background from out-of-focus areas by a thousand-fold relative to wide-field microscopy.

The sample preparation of confocal spectroscopy includes fixation, application of fluorophores, and mounting of the specimen. A standard fixative for fluorescence microscopy is 2% to 4% formaldehyde in PBS. Formaldehyde penetrates cells rapidly and preserves the antigen-recognition sites for many antibodies. However, formaldehyde cross-links proteins slowly and may cause vesiculation of membranes. An alternative procedure for preparing specimens is to immerse them in the cold (-20 °C) methanol or acetone, but fixation by this method causes severe shrinkage. The choice of fluorophores should take into account the available laser lines and the detector channels of the confocal microscope. Excitation is most efficient at wavelengths near the peak of the excitation spectrum of the fluorophore, but a precise match is not required. A recommended combination of fluorophores for excitation at 405 nm,

488 nm, 543/561 nm, and 633 nm would comprise Marina Blue, Alexa 488, Alexa 555, and Alexa 647 (all available from Molecular Probes/Invitrogen). The nucleic acid stain DAPI can be excited by illumination at 405 nm, although ultraviolet excitation (350 nm) is more optimal. The cyanine dyes Cy2, Cy3, and Cy5 (available from Jackson ImmunoResearch Laboratories) are also suitable for confocal microscopy. For multiwavelength imaging, it is important to select fluorophores that have distinct emission spectra, but there is no advantage in using fluorophores that have differing excitation spectra. Indeed, it is best to use fluorophores that have similar excitation maxima so that they can be excited with a single laser line reflected into the microscope with a single-wavelength dichroic mirror. The selection of a mounting medium should consider the type of microscope objective that will be used to observe the specimen. In order for an objective to perform optimally, the mounting medium should have the same refractive index as the objective immersion medium. Mismatches in the refractive indices produce spherical aberration leading to loss of light at the detector, as well as decreased z-axis resolution and incorrect depth discrimination. Image deterioration caused by spherical aberration increases with depth into the specimen; therefore, matching the immersion and mounting medium refractive indices is particularly important for thick specimens.

References

1.   AlSawaftah, N., et al., *A comprehensive review on membrane fouling: Mathematical modelling, prediction, diagnosis, and mitigation.* Water, 2021. **13**(9): p. 1327.

2.   Baghban, R., et al., *Yeast expression systems: overview and recent advances.* Molecular biotechnology, 2019. **61**(5): p. 365-384.

3.   Carta, G. and A. Jungbauer, *Protein chromatography: process development and scale-up.* 2020: John Wiley & Sons.

4.   Mehta, A., *Downstream processing for biopharmaceuticals recovery*, in *Pharmaceuticals from Microbes*. 2019, Springer. p. 163-190.

5.   Liu, Z., S.R. Wickramasinghe, and X. Qian, *Membrane chromatography for protein purifications from ligand design to functionalization.* Separation Science and Technology, 2017. **52**(2): p. 299-319.

6.   Stressmann, M. and C. Moresoli, *Effect of pore size, shear rate, and harvest time during the constant permeate flux microfiltration of CHO cell culture supernatant.* Biotechnology progress, 2008. **24**(4): p. 890-897.

7.   Kelley, B., *Very large scale monoclonal antibody purification: the case for conventional unit operations.* Biotechnology progress, 2007. **23**(5): p. 995-1008.

8.   Singh, N., et al., *Clarification technologies for monoclonal antibody manufacturing processes: Current state and future perspectives.* Biotechnology and bioengineering, 2016. **113**(4): p. 698-716.

9.   Dryden, W.A., et al., *Technical and economic considerations of cell culture harvest and clarification technologies.* Biochemical Engineering Journal, 2021. **167**: p. 107892.

10.   Coronel, J., et al., *Application of an inclined settler for cell culture-based influenza A virus production in perfusion mode.* Frontiers in Bioengineering and Biotechnology, 2020. **8**: p. 672.

11.   Willoughby, N., P. Martin, and N. Titchener-Hooker, *Extreme scale-down of expanded bed adsorption: Purification of an antibody fragment directly from recombinant E. coli culture.* Biotechnology and bioengineering, 2004. **87**(5): p. 641-647.

12.   Najjar, Y.S. and A. Abu-Shamleh, *Harvesting of microalgae by centrifugation for biodiesel production: A review.* Algal Research, 2020. **51**: p. 102046.

13.   Chatel, A., P. Kumpalume, and M. Hoare, *Ultra scale-down characterization of the impact of conditioning methods for harvested cell broths on clarification by continuous centrifugation—Recovery of domain antibodies from rec E. coli.* Biotechnology and Bioengineering, 2014. **111**(5): p. 913-924.

14.   Kempken, R., A. Preissmann, and W. Berthold, *Assessment of a disc stack centrifuge for use in mammalian cell separation.* Biotechnology and bioengineering, 1995. **46**(2): p. 132-138.

15.   Kempken, R., A. Preissmann, and W. Berthold, *Clarification of animal cell cultures on a large scale by continuous centrifugation.* Journal of industrial microbiology, 1995. **14**(1): p. 52-57.

16.   Melinek, B.J., et al., *Ultra scale-down approaches to study the centrifugal harvest for viral vaccine production.* Biotechnology and Bioengineering, 2018. **115**(5): p. 1226-1238.

17.   Liu, H.F., et al. *Recovery and purification process development for monoclonal antibody production*. in *MAbs*. 2010. Taylor & Francis.

18.   Gimenez, L., et al. *Overcoming the clarification challenges of high cell density culture*. in *BMC Proceedings*. 2015. BioMed Central.

19.   Parau, M., et al., *Analysis of fouling and breakthrough of process related impurities during depth filtration using confocal microscopy.* Biotechnology Progress, 2022: p. e3233.

20.   Ikeda, Y., S. Iwakiri, and T. Yoshimori, *Development and characterization of a novel host cell DNA assay using ultra-sensitive fluorescent nucleic acid stain "PicoGreen".* Journal of pharmaceutical and biomedical analysis, 2009. **49**(4): p. 997-1002.

21.   Goey, C.H., et al., *Cascading effect in bioprocessing—the impact of mild hypothermia on CHO cell behavior and host cell protein composition.* Biotechnology and Bioengineering, 2017. **114**(12): p. 2771-2781.

22.   Goey, C.H., D. Bell, and C. Kontoravdi, *CHO cell cultures in shake flasks and bioreactors present different host cell protein profiles in the supernatant.* Biochemical Engineering Journal, 2019. **144**: p. 185-192.

23.   Tait, A.S., et al., *Host cell protein dynamics in the supernatant of a mAb producing CHO cell line.* Biotechnology and Bioengineering, 2012. **109**(4): p. 971-982.

24.   Valente, K.N., A.M. Lenhoff, and K.H. Lee, *Expression of difficult-to-remove host cell protein impurities during extended Chinese hamster ovary cell culture and their impact on continuous bioprocessing.* Biotechnology and Bioengineering, 2015. **112**(6): p. 1232-1242.

25.   Paul, A.J., et al., *Identification of process conditions influencing protein aggregation in Chinese hamster ovary cell culture.* Biotechnology and Bioengineering, 2018. **115**(5): p. 1173-1185.

26.   Apostolidis, P.A., et al., *Investigation of low viability in sparged bioreactor CHO cell cultures points to variability in the Pluronic F-68 shear protecting component of cell culture media.* Biochemical Engineering Journal, 2015. **98**: p. 10-17.

27.   Velez-Suberbie, M.L., et al., *Impact of aeration strategy on CHO cell performance during antibody production.* Biotechnology progress, 2013. **29**(1): p. 116-126.

28.   van Reis, R. and A. Zydney, *Bioprocess membrane technology.* Journal of Membrane Science, 2007. **297**(1-2): p. 16-50.

29.   Gilgunn, S., et al., *Identification and tracking of problematic host cell proteins removed by a synthetic, highly functionalized nonwoven media in downstream bioprocessing of monoclonal antibodies.* Journal of Chromatography A, 2019. **1595**: p. 28-38.

30.   Tomic, S., et al., *Complete clarification solution for processing high density cell culture harvests.* Separation and Purification Technology, 2015. **141**: p. 269-275.

31.   Yigzaw, Y., et al., *Exploitation of the adsorptive properties of depth filters for host cell protein removal during monoclonal antibody purification.* Biotechnology progress, 2006. **22**(1): p. 288-296.

32.   Westoby, M., et al., *Effects of solution environment on mammalian cell fermentation broth properties: enhanced impurity removal and clarification performance.* Biotechnology and bioengineering, 2011. **108**(1): p. 50-58.

33.   Wong, F.W.F., A.B. Ariff, and D.C. Stuckey, *Downstream protein separation by surfactant precipitation: a review.* Critical reviews in biotechnology, 2018. **38**(1): p. 31-46.

34.   Brodsky, Y., et al., *Caprylic acid precipitation method for impurity reduction: an alternative to conventional chromatography for monoclonal antibody purification.* Biotechnology and bioengineering, 2012. **109**(10): p. 2589-2598.

35.   Bhat, R. and S.N. Timasheff, *Steric exclusion is the principal source of the preferential hydration of proteins in the presence of polyethylene glycols.* Protein Science, 1992. **1**(9): p. 1133-1143.

36.   Yoshikawa, H., et al., *Mechanistic insights into protein precipitation by alcohol.* International journal of biological macromolecules, 2012. **50**(3): p. 865-871.

37.   Kim, J.-Y., et al., *Genetically engineered elastin-protein A fusion as a universal platform for homogeneous, phase-separation immunoassay.* Analytical Chemistry, 2005. **77**(8): p. 2318-2322.

38.   Sardari, K., et al., *Aluminum electrocoagulation followed by forward osmosis for treating hydraulic fracturing produced waters.* Desalination, 2018. **428**: p. 172-181.

39.   Han, B., et al., *Arsenic removal from drinking water by flocculation and microfiltration.* Desalination, 2002. **145**(1-3): p. 293-298.

40.   Wickramasinghe, S.R., et al., *Influence of cationic flocculant properties on the flocculation of yeast suspensions.* Advanced Powder Technology, 2010. **21**(4): p. 374-379.

41.   Wickramasinghe, S.R., et al., *Clearance of minute virus of mice by flocculation and microfiltration.* Biotechnology and bioengineering, 2004. **86**(6): p. 612-621.

42.   McNerney, T., et al. *PDADMAC flocculation of Chinese hamster ovary cells: enabling a centrifuge-less harvest process for monoclonal antibodies*. in *MAbs*. 2015. Taylor & Francis.

43.   Gómez, I.A., et al., *Flocculation of CHO cells for primary separation of recombinant glycoproteins: Effect on glycosylation profiles.* Biochemical Engineering Journal, 2018. **132**: p. 244-254.

44.   Pabst, T.M., J. Thai, and A.K. Hunter, *Evaluation of recent Protein A stationary phase innovations for capture of biotherapeutics.* Journal of Chromatography A, 2018. **1554**: p. 45-60.

45.   Hober, S., K. Nord, and M. Linhult, *Protein A chromatography for antibody purification.* Journal of Chromatography B, 2007. **848**(1): p. 40-47.

46.   Linhult, M., et al., *Improving the tolerance of a protein a analogue to repeated alkaline exposures using a bypass mutagenesis approach.* Proteins: structure, function, and bioinformatics, 2004. **55**(2): p. 407-416.

47.   González-Valdez, J., et al., *Toward improving selectivity in affinity chromatography with PEG ylated affinity ligands: The performance of PEG ylated protein A.* Biotechnology progress, 2014. **30**(6): p. 1364-1379.

48.   Verdoliva, A., et al., *Affinity purification of polyclonal antibodies using a new all-D synthetic peptide ligand: comparison with protein A and protein G.* Journal of immunological methods, 2002. **271**(1-2): p. 77-88.

49.   Fekete, S., et al., *Ion-exchange chromatography for the characterization of biopharmaceuticals.* Journal of Pharmaceutical and Biomedical Analysis, 2015. **113**: p. 43-55.

50.   Kastner, M., *Protein Liquid Chromatography*. 2000: Elsevier Science.

51.   Pepaj, M., et al., *Two-dimensional capillary liquid chromatography: pH Gradient ion exchange and reversed phase chromatography for rapid separation of proteins.* Journal of chromatography A, 2006. **1120**(1-2): p. 132-141.

52.   Zheng, S., et al., *Two-dimensional liquid chromatography protein expression mapping for differential proteomic analysis of normal and O157: H7 Escherichia coli.* BioTechniques, 2003. **35**(6): p. 1202-1212.

53.   Fekete, S., et al., *Hydrophobic interaction chromatography for the characterization of monoclonal antibodies and related products.* Journal of Pharmaceutical and Biomedical Analysis, 2016. **130**: p. 3-18.

54.   Chen, B., et al., *Online hydrophobic interaction chromatography–mass spectrometry for top-down proteomics.* Analytical chemistry, 2016. **88**(3): p. 1885-1891.

55.   Hermia, J., *Constant pressure blocking filtration law application to powder-law non-Newtonian fluid.* Trans. Inst. Chem. Eng., 1982. **60**: p. 183-187.

56.   Ho, C.-C. and A.L. Zydney, *A combined pore blockage and cake filtration model for protein fouling during microfiltration.* Journal of colloid and interface science, 2000. **232**(2): p. 389-399.

57.   Bolton, G., D. LaCasse, and R. Kuriyel, *Combined models of membrane fouling: development and application to microfiltration and ultrafiltration of biological fluids.* Journal of Membrane Science, 2006. **277**(1-2): p. 75-84.

58.   Bolton, G.R., A.W. Boesch, and M.J. Lazzara, *The effects of flow rate on membrane capacity: development and application of adsorptive membrane fouling models.* Journal of Membrane Science, 2006. **279**(1-2): p. 625-634.

59.   Davis, R.H. and J.D. Sherwood, *A similarity solution for steady-state crossflow microfiltration.* Chemical Engineering Science, 1990. **45**(11): p. 3203-3209.

60.   Juang, R.-S., H.-L. Chen, and Y.-S. Chen, *Resistance-in-series analysis in cross-flow ultrafiltration of fermentation broths of Bacillus subtilis culture.* Journal of Membrane Science, 2008. **323**(1): p. 193-200.

61.   Fan, R., et al., *Lactic acid production in a membrane bioreactor system with thermophilic Bacillus coagulans: Fouling analysis of the used ceramic membranes.* Separation Science and Technology, 2015. **50**(14): p. 2177-2189.

62.   Zhang, Z., et al., *Prediction of carbon dioxide adsorption via deep learning.* Angewandte Chemie, 2019. **131**(1): p. 265-269.

63.   Zhou, Y., et al., *Predicting the oxidation of carbon monoxide on nanoporous gold by a deep-learning method.* Chemical Engineering Journal, 2022. **427**: p. 131747.

64.   Marcato, A., G. Boccardo, and D. Marchisio, *A computational workflow to study particle transport and filtration in porous media: Coupling CFD and deep learning.* Chemical Engineering Journal, 2021. **417**: p. 128936.

65.   Li, Y., *Effective strategies for host cell protein clearance in downstream processing of monoclonal antibodies and Fc-fusion proteins.* Protein Expression and Purification, 2017. **134**: p. 96-103.

66.   Baycin-Hizal, D., et al., *Proteomic analysis of Chinese hamster ovary cells.* Journal of proteome research, 2012. **11**(11): p. 5265-5276.

67.   Zydney, A.L., *New developments in membranes for bioprocessing–a review.* Journal of Membrane Science, 2021. **620**: p. 118804.

68.   Hogwood, C.E., et al., *The dynamics of the CHO host cell protein profile during clarification and protein A capture in a platform antibody purification process.* Biotechnology and bioengineering, 2013. **110**(1): p. 240-251.

69.   Walther, J., et al., *Perfusion cell culture decreases process and product heterogeneity in a head-to-head comparison with fed-batch.* Biotechnology Journal, 2019. **14**(2): p. 1700733.

70.   Castilho, L.R. and R.A. Medronho, *Cell retention devices for suspended-cell perfusion cultures.* Tools and applications of biochemical engineering science, 2002: p. 129-169.

71.   Dowd, J.E., et al., *Optimization and control of perfusion cultures using a viable cell probe and cell specific perfusion rates.* Cytotechnology, 2003. **42**(1): p. 35-45.

72.   Warikoo, V., et al., *Integrated continuous production of recombinant therapeutic proteins.* Biotechnology and bioengineering, 2012. **109**(12): p. 3018-3029.

73.   Xu, S. and H. Chen, *High-density mammalian cell cultures in stirred-tank bioreactor without external pH control.* Journal of biotechnology, 2016. **231**: p. 149-159.

74.   Bielser, J.-M., et al., *Perfusion cell culture for the production of conjugated recombinant fusion proteins reduces clipping and quality heterogeneity compared to batch-mode processes.* Journal of biotechnology, 2019. **302**: p. 26-31.

75.   Karst, D.J., et al., *Characterization and comparison of ATF and TFF in stirred bioreactors for continuous mammalian cell culture processes.* Biochemical Engineering Journal, 2016. **110**: p. 17-26.

76.   Liu, Z., et al., *The application of Raman spectroscopy for monitoring product quality attributes in perfusion cell culture.* Biochemical Engineering Journal, 2021. **173**: p. 108064.

77.   Mercier, S.M., et al., *Process analytical technology tools for perfusion cell culture.* Engineering in life Sciences, 2016. **16**(1): p. 25-35.

78.   Pinto, N.D. and M. Brower, *Wide-surface pore microfiltration membrane drastically improves sieving decay in TFF-based perfusion cell culture and streamline chromatography integration for continuous bioprocessing.* Biotechnology and Bioengineering, 2020. **117**(11): p. 3336-3344.

79.   Wang, S., et al., *Shear contributions to cell culture performance and product recovery in ATF and TFF perfusion systems.* Journal of Biotechnology, 2017. **246**: p. 52-60.

80.   Garfin, D.E., *One-dimensional gel electrophoresis*, in *Methods in enzymology*. 1990, Elsevier. p. 425-441.

81.   Bandow, J.E., et al., *Improved image analysis workflow for 2-D gels enables large-scale 2-D gel-based proteomics studies–COPD biomarker discovery study.* Proteomics, 2008. **8**(15): p. 3030-3041.

82.   Sengar, R.S., et al., *Analysis of 2D-gel images for detection of protein spots using a novel non-separable wavelet based method.* Biomedical Signal Processing and Control, 2016. **25**: p. 62-75.

83.   Goez, M.M., et al., *Preprocessing of 2-dimensional gel electrophoresis images applied to proteomic analysis: a review.* Genomics, proteomics & bioinformatics, 2018. **16**(1): p. 63-72.

84.   Rabilloud, T., et al., *Two-dimensional gel electrophoresis in proteomics: Past, present and future.* Journal of proteomics, 2010. **73**(11): p. 2064-2077.

85.   Cramer, R., *Maldi Ms*, in *Proteomics*. 2009, Springer. p. 85-103.

86.   Singhal, N., et al., *MALDI-TOF mass spectrometry: an emerging technology for microbial identification and diagnosis.* Frontiers in microbiology, 2015. **6**: p. 791.

87.   Hosseini, S. and S.O. Martinez-Chapa, *Principles and mechanism of MALDI-ToF-MS analysis.* Fundamentals of MALDI-ToF-MS Analysis, 2017: p. 1-19.

Chapter 2.   Modeling tangential flow filtration using reverse asymmetric membranes for bioreactor harvesting

Summary

Tangential flow filtration has many advantages for bioreactor harvesting as the permeate could be introduced directly to the subsequent capture step. However, membrane fouling has limited its widespread use. This is particularly problematic given the high cell densities encountered today. Here a reverse asymmetric membrane, where the more open surface faces the feed stream and the tighter barrier layer faces the permeate stream, has been investigated. The open surface contains pores up to 40 µm in diameter while the tighter barrier layer has an average pore size of 0.4 µm. Filtration of yeast suspensions has been conducted under a range of conditions. The yeast cells are trapped in the open pore structure. The membrane stabilizes an internal porous cake that acts like a depth filter. This stabilized cake layer can remove particulate matter that would foul the barrier layer if it faced the feed stream. As filtration continues a surface cake layer forms on the membrane surface. A resistance in series model has been developed to describe the permeate flux during tangential flow filtration. The model contains three fitted parameters which can easily be determined from constant pressure normal flow filtration experiments and total recycle constant flux tangential flow filtration experiments. The model can be used to estimate the capacity of the filter for a given feed stream. Our results suggest that using a reverse asymmetric membrane could avoid severe flux decline associated with fouling of the barrier during bioreactor harvesting.

2.1   Introduction

Bioreactor harvesting represents the first of the downstream purification operations in the manufacture of biopharmaceuticals. The product of interest, typically a protein based therapeutic,

is separated from the particulate matter in the bioreactor: the cells and cell debris. The harvesting method of choice depends on the type of cells, mode of bioreactor operation, scale of manufacturing, and product properties. Typical unit operations include centrifugation, expanded bed chromatography, depth filtration, and tangential flow filtration (TFF). Frequently more than one unit operation is required[1]. Today centrifugation and depth filtration and are preferred over TFF even though TFF has many potential advantages[2]. In particular there is growing interest in continuous biomanufacturing. Continuous cell cultivation will require the development of continuous cell harvesting operations. The use of an external TFF unit is ideal since by using an appropriate membrane pore size, a cell free permeate may be recovered that can be directly introduced to the subsequent capture step.

TFF based harvesting processes typically use 0.2 µm pore sized membranes. Unlike centrifugation, a particle free solution is obtained that needs no further clarification before the subsequent product capture step. However, as cell densities have increased, increases in cell debris have caused high levels of fouling and lower product recoveries which has limited the use of TFF[3]. Wang et al.[4] compared centrifugation followed by depth filtration, centrifugation followed by filter aid enhanced depth filtration and TFF for harvesting a therapeutic protein from a high-density yeast fermentation broth. Given the fact that membrane processes are linearly scalable and the product from a TFF step can be directly introduce to a capture step, TFF displayed the greatest of ease of manufacturability. This is however offset by capital costs and consumable costs due to membrane fouling.

Over the years numerous attempts have been made to design membranes, modules and choose appropriate operating conditions that minimize fouling and maximize product recovery during TFF. Naja et al.[5] compare TFF for microbial cultures under different operating

conditions. Wang et al.[6] in a recent study suggest the use of larger pore sizes, up 0.65 μm, in order to minimize product retention. Stressmann and Moresoli[7] indicate the importance of pore size and shear rate on permeate flux during TFF of CHO cells. Hopper et al.[8] indicate that adjusting the feed pH can improve the filterability of bacterial cell broths. Periodic permeate flow reversal has been shown to help limit fouling[9, 10]. Others have considered the use of flow instabilities such as rotating disk filters[11], Taylor vortex devices[12] and Dean vortices[13] to suppress cake formation. Russotti et al.[14] highlight the importance of selecting appropriate operating conditions in order to maximize product recovery. More recently periodic reversal of the feed flow (alternating tangential flow) has been shown to improve product recovery especially for perfusion bioreactors[15].

In an early study Arora and Davis[16] considered normal flow microfiltration of bovine serum albumin through yeast cake layers. They indicate that the formation of a thin secondary cake layer on the membrane surface led to higher fluxes compared to the absence of a cake layer. The yeast cake layer was found to act as a filter aid, removing foulants which would have adsorbed onto the membrane leading to a reduction in product transmission and permeate flux. These studies were extended to TFF by Kuberkar and Davis[17], and Güell et al[18]. These later studies indicate that the formation of a thin secondary membrane can be beneficial and lead to higher stable permeate fluxes and product transmission compared to the absence of a secondary membrane. However, it is important that the secondary membrane is thin. Given the high cell densities encountered today this will not be feasible.

An early study by Guerra et al.[19] suggest a method of ensuring the secondary membrane can be stabilized on the membrane. They used reverse asymmetric membranes where the larger pore surface of the membrane faces the feed stream and the tighter barrier layer faces

the permeate stream. This results in the accumulation of particulate matter within the membrane structure facing the feed. The more open surface of the membrane ensures that the deposited species have an open structure which minimizes the increase in resistance to permeate flow. Similar to the results obtained by Arora and Davis[16], Kuberkar and Davis[17] and Güell et al.[18] show that an open, low resistance secondary cake layer can lead to higher stable permeate fluxes and product recovery. Gan[20] showed a similar effect of reverse asymmetry for beer clarification. In fact, today commercially available virus filtration membranes are reverse asymmetric membranes[21]. The more open support structure acts as an inline prefilter removing any product dimers, trimers etc. that could foul the membrane.

In this work a TFF module which contains a unique reverse asymmetric membrane has been investigated. The BioOptimal[TM] MF-SL Microfilter (Asahi Kasei, Glenview, IL, USA), is a commercially available hollow fiber module that contains a reverse asymmetric membrane. The polysulfone hollow fiber membrane has an effective membrane surface area of 0.005 m² and an inside diameter of 1.4 mm. The inside surface has pores up to 40 mm in diameter while the outside surface has 0.4 μm pores. Since the feed is pumped inside the fibers, it is the more open membrane surface that contacts the feed. Reverse asymmetric microfiltration membranes could overcome severe flux decline and low product recoveries that occur due to the formation of a low permeability cake layer.

Though the use of reverse asymmetric microfiltration membranes has been proposed for several years the BioOptimal[TM] microfilter is the first such module to be used commercially on a wide scale. Further there have been few studies that have attempted to model the performance of the filter. Here we have developed a resistance in series model to describe the performance of the BioOptimal[TM] microfilter. The model parameters may be determined by conducting two

experiments: normal flow filtration at constant pressure and TFF under total recycle and constant flux conditions. Our feed stream consisted of yeast cells. Yeast cells are good model system as they are incompressible. The presence of a cell wall results in their being relatively robust and resistant to lysis under an imposed shear stress.

2.2 Background and Theory

Given the reverse asymmetry of the membrane, at the commencement of microfiltration the filter will behave like a depth filter where yeast cells are captured in the membrane pores. This internal cake is stabilized by the membrane morphology. The analysis used here is based on that proposed by Carrère et al.[22] to model clarification of yeast fermentation broths by TFF. Juang et al.[23] and Fan et al.[24] used a similar approach to model fermentation broths of *Bacillus subtilis* and thermophilic *Bacillus coagulans,* respectively. It is assumed that the resistance to permeate flow is given by the sum of the individual resistance in series[25, 26].

$$\frac{Q_P}{A} = \frac{\Delta P}{\mu(R_m + R_c)}$$ [2.1]

where Q_P is the permeate flow, A is the membrane surface area, ΔP is the pressure driving force across the membrane, μ is the permeate viscosity and R_m and R_c are the membrane and cake resistances, respectively. Experimentally, Qp is obtained by measuring the permeate volume at certain intervals.

$$Q_P = \frac{dV}{dt}$$ [2.2]

where V is permeate volume at time t.

The membrane resistance may be found from the permeate flux for DI water where R_c is zero in Equation[2.1]. Experimentally this is achieved by closing the retentate line and operating the BioOptimal™ Microfilter in normal flow mode (see Figure 2.1(a)).

The cake resistance is given by

$$R_c = \frac{m}{A}\alpha \qquad [2.3]$$

where m it the mass of yeast cells deposited on the membrane and α is the resistance coefficient of the cake which is given by

$$\alpha = \alpha_0 \times \Delta P^n \qquad [2.4]$$

where α_0 is a constant that depends on the particle size and shape and n is the compressibility index of the cake. Substituting equation [2.4] into [2.3] yields,

$$log(R_c) = log\left(\frac{m \times \alpha_0}{A}\right) + nlog(\Delta P) \qquad [2.5]$$

Equation [2.5] assumes the cake resistance varies with the mass of the deposited cake. Here the cake resistance is also determined in normal flow mode (see Figure 2.1 (b)) with the feed introduced outside the fibers. The value of R_c may be determined from Equation[2.1] where R_m is determined from the DI water flux. Experimentally the flux is determined as function of pressure drop. Equation [2.5] is used to calculate n and α_0. In determining the membrane resistance (Figure 2.1 (a)) the direction of flow makes no difference. However, when determining the cake resistance, the module was run in normal flow mode with the feed introduce outside the hollow fibers. This is opposite to industrial practice where the feed is introduced inside the fibers. By determining α_0 and n when the barrier layer faces the feed stream, we ensure the structure of the cake within the more open membrane surface does not affect the values of α_0 and n.

Unlike normal flow filtration, the rate of change of cake mass for TFF is given by

$$\frac{dm}{dt} = cQ_P - KQ_F m \qquad [2.6]$$

where c is the concentration of yeast at time t. Suppression of cake formation is assumed to depend on the mass of cake already deposited as well as the feed flow rate, Q_F, and a cake attrition factor, K as given by the second term on the right-hand side of Equation [2.6].

52

Integrating Equation [2.6]gives:

$$m = \frac{cQ_P}{KQ_F}(1 - e^{-KQ_F t})$$ [2.7]

Substituting Equation[2.5] and [2.7] into [2.1] with R_m taken as 0, gives the increase in TMP due to cake formation,

$$TMP_c = \frac{\alpha \mu c Q_P{}^2}{A^2 KQ_F}(1 - e^{-KQ_F t})$$ [2.8]

where TMP_c is the increase in TMP due to fouling. The TMP due to resistance to flow through the clean membrane is given by TMP_m. It is noted that the total TMP is comprised of TMP_c plus TMP_m. The attrition factor K is the only unknown coefficient and can be determined from constant flux experiments in total recycle mode (Figure 2.1 (c)). The permeate flux may be predicted in concentration mode under constant pressure (see Figure 2.1 (d)) using the values of the three parameters n, α_0 and K from normal flow and total recycle TFF.

The yeast concentration in the feed at any time t, is obtained from a mass balance

$$c = \frac{c_0 V_0 - m}{V_0 - V}$$ [2.9]

where V_0 is the initial feed volume and V is the permeate volume at time t. The permeate flux may be determined by combining Equations [2.1], [2.2], [2.5], [2.6]and[2.9].
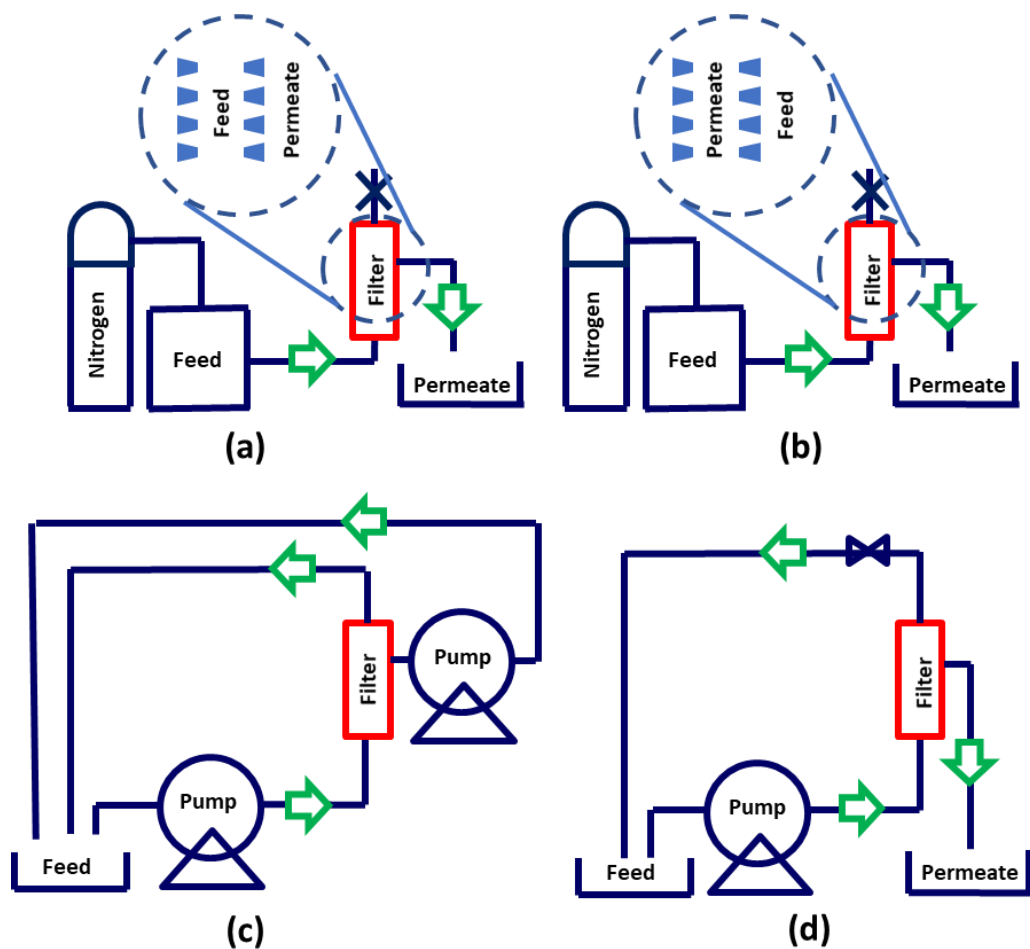
Figure 2.1 Experimental set up (a) normal flow and constant pressure, feed inside the hollow fibers; (b) normal flow and constant pressure, feed outside the hollow fibers; (c) TFF, total recycle and constant flux, feed inside the hollow fibers; (d) TFF, concentration mode and constant pressure, feed inside the hollow fibers.

2.3 Material and Methods

2.3.1 Materials

All reagents purchased were ACS grade or higher unless specified. Yeast suspensions were prepared with Fleischmann's baker's yeast (Memphis, TN, USA). Sodium chloride, sodium phosphate monobasic and sodium phosphate dibasic were purchased from MilliporeSigma (Billerica, MA, USA). BioOptimal™ MF-SL filters (Catalog Number: MFSL0005) and a

filtration vessel were provided by Asahi Kasei Bioprocess (Glenview, IL, USA). The outer

surface of the hollow fibers present in the BioOptimal™ microfilter is the barrier layer for

filtration. Pressure sensors and a peristaltic pump were obtained from SciLog (Oxnard, CA,

USA). Sodium hydroxide, sodium hypochlorite, a digital hotplate stirrer, and a pressure gauge

were purchased from VWR (Radnor, PA, USA). An electronic balance was purchased from

Mettler Toledo (Columbus, OH, USA). All rubber tubing used to deliver fluid were purchased

from Masterflex (Vernon Hills, IL, USA). DI water used in this work was obtained from a

ThermoFisher 18MΩ Barnstead Smart2pure system (Schwerte, Germany).

2.3.2 Filtration experiments

In normal flow filtration, the permeate port was closed and yeast feed solution was

loaded into the pressurized filtration cell. The feed solution was stirred using a magnetic stirrer.

A nitrogen tank was connected to the filtration cell. Permeate was collected on the balance. The

flux was calculated based on the change in the permeate weight during a specified time interval.

The density of the permeate was taken as 1000 kg/m³.

In TFF, the feed was pumped as shown in Figure 2.1(c) and (d). The pump flow rate was

set to provide the desired wall shear rate according to

$$\gamma = \frac{4Q_F}{\pi r^3} \qquad [2.10]$$

where γ is the shear rate and r is the fiber radius. In constant flux total recycle mode, both

retentate and permeate were returned to the feed reservoir. Two pumps were used as show in

Figure 2.1(c). The variation in TMP was determined where the TMP is given by

$$\frac{P_F + P_R}{2} - P_P \qquad [2.11]$$

where P_F, P_R and P_P are the feed retentate and permeate pressures, respectively. In concentration

mode at constant pressure, the permeate was collected on a balance.

The BioOptimal™ MF-SL was reused after each run. The regeneration protocol consisted of overnight incubation with 0.5 N NaOH with 3,000 ppm. NaOCl followed by backflushing with the same solution. Finally, the module was flushed with DI water till the permeate was at pH 7. If the DI water flux varied from the original DI water flux of the clean membrane by more than 5% a new module was used. All experimental results represent average values. The variation between repeat runs was found to be 5%.

2.3.3 Feed preparation

The yeast suspensions were prepared with Fleischmann's baker's yeast (Saccharomyces cerevisiae). The volume-based modal particle size was found to around 5 µm using laser diffraction particle sizing. Yeast powder was suspended with 20 mM phosphate buffer (pH 7), which consisted of 1.07 g/L sodium phosphate monobasic, 1.73 g/L sodium phosphate dibasic, and 9 g/L sodium chloride. Table 2.1 summarizes the filtration experiments. Shear rates around 2000 s^{-1} were chosen as this is common in indusial practice.

Table 2.1 Yeast filtration experimental conditions. For TFF operation, pressure difference across the membrane refers to TMP.

Operating mode	Feed volume (mL)	Yeast concentration (g/L)	Pressure difference across membrane (Pa)	Wall shear rate (s-1)
Normal flow, constant pressure	500	1.6	6894-20,684	N/A
TFF, total recycle, constant flux	500	0.7	N/A	2000
TFF, concentration mode, constant pressure	2000	0.4, 0.6, 0.8, 1.0, 1.2	6894	2000
	2000	1	6894	1750, 2000, 2250, 2500, 2850

2.4   Results and Discussion

2.4.1   Normal flow filtration

Normal flow filtration experiments with DI water gave a membrane resistance, R_m of 1.8 x 10^{10} (m^{-1}). The viscosity of the permeate at 22 °C, the average temperature in the feed reservoir, was taken as 9.6 x10^{-4} (Pa·s). Figure 2.2 Figure 2.2 Variation of R_c with TMP.gives the variation of Log(Rc) with Log(ΔP) as given by Equation [2.5]. Rc was calculated using Equation [2.1] and then plotted against the experimental value of log($\triangle$P) to obtain n and α_0 using

Equation[2.5]. The R^2 value was 0.96 indicating a good fit to the data.
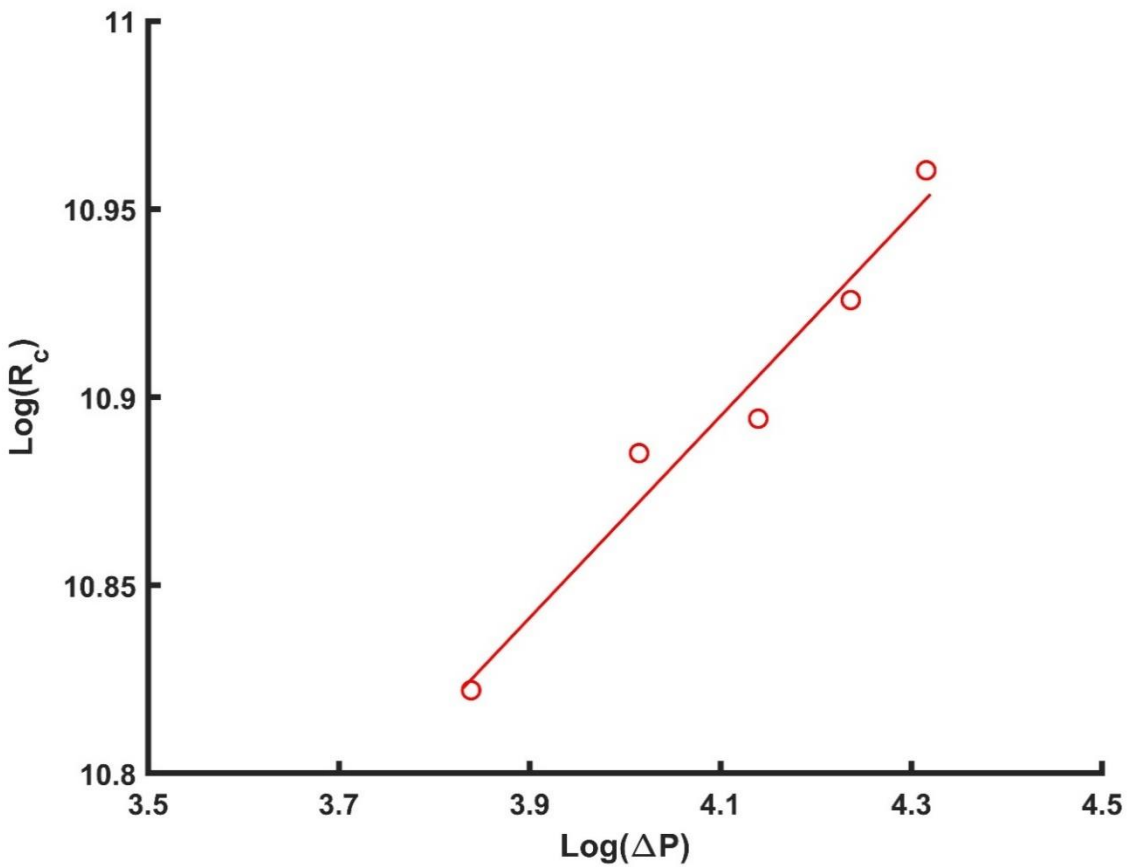
Figure 2.2 Variation of R_c with TMP.

      The compressibility index, n, was found to be 0.268 and resistance coefficient α_0

6.4×10^{10} (m kg^{-1} pa$^{-0.268}$). The low compressibility indicates a relatively incompressible cake as

expected for yeast cells. The compressibility index depends on the microorganisms[24].

2.4.2 TFF

      Next TFF experiments were conducted under total recycle and constant flux conditions to

determine K, the attrition coefficient. The variation of TMP with time is plotted in Figure 2.3.

Results are given for 5 different fluxes. The initial yeast concentration was 0.7 g/L and the wall

shear rate 2000 s^{-1}. The solid curves give the model fit based on n and a0 determined from

normal flow filtration experiments. The y axis gives TMPC. The value of the attrition coefficient that gave the best fit for all the data excluding data for a permeate flux of 840 LMH is given by

$$K = 10^9 \times Q_p + 300 \qquad [2.12]$$

Figure 2.3 indicates that at low permeate fluxes a pseudo steady state flux is obtained. At intermediate fluxes, an extended period of slow TMP increase is observed. However, at high permeate fluxes the TMP continues to increase rapidly with time. While the results for a permeate flux of 840 L m^{-2} h^{-1} are not included in the determination of K, the prediction based on Equation [2.12]is included. The results indicate the presence of a critical flux. If the permeate flux is below the critical flux, fouling is negligible in this case around 360 L m^{-2} h^{-1}.[27]
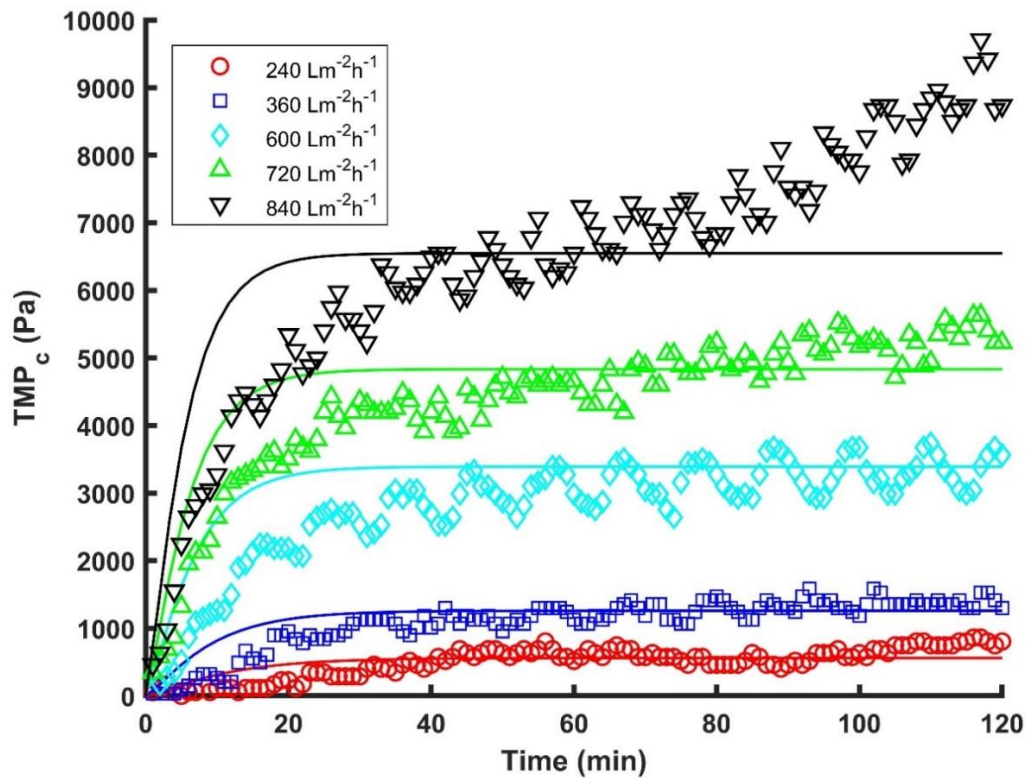
Figure 2.3 Variation of TMP with time for TFF under total recycle and constant flux. The yeast concentration was 0.7 g/L and the wall shear rate 2000 s^{-1}. Symbols give experimental data; curves are model fits.

More recently the concept of a threshold flux has been proposed. The threshold flux defines the boundary between low and high fouling. Fouling however depends on the membrane properties, feed properties and operating conditions. Above the threshold flux high fouling which leads to unsustainable operation results. In this case the threshold flux is around 720 L m^{-2} h^{-1}.[28]

In this work we have used an empirical approach to describe the migration of yeast cells away from the membrane. Several back-migration mechanisms have been described such as Brownian diffusion, shear enhanced diffusion, inertial lift forces and surface transport[3]. However, as the feed stream contains a mixture of intact yeast cells as well as cell debris, a range of particle sizes exists. The different back migration mechanism will contribute to different degrees to the overall back migration of a given particle size. The situation is complicated by the fact that yeast cells do interact with each other and can aggregate. Further the presence of a stabilized internal cake within the membrane will lead to surface yeast cells interacting with both the membrane and yeast cells that from part of the stabilized internal cake layer. All of these effects make it difficult for practical application of the theoretical models to predict the permeate flux.

The model we have developed ignores the effects of adsorption of foulants on the membrane surface. However due to the formation of a stabilized cake layer in the membrane pores, adsorption on the membrane surface is minimized. The internal cake acts as a depth filter. In effect the internal cake layer protects the tighter membrane barrier layer from foulants.

Theoretical models indicate the back migration mechanism depends on variables such as the shear rate, particle size, particle concentration, suspension viscosity, and length of the flow channel. From a practical perspective we have chosen to relate the attrition coefficient to the

permeate flow rate (Equation [2.12]). Since yeast cells interact with each other as the permeate flow rate increases, convection of particle to the membrane surface increases. The particles interact with each other limiting their back migration. Equation [2.12]suggests that at a permeate flux of zero, K is not zero. In reality cake attrition and back migration of particles applies only to particles in the surface cake layer. Particles in the internal cake within the membrane are less likely to return to the feed stream. However, we have combined the resistance of both internal and surface cakes.

TFF was conducted under concentration mode at constant TMP. Figure 2.4 gives results for different yeast concentrations while Figure 2.5 gives results for different shear rates (feed flow rates). Model fits are based on values for the three parameters α_0, n and K estimated for normal flow and TFF under total recycle and constant flux conditions. Figure 2.4 and Figure 2.5 give the variation of permeate flux with time. The experimental data are given by symbols while the solid lines gives give the corresponding variation of the calculated flux with time as given by Equation [2.1]. In Equation [2.1], R_m is determined experimentally, R_c is obtain from Equations [2.5] and [2.6] as a function of time. The TMP was set experimentally (see Table 2.1).
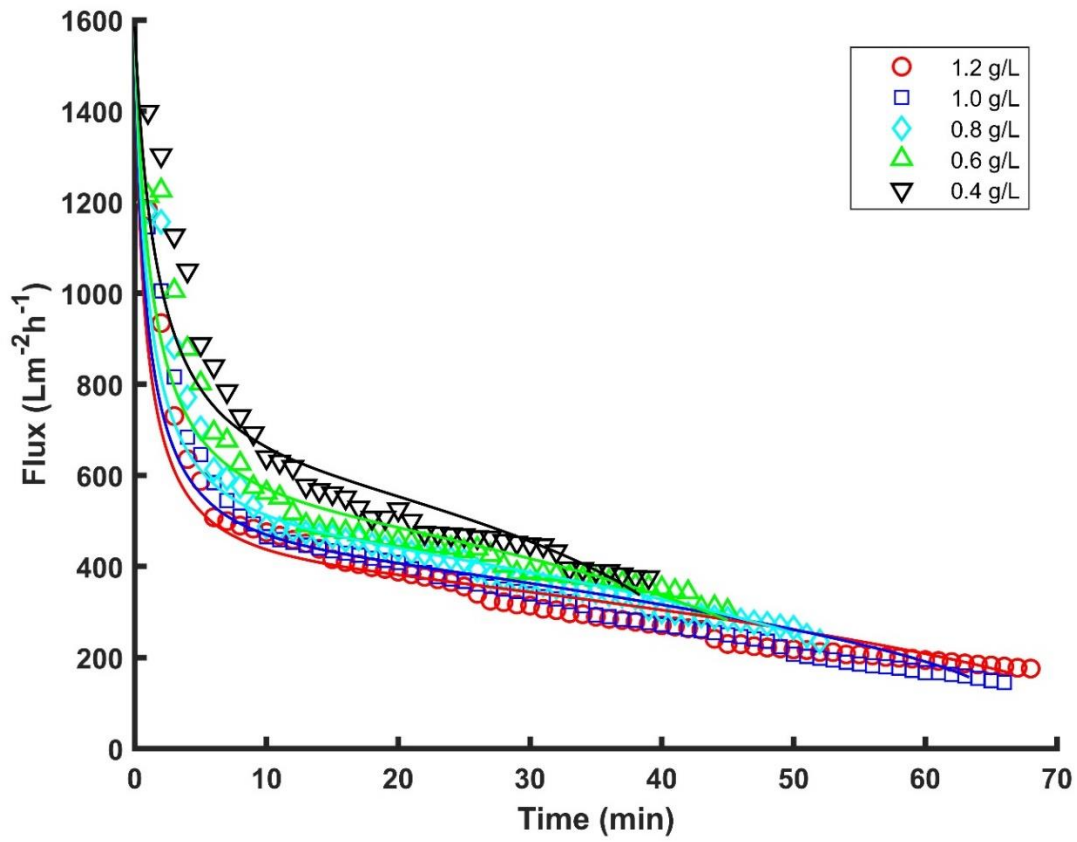
Figure 2.4 Variation of permeate flux with permeate volume for different yeast concentrations. The wall shear rate was 2000 s^{-1}. Symbols give experimental data; curves are model fits.
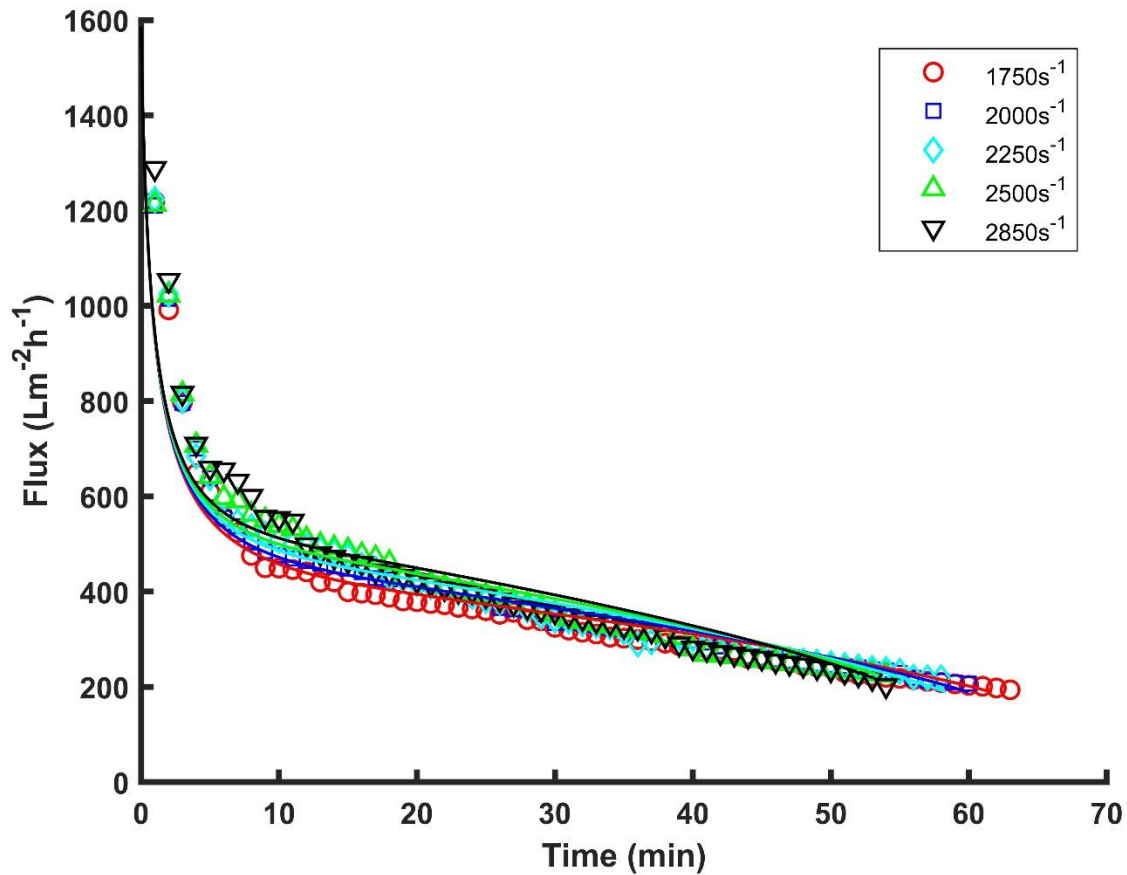
Figure 2.5 Variation of permeate flux with permeate volume for different wall shear rates. The initial yeast concentration was 1 g/L. Symbols give experimental data, curves are model fits.

Figure 2.4 and Figure 2.5indicate that the calculated values fit the experimental data very well. As the initial yeast concentration increases, the permeate flux decreases as expected. As the wall shear rate increases, there is very little change in permeate flux indicating that back migration of yeast cells is affected by interactions between yeast cells.

Equation [2.7]is used to calculate the cake mass as function of permeate volume. Figure 2.6 gives the change in calculated cake mass with permeate volume for different yeast concentrations for concentration mode, constant pressure TFF. The wall shear rate was 2000 s^{-1}.

As expected, for a given permeate volume the cake mass increases with increasing initial yeast concentration. Three zones of operation are easily identified. Initially the cake mass increases due to deposition within the membrane structure. A period of slower increase in cake mass is observed as the external cake layer forms. As permeate is removed, the yeast concentration of the yeast in the feed increases. Eventually the increasing concentration of yeast in the feed leads to a rapid increase in cake mass. The experiments were stopped after 1900 mL of permeate were removed as the residual 100 mL feed volume was insufficient to fill the external tubing.
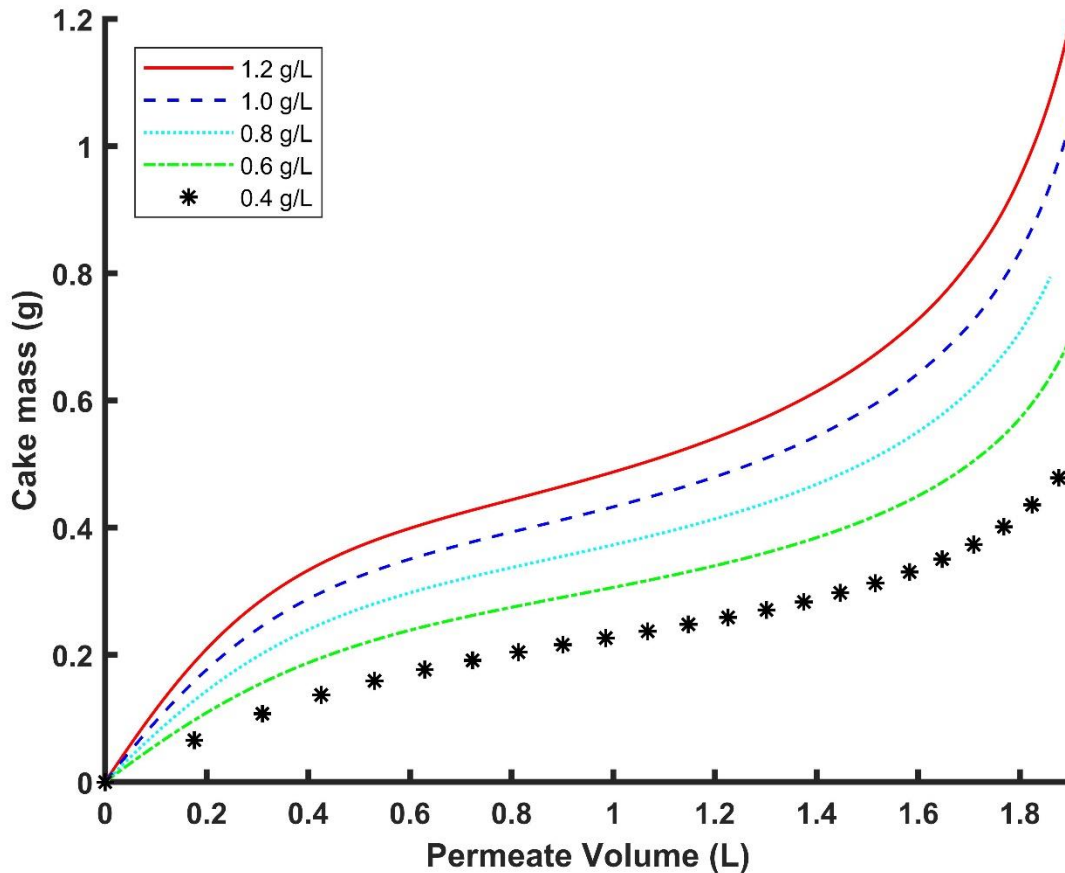
Figure 2.6 Variation of deposited cake mass with permeate volume for various initial yeast concentrations. The wall shear rate was 2000 s^{-1}.

Porosity, ε, is the void fraction divided by the total volume of the membrane. UF and MF membrane porosity typically ranges from 0.3 to 0.7[29]. The porosity of BioOptimal^{TM} MF-SL is expected to be slightly larger than conventional micorfiltration membranes due to the presence of an integrated depth filter.

The porosity of the membrane used in the BioOptimal MF-SL filter was estimated by weight difference between the membrane pores filled with water and air. A short piece of hollow fiber, around 9 cm was incubated in DI water for 5 hours. Next the outside surface was carefully padded dry, making sure no water was adsorbed from the filled membrane pores. Using a glass pipette, water in the fiber lumen was blown out. Then the fiber was weighted. This is the wet mass in Table 2.2.

The hollow fiber was placed in an oven at 60 °C and dried overnight. The fiber was then reweighed. This is the dry weight in Table 2.2. The void fraction of the membrane can be determined from the difference in the wet and dry weight of the hollow fiber assuming the density of the water is 1 kg m^{-3}. The total volume of the hollow fiber membrane is the difference in volume calculated when using the outer and inner diameter. The porosity is the void volume divided by this total volume as given in Table 2.2. The measurement is performed in triplicate. The results for porosity measurement are shown in Table 2.2

Table 2.2 Determination of porosity of BioOptimal[TM] MF-SL

Wet mass, mg	Dry mass, mg	Length, cm	Void fraction, mm^3	Total volume, mm^3	Porosity,%
241.5	48.8	9.3	192.7	243.1	79.2
239.5	48.2	9	191.3	235.2	81.3
218.2	43.7	8.2	174.5	214.3	81.4

Therefore porosity of BioOptimal[TM] MF-SL is 80%, the total void volume for BioOptimal[TM] MF-SL 0.005 m^2 module is calculated to be 27,604 mm^3

The diameter of the yeast cell is 3 um. Therefore, the void fraction accommodates around 3.9E9 yeast cells. The single mass of the yeast cell (dry mass) is 47.65 ± 1.05 pg[30]. The wet mass of a single yeast cell is in the range of 50-200 pg, depending on the cell cycle phases and budding[31]. Here we took 100 pg as a single mass. Therefore the total mass of yeast in the pore is 391 mg

From Figure 2.6 we can see the transition of the curve is around 0.4 g, when the yeast just fills up the open pores. The experimental result is in reasonable agreement with the approximate calculated mass of yeast in the membrane pores. The next stage of the fouling will take place on the surface, with the restriction of tangential flow. Therefore the fouling in the second stage is flatter. At the end of the filtration, the concentration of the yeast dominates, which enhances the convection of the yeast cell to the membrane; therefore, the mass of the cake increases rapidly in the last stage.

Figure 2.7 gives the variation of deposited cake mass with permeate volume for a range

of wall shear rates and an initial yeast concentration of 1 g/L. The curves are similar toFigure

2.6. However increasing wall shear rate has a much smaller effect than the initial yeast

concentration on the increase in cake mass. Table 2.3 gives the dependence of the long term flux

on shear rate and particle concentration for four different back migration mechanisms. The

permeate flux is expressed as

$$\frac{Q_p}{A} = \eta \gamma^x \phi^y \qquad\qquad [2.13]$$

where η is a constant and the values of x and y are given in Table 2.3. As can be seen standard

back migration models indicate a much stronger effect of wall shear rate on permeate flux

compared to feed concentration. This is opposite to what we observe here indicating the

importance of interactions between yeast particles.
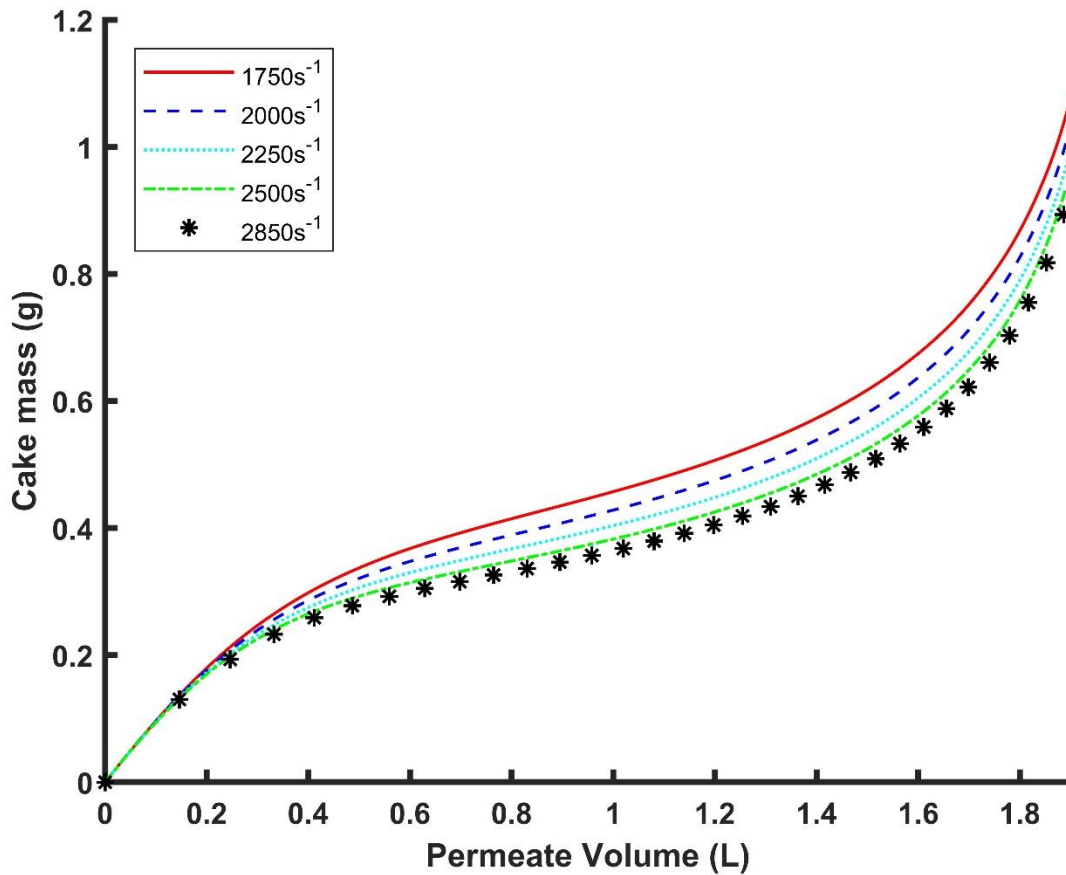
Figure 2.7 Variation of deposited cake mass with permeate volume for various shear rates concentrations. The initial yeast concentration was 1 g/L.

Table 2.3 Predicted dependence of permeate flux on wall shear rate and particle concentration for various back transport mechanisms.

	Brownian diffusion	Shear-enhanced diffusion	Inertial lift	Surface transport
Shear rate	x = 0.33	x = 0.33	x = 0.33	x = 0.33
Particle concentration	y = -0.33	y = -0.33	y = 0	y = 0

The empirical model developed here is the first attempt to describe the permeate flux when using reverse asymmetric microfiltration membranes. It should be noted that we only considered two resistances in series, the membrane and cake resistance. Combining the

68

resistance of the stabilized cake layer and the external cake layer into a single resistance term is a simplification. Further we have not accounted for adsorption onto the membrane surface as this is significantly reduced as foulant species will now adsorb onto the stabilized cake layer. We made these simplifications in order to develop a practical model.

The model can be used during TFF in concentration mode under constant pressure conditions to describe the change in permeate flux with permeate volume. In addition, calculation of the mass of deposited cake can provide guidance on the product volume that can be processed prior to membrane regeneration. In Figure 2.6 and Figure 2.7, membrane regeneration should be commenced prior to the rapid rise in cake mass observed towards the end of the filtration

Here we have investigated the filtration of yeast cells. However harvesting yeast cell cultures are not representative of typical cell cultures used in the biopharmaceutical industry. Nevertheless, by using a cell culture that leads to a relatively incompressible cake we have been able to analyze the behavior of the reverse asymmetric membranes used here. Our future studies will focus on harvesting mammalian cell cultures.

The focus here has been constant pressure tangential flow filtration as shown schematically in Figure 2.1(d). As can be seen a pressure reducing valve was placed on the retentate side to ensure a constant TMP. In industrial practice most cell clarifications are typically run in constant flux mode. This is essential for conventional non-reverse asymmetric membranes in order to maximize both permeate flux and product protein passage. However, due to its unique reverse asymmetric membrane geometry the BioOptimal^{TM} Microfilter performance is superior when the pressure is kept as low as possible.

Figure 2.4 and Figure 2.5 indicate that even at a TMP of 6894 Pa, the initial permeate flux is well above the observed threshold flux of around 720 $Lm^{-2}h^{-1}$. However, there is a rapid flux decline to values below the threshold flux. Nevertheless, the calculated fluxes fit the experimental data very well. On the other hand, Figure 2.3 indicates that under constant flux conditions, if one imposes a constant flux of ($840\ Lm^{-2}h^{-1}$) which is only about 16% higher than the threshold flux (Figure 2.3), a constant increase in TMP is observed and the model fails. These results suggest that the initial rapid decrease in flux is due to the formation of the stabilized cake layer. Once formed the flux decreases to values below the threshold flux. However, imposing a flux that is higher than the threshold flux will lead to a continual increase in the TMP due to continual growth of the external cake. The success of the model arises from the fact that it accounts for deposition of yeast cells as well as removal of yeast cells due to cross flow of the feed once the stabilized cake layer has formed. Form a practical perspective the results indicate that operating the BioOptimal^{TM} microfilter under constant flux conditions will not be beneficial.

A higher TMP will lead to compaction of the internal cake which is undesirable. Consequently, only the feed flow rate is controlled. This leads to simplification of the external circuit used to run the BioOptimal^{TM} Microfilter. Here we control the TMP via a pressure reducing valve in order to model the observed flux behavior. It should also be noted that superior performance will be observed when the feed stream contacts the more open pore structure of the membrane rather than the barrier layer, if the more open pore structure is able to prevent the smaller particulate matter present from reaching and fouling the barrier layer. Thus, performance will depend on feed properties.

2.5 Conclusion

The performance BioOptimal^{TM} Microfilter which contains a reverse asymmetric membrane has been investigated using feed streams consisting of yeast cells. Since the more open surface of the membrane faces the feed stream the membrane stabilizes an internal cake layer that is highly porous. This internal cake layer acts as a depth filter removing foulants that could foul the much tighter barrier layer. The performance of the BioOptimal^{TM} Microfilter was investigated using yeast feed stream.

A resistance in series model was developed to describe the variation of permeate flux with permeate volume. Three model parameters are easily estimated from normal flow filtration experiments at constant pressure and TFF in total recycle mode at constant flux. The model can be used to help estimate the flux and capacity of the filter before regeneration of the membrane is necessary.

2.6 Acknowledgements

References

1.   Turner, R., et al., *Manufacturing of Proteins and Antibodies: Chapter Downstream Processing Technologies*, in *New Bioprocessing Strategies: Development and Manufacturing of Recombinant Antibodies and Proteins*. 2017, Springer. p. 95-114.

2.   Van Reis, R. and A. Zydney, *Membrane separations in biotechnology.* Current Opinion in Biotechnology, 2001. **12**(2): p. 208-211.

3.   Belfort, G., R.H. Davis, and A.L. Zydney, *The behavior of suspensions and macromolecular solutions in crossflow microfiltration.* Journal of membrane science, 1994. **96**(1-2): p. 1-58.

4.   Wang, A., R. Lewus, and A.S. Rathore, *Comparison of different options for harvest of a therapeutic protein product from high cell density yeast fermentation broth.* Biotechnology and bioengineering, 2006. **94**(1): p. 91-104.

5.   Naja, G., B. Volesky, and A. Schnell, *Comparative testing of tangential microfiltration for microbial cultures.* Biotechnology and bioengineering, 2006. **95**(4): p. 584-598.

6.   Wang, S.B., et al., *Larger Pore Size Hollow Fiber Membranes as a Solution to the Product Retention Issue in Filtration-Based Perfusion Bioreactors.* Biotechnology Journal, 2019. **14**(2): p. 1800137.

7.   Stressmann, M. and C. Moresoli, *Effect of pore size, shear rate, and harvest time during the constant permeate flux microfiltration of CHO cell culture supernatant.* Biotechnology progress, 2008. **24**(4): p. 890-897.

8.   Hooper, L.A., H.C. Hollein, and C.S. Slater, *Microfiltration of Streptomyces rimosus: cell harvesting process studies.* Separation Science and technology, 1998. **33**: p. 1747-1765.

9.   Carstensen, F., et al., *Reverse-flow diafiltration for continuous in situ product recovery.* Journal of membrane science, 2012. **421**: p. 39-50.

10.   Carstensen, F., T. Kasperidus, and M. Wessling, *Overcoming the drawbacks of microsieves with micromeshes for in situ product recovery.* Journal of membrane science, 2013. **436**: p. 16-27.

11.   Lee, S.S., et al., *Microfiltration of recombinant yeast cells using a rotating disk dynamic filtration system.* Biotechnology and bioengineering, 1995. **48**(4): p. 386-400.

12.   Parnham III, C.S. and R.H. Davis, *Protein recovery from cell debris using rotary and tangential crossflow microfiltration.* Biotechnology and bioengineering, 1995. **47**(2): p. 155-164.

13.   Luque, S., et al., *A new coiled hollow-fiber module design for enhanced microfiltration performance in biotechnology.* Biotechnology and bioengineering, 1999. **65**(3): p. 247-257.

14.   Russotti, G., et al., *Pilot-scale harvest of recombinant yeast employing microfiltration: a case study.* Journal of Biotechnology, 1995. **42**(3): p. 235-246.

15.   Karst, D.J., et al., *Characterization and comparison of ATF and TFF in stirred bioreactors for continuous mammalian cell culture processes.* Biochemical Engineering Journal, 2016. **110**: p. 17-26.

16.   Arora, N. and R.H. Davis, *Yeast cake layers as secondary membranes in dead-end microfiltration of bovine serum albumin.* Journal of membrane science, 1994. **92**(3): p. 247-256.

17.   Kuberkar, V.T. and R.H. Davis, *Modeling of fouling reduction by secondary membranes.* Journal of Membrane Science, 2000. **168**(1-2): p. 243-258.

18.   Güell, C., P. Czekaj, and R. Davis, *Microfiltration of protein mixtures and the effects of yeast on membrane fouling.* Journal of Membrane Science, 1999. **155**(1): p. 113-122.

19.   Guerra, A., et al., *Low cross-flow velocity microfiltration of skim milk for removal of bacterial spores.* International Dairy Journal, 1997. **7**(12): p. 849-861.

20.   Gan, Q., *Beer clarification by cross-flow microfiltration—effect of surface hydrodynamics and reversed membrane morphology.* Chemical Engineering and Processing: Process Intensification, 2001. **40**(5): p. 413-419.

21.   Wickramasinghe, S.R., et al., *Understanding virus filtration membrane performance.* Journal of Membrane Science, 2010. **365**(1-2): p. 160-169.

22.   Carrère, H., F. Blaszkow, and H.R. de Balmann, *Modelling the clarification of lactic acid fermentation broths by cross-flow microfiltration.* Journal of Membrane Science, 2001. **186**(2): p. 219-230.

23.   Juang, R.-S., H.-L. Chen, and Y.-S. Chen, *Resistance-in-series analysis in cross-flow ultrafiltration of fermentation broths of Bacillus subtilis culture.* Journal of Membrane Science, 2008. **323**(1): p. 193-200.

24.   Fan, R., et al., *Lactic acid production in a membrane bioreactor system with thermophilic Bacillus coagulans: Fouling analysis of the used ceramic membranes.* Separation Science and Technology, 2015. **50**(14): p. 2177-2189.

25.   Shimizu, Y., K.-I. Shimodera, and A. Watanabe, *Cross-flow microfiltration of bacterial cells.* Journal of fermentation and bioengineering, 1993. **76**(6): p. 493-500.

26.   Tanaka, T., et al., *Filtration behaviors of rod-shaped bacterial broths in unsteady-state phase of cross-flow filtration.* Journal of chemical engineering of Japan, 1996. **29**(6): p. 973-981.

27.   Field, R.W., et al., *Critical flux concept for microfiltration fouling.* Journal of membrane science, 1995. **100**(3): p. 259-272.

28.   Field, R.W. and G.K. Pearce, *Critical, sustainable and threshold fluxes for membrane filtration with water industry applications.* Advances in colloid and interface science, 2011. **164**(1-2): p. 38-44.

29.   Baker, R.W., *Membrane technology and applications.* 2012: John Wiley & Sons.

30.   Łabędź, B., A. Wańczyk, and Z. Rajfur, *Precise mass determination of single cell with cantilever-based microbiosensor system.* PloS one, 2017. **12**(11): p. e0188388.

31.   Cuny, A.P., et al., *High-resolution mass measurements of single budding yeast reveal linear growth segments.* Nature communications, 2022. **13**(1): p. 1-11.

Chapter 3.   Modeling flux in tangential flow filtration using a reverse asymmetric membrane for CHO cell clarification

Summary

Tangential flow filtration is advantageous for bioreactor clarification as the permeate stream could be introduced directly to the subsequent product capture step. However, membrane fouling coupled with high product rejection has limited its use. Here the performance of a reverse asymmetric hollow fiber membrane where the more open pore structure faces the feed stream, and the barrier layer faces the permeate stream has been investigated. The open surface contains pores up to 40 µm in diameter while the tighter barrier layer has an average pore size of 0.4 µm. Filtration of Chinese hamster ovary cell feed streams has been investigated under condition that could be expected in fed batch operations. The performance of the reverse asymmetric membrane is compared to that of symmetric hollow fiber membranes with nominal pore sizes of 0.2 and 0.65 µm. Laser scanning confocal microscopy was used to observe the location of particle entrapment. The throughput of the reverse asymmetric membrane is significantly greater than the symmetric membranes. The membrane stabilizes an internal high permeability cake that acts like a depth filter. This stabilized cake can remove particulate matter that would foul the barrier layer if it faced the feed stream. An empirical model has been developed to describe the variation of flux and transmembrane pressure drop during filtration using reverse asymmetric membranes. Our results suggest that using a reverse asymmetric membrane could avoid severe flux decline associated with fouling of the barrier layer during bioreactor clarification.

3.1   Introduction

Chinese Hamster Ovary (CHO) cells are frequently used to produce glycosylated protein based therapeutics. Bioreactor clarification is the first of the downstream purification operations

used to remove cells and cell debris from the supernatant which contains the product of interest. Commonly centrifugation and filtration are used, sometimes in combination [1]. Tangential flow filtration (TFF), typically using 0.2 μm pore size membranes, is one of the filtration methods that is used for bioreactor clarification. Unlike centrifugation, TFF produces a permeate that is free of particulate matter and can be introduced directly to the next capture step [2]. However larger pore size membranes are frequently used to improve throughput and product yield requiring the use of an additional clarification step [2, 3].

Major drawbacks of TFF include membrane fouling and product rejection leading to unacceptably low product recoveries [4]. Today TFF is run at constant permeate flux in order to prevent operating at fluxes above the critical flux especially at the start of the filtration [5, 6]. By controlling the permeate flux rather than the transmembrane pressure, both product yield and average flux are increased [7]. However, as cell densities in the cell culture operations have increased, the increase in cell debris often causes unacceptable levels of membrane fouling, reducing the economic viability of TFF.

Though the majority of recombinant protein manufacturing facilities use fed-batch cultures, there is growing interest in developing continuous manufacturing processes [8]. This interest is driven by the demand for cheaper and higher volume production methods. Continuous cell cultivation will require the development of continuous clarification operations if a continuous process is to be developed [9]. The use of an external TFF unit is ideal since by using an appropriate membrane pore size, a cell free permeate may be recovered that can be directly introduced to the subsequent capture step. Nevertheless, membrane fouling remains a major concern that limits the productivity of the TFF module. Changing out a TFF module during a batch clarification operation is not practical. More recently alternating tangential flow has been

developed where the feed is periodically cycled through a hollow fiber module. The periodic change in feed flow direction and resulting pressure gradient has been shown to reduce fouling [10]. In addition, the use of single pass TFF has been proposed as an inline concentration step during bioreactor clarification [11].

Here we have developed a model to describe the permeate flux during fed batch operations using asymmetric hollow fibers where the inside fiber lumen surface has a large pore size while the outer fiber surface has a pore size of 0.4 μm. The feed flows inside the fiber lumen. Consequently, cells and cell debris will be trapped in the open pore structure on the inner lumen surface. The benefits of stabilizing a permeable cake layer that can act as a filter aid removing foulants which could adsorb onto the membrane have been highlighted by earlier studies [12]. Kuberkar and Davis [13] and Güell et al. [14] indicate that the formation of a thin secondary membrane can be beneficial and leads to higher stable permeate fluxes and product transmission compared to the absence of a secondary membrane. However, the secondary membrane must be highly permeable.

Guerra et al. [15] suggested a method of ensuring that a permeable secondary membrane can be stabilized on the membrane. They used reverse asymmetric membranes where the larger pore surface of the membrane faced the feed stream and the tighter barrier layer faced away from the feed stream. This resulted in the accumulation of particulate matter within the membrane structure facing the feed. The more open surface of the membrane ensures that the deposited species have an open structure which minimizes the increase in resistance to permeate flow. Gan [16] showed a similar effect for beer clarification. In fact, today commercially available virus filtration membranes are reverse asymmetric membranes [17]. The more open support structure

acts as an inline prefilter removing any product dimers, trimers, etc. that could foul the membrane.

The BioOptimal™ MF-SL microfilter (Asahi Kasei, Glenview, IL, USA), is a commercially available hollow fiber module that contains a reverse asymmetric membrane. The inside surface has pores up to 40 μm in diameter while the outside surface has 0.4 μm pores. Since the feed is pumped inside the fibers, it is the more open membrane surface that contacts the feed. Though many investigators have attempted to model the flux performance of TFF [18, 19] there has been no attempt to model the flux performance of TFF when using reverse asymmetric membranes.

The model we have developed to describe the performance of the BioOptimal™ MF-SL microfilter may be used to predict the permeate flux during bioreactor clarification for fed batch operations. The model parameters were determined by conducting normal flow filtration at constant pressure. Experiments were conducted using a CHO cell feed stream. In addition, the performance of two symmetric membranes with nominal pore sizes of 0.2 and 0.65 μm was evaluated and compared to the reverse asymmetric membrane. Confocal laser scanning microscopy was used to identify the location of cell entrapment within and on the membrane.

3.2   Materials and methods

3.2.1   Materials

All reagents were biotechnology grade or higher unless specified. FreeStyle™ CHO-S cells were obtained from ThermoFisher (Waltham, MA, USA). Phosphate buffered saline was purchased from MilliporeSigma (Billerica, MA, USA). CHOgro® Expression Media, and poloxamer 188 solution, 10% w/v in cell culture grade water were purchased from Mirus Bio

(Madison, WI, USA). Paraformaldehyde, 97% was obtained from Alfa Aesar (Haverhill, MA, USA). 4',6'-Diamidino-2-phenylindole dihydrochloride (DAPI) was purchased from Anaspec Inc (Fremont, CA, USA). A MemBrite^{TM} fix cell surface staining kit was purchased from Biotium (Fremont, CA, USA). Pressure sensors and a peristaltic pump were obtained from SciLog (Oxnard, CA, USA). TRITON™ X-100, sodium hydroxide, sodium hypochlorite, a digital hotplate stirrer, and a pressure gauge were purchased from VWR (Radnor, PA, USA). An electronic scale (PL602-S) was purchased from Mettler Toledo (Columbus, OH, USA). All the rubber tubing used to deliver fluid was purchased from Masterflex (Vernon Hills, IL, USA). All water used in this work was obtained from a ThermoFisher 18MΩ Barnstead Smart2pure system (Schwerte, Germany). BioOptimal™ MF-SL filters with membrane surface area of 0.00041 m^2, pore size of 0.4 µm on the permeate side and 40 µm on the feed side; UJP microfilter with membrane surface area of 0.00032 m^2, nominal pore size of 0.65 µm and UMP microfilter with membrane surface area of 0.00041 m^2, nominal pore size of 0.2 µm were provided by Asahi Kasei Bioproces (Glenview, IL, USA). All the filters contained 1 hollow fiber. Table 3.1 summarizes some of the properties of the three membranes investigated here.

Table 3.1 Properties of the three membranes investigated in this study

	BioOptimal™ MFSL	UMP	UJP
Material	Polysulfone hollow fiber	Polyvinyldenedifluoride (PVDF) hollow fiber	Polyvinyldenedifluoride (PVFD) hollow fiber
Pore size (μm)	Asymmetric, Inner surface: 40 outer surface: 0.4	Symmetric, 0.2 inner and outer surface	Symmetric, 0.65 inner and outer surface
Dense layer location	Outer surface	Inner and outer surface	Inner and outer surface
Surface area (cm^2)	4.1	4.1	3.2
Hollow fiber ID (mm)	1.4	1.4	1.1
Permeability (L m^{-2}h^{-1} kPa^{-1})	323	17	84

3.2.2 Cell culture

FreeStyle™ CHO-S Cells were cultured using a shaking incubator. Culture conditions were: temperature of 37 °C and a CO$_2$ concentration of 8%. The cell culture medium consisted of CHOgro® Expression Media, supplemented at a final concentration of 8 mM L-glutamine, 0.3% poloxamer 188, and 0.5× penicillin-streptomycin. Initially, a 30 mL inoculum of CHO cells was grown in a 200 mL shaker flask. Once the cell density was higher than 8 million cells/mL and

cell culture was scaled up to 200 mL in a 1L shaker flask by seeding a portion of culture to the fresh growth medium at a cell density of 1.5 million cells/mL.

3.2.3   Normal flow filtration for determining cake parameter

Normal flow filtration was conducted using the BioOptimal™ MF-SL microfilter in order to determine the model cake parameters. In this mode of operation, the retentate port was closed. The feed suspension was loaded into a pressurized filtration cell and stirred using a magnetic stirrer. A nitrogen source was connected to the filtration cell, and the feed pressure was maintained by adjusting the regulator on the nitrogen cylinder. Permeate was collected on an electronic scale. The flux was calculated based on the change in permeate weight over a specified time. The CHO cell density of the feed was 0.5, 1.0 and 2.0 million cells/mL and the feed volume was 50 mL, giving a throughput of 120 L m^{-2}. The TMP ranged from 4.1 to 11 kPa (0.6-1.6 psi). The experimental set-up is shown in Figure 3.1(a).
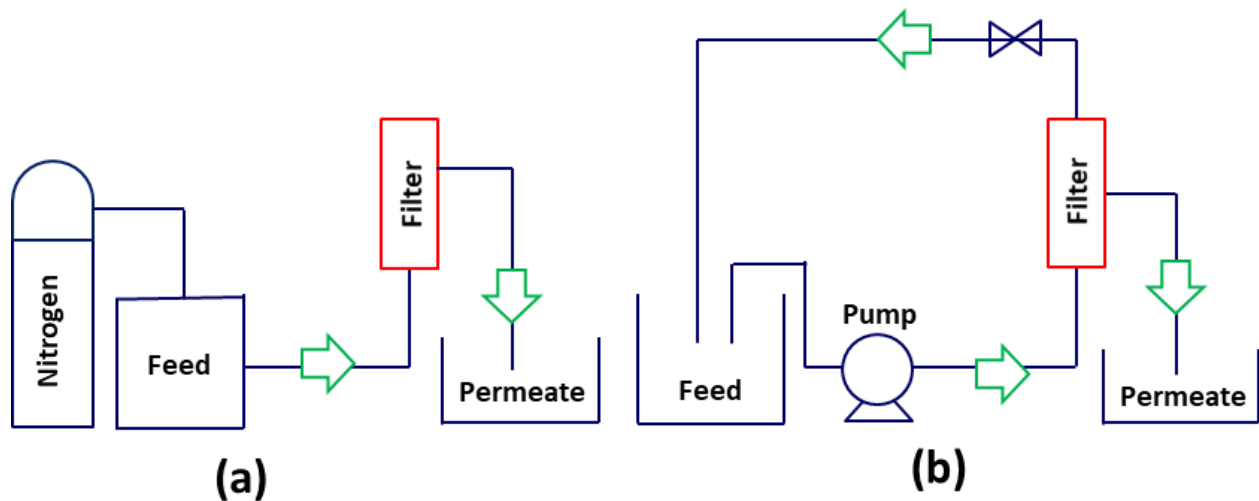
Figure 3.1 Experimental set up (a) normal flow filtration at constant pressure, (b) TFF, concentration mode with initial TMP set at a specified value

3.2.4 TFF for determining resistance parameter

A peristaltic pump was used to pump the feed. Three pressure sensors were mounted on the feed (P_F), retentate (P_R), and permeate (P_P) lines of the filter, respectively. The transmembrane pressure (TMP) is defined as:

$$\text{TMP} = \frac{P_F + P_R}{2} - P_P \qquad [3.1]$$

Assuming laminar tube flow, the wall shear rate within the fiber is given by

$$\Upsilon = \frac{4Q_F}{\pi r^3} \qquad [3.2]$$

where Υ is shear rate (s^{-1}), Q_F is volumetric flow rate (m^3 s^{-1}) and r is radius of the fiber lumen (m).

The feed volume was 50 mL and the cell density of 9 million cells/mL. A wall shear rate of 2,000 s^{-1} was used as recommended by the manufacturer. The permeate was collected on a balance. The retentate was returned to the feed tank. Experiments were conducted using the BioOptimal™ MF-SL microfilter, UMP, and UJP microfilters. Before each experiment, the DI water flux was determined at a TMP of 3.4 kPa (0.5 psi) for the BioOptimal™ MF-SL microfilter and was found to be 1100 Lm^{-2}h^{-1}. In order to compare the performance of the BioOptimal™ MF-SL microfilter with the UJP and UMP microfilters, the TMP for the same DI water flux as the BioOptimal™ MF-SL microfilter was determined. The initial TMPs were 13 kPa (2 psi) and 62 kPa (9 psi) for UJP and UMP microfilters, respectively.

3.2.5 Confocal imaging

DAPI was used to label DNA. It displays a blue, fluorescent signal. MemBrite™ was used to label cell membrane proteins. It displays an orange, fluorescent signal. A stock 5 mg mL^{-1} DAPI solution was prepared in DI water. Based on screening experiments, a concentration of 2

µg mL^{-1} was used for all staining experiments. The MemBrite™ staining solution was prepared according to the manufacturer's instructions.

After filtration, the module was opened, and the fouled hollow fiber was soaked in PBS to remove unbound cells and cell debris. Next, the fiber was incubated with 4 % paraformaldehyde for 20 min, then washed again with PBS buffer. The fiber was then incubated with 0.5 % Triton-X 100 for 10 min and washed again with PBS buffer. The fiber was quickly dipped into liquid nitrogen and sectioned into small pieces. The fiber samples were first incubated with DAPI for 30 min in the dark and washed twice with PBS to remove excess dye. Next, MemBrite™ labeling was carried out. The fiber samples were incubated in a pre-staining solution (provided by MemBrite™ dye kit) for 5 min at 37 °C followed by incubation in the staining solution (provided by MemBrite™ dye kit) for 5 min at 37 °C. After incubation, the fiber sections were washed twice with PBS buffer to remove excess dye. The fibers were mounted on slides and then imaged with a Leica TCS SP5 Confocal Laser Scanning Microscope (Buffalo Grove, IL, USA). The excitation/emission wavelength for DAPI is 405/461, and MemBrite™ is 594/615 nm.

3.3   Modeling

In industrial practice, cell clarifications are typically run in constant flux mode. However, due to its unique reverse asymmetric membrane geometry, the BioOptimal™ MF-SL microfilter performance is superior when the pressure is kept as low as possible in order to minimize cake compression. A higher TMP will lead to compaction of the internal cake which is undesirable. Consequently, only the feed flow rate is controlled. In this work, we set the initial TMP by placing a valve on the retentate line (see Figure 3.1). The feed entering the hollow fiber has two

flow paths. It can go through the fiber lumen and exit via the retentate outlet or go through the

membrane and exit via the permeate outlet. The pressure drop for flow through both paths must

be the same which will determine the retentate and permeate flow rates. Figure 3.2 is a schematic

diagram of the resistance to flow through the two different paths. The resistance to retentate flow

may be modeled by the valve on the retentate line. The resistance to permeate flow is modeled

by the membrane and cake resistances.
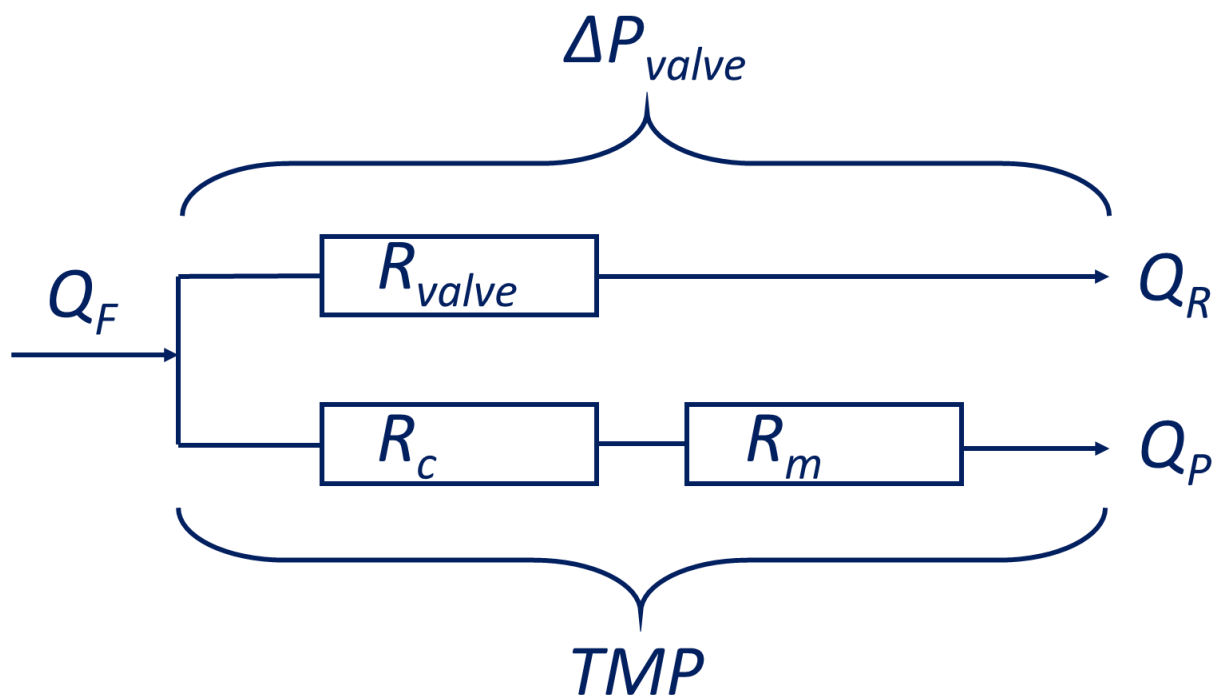
Figure 3.2. Schematic diagram of the flow path in BioOptimal™ MF-SL microfilter.
Since CHO cell feed streams are highly compressible, a correlation between the

resistance of deposited CHO cells and the TMP is needed. This may be obtained from normal

flow filtration data using a combined pore blockage and cake filtration model developed by Ho

and Zydney [20]. The model assumes initial pore blockage followed by the formation of a

surface cake layer. The model is based on the classical fouling models [21, 22]. The permeate

flux and cake resistance are given by the following equations where the symbols are defined in the nomenclature.

$$J = J_0 \left[e^{-\frac{\alpha \Delta pc}{\mu R_m} t} + \int_0^t \frac{\alpha \Delta pc}{\mu (R_m + R_C)} \times e^{-\frac{\alpha \Delta pc}{\mu R_m} t_c} dt_c \right]$$
[3.3]

$$R_c = (R_m + R_{c0}) \sqrt{1 + \frac{2 f' \alpha' \Delta pc}{\mu (R_m + R_{c0})^2} (t - t_c)} - R_m$$
[3.4]

In the above equations, it is assumed that all cells and cell debris are completely rejected by the tighter barrier layer, thus f' is 1.0. Three parameters need to be determined: pore blockage parameter α, the resistance of single cell, R_{c0} and specific cake layer resistance, α'. The specific cake layer resistance is assumed to depend on the TMP as follows [23].

$$\alpha' = \alpha_0 \times \Delta p^n$$
[3.5]

where n is the compressibility index and α_0 is the resistance coefficient of the cake. If n is 0, the cake is incompressible. R_m is determined from the DI water flux and was found to be 1.3×10^{10} (m^{-1}) for the BioOptimal™ MF-SL microfilter. The value of R_m for the UMP and UJP microfilters was 2.2×10^{11} and 5×10^{10} (m^{-1}) respectively. As can be seen the BioOptimal™ MF-SL microfilter has the highest permeability (lowest membrane resistance) of the three filters. The UJP microfilter which has a larger nominal pore size (0.65 µm) than the UMP microfilter (0.2 µm), has a higher permeability as expected. By substituting equation [3.] and [3.5] into [3.5], the values of α, α_0, R_{C0} and n can be obtained by fitting the experimental flux data from normal flow filtration. Since α_0 and n are foulant properties they should be independent of the mode of operation. The values obtained here will be used in TFF.

Juang et al. [24] have used a resistance in series analysis to model the permeate flux during TFF.

$$J = \frac{TMP}{\mu (R_m + R_c + R_P)}$$
[3.6]

85

$$R_c = \frac{m}{A} * \alpha' \qquad [3.7]$$

where R_m and R_c are the membrane and cake resistance. R_c is given by Equation [3.7] where m is the mass of deposited cake and A is the membrane area. R_p is the resistance due to concentration polarization which is ignored here. The growth of the cake during TFF depends upon the convection of particulate matter towards the membrane due to the permeate flow and back migration away from the membrane. Several back-migration mechanisms have been described such as Brownian diffusion, shear enhanced diffusion, inertial lift forces and surface transport [19]. However, as the feed stream contains a mixture of intact CHO cells and cell debris, and the cake is highly compressible, a range of particle sizes exists. The different back migration mechanisms will contribute to different degrees to the overall back migration of a given particle size. Further, the presence of a stabilized internal cake within the membrane will lead to some CHO cells interacting with both the membrane and CHO cells that from part of the stabilized internal cake layer. All of these effects make it difficult for practical application of the theoretical models to predict the permeate flux.

Instead, we assume the growth of the cake is given by the product of the permeate flow rate multiplied by the concentration of CHO cells in the feed. Suppression of cake formation is assumed to depend on the mass of cake already deposited, m, as well as the feed flow rate, Q_F, and a cake attrition factor, K, as given by the second term on the right-hand side of Equation [3.8]

$$\frac{dm}{dt} = cQ_P - KQ_F m \qquad [3.8]$$

The concentration of CHO cells in the feed increases with time and is given by [3.9]

$$c = \frac{c_0 v_0 - m}{v_0 - v} \qquad [3.9]$$

where c_0, v_0 are the initial concentration and volume of the feed, respectively.

86

In this work, the initial TMP was set via the retentate valve. The TMP was free to increase as the feed is concentrated (see Figure 3.1). The pressure drop for flow through the fiber lumen (ΔP) must equal the TMP. These two pressure drops are related to the retentate and permeate flow rates Q_R and Q_P by Darcy's law as follow.

$$\text{TMP} = \mu \times R_{valve} \times \frac{Q_R}{A_{valve}} = \mu \times (R_c + R_m) \times \frac{Q_P}{A} \qquad [3.10]$$

$$Q_F = Q_R + Q_P \qquad [3.11]$$

R_{valve} is the resistance for flow through the valve and is the only unknown parameter. Equation [3.10] implies the TMP increases with an increase of the retentate flow rate. Since R_{valve} is a property of the valve and independent of the fluid it is easily determined experimentally. The pressure drop across the valve is measured at different constrictions of the valve. The slope of the pressure drop with respect to the flow rate is $\frac{\mu R_{valve}}{A_{valve}}$ enabling calculation of the TMP via

$$TMP = TMP_0 + \frac{\mu R_{valve} Q_R}{A_{valve}} \qquad [3.12]$$

where TMP_0 is the initial TMP. The only unknown is K, the attrition factor, which may be obtained from fitting the experimental data. The permeate flux is obtained by combining and solving equations [3.5] - [3.9] and [3.12]. The values of the fitted parameters were obtained by "NonlinearModelFit" package from Mathematica (Champaign, IL, USA) Version 11.3. The fitting method was set as "Automatic".

3.4   Results and Discussion

3.4.1   Normal flow filtration for determining cake parameters

Normal flow filtration of CHO cells was utilized to determine the cake parameters and was conducted at pressure drops ranging from 4.1 kPa to 11 kPa (0.6 psi to 1.6 psi). Figure 3.3 gives the experimental data (symbols) for a cell density of 0.5 million cells/L and curves

generated from Equation[3.3]. Coefficients of determination, (r^2 values) are given in the figure legend. As can be seen the quality of the fit is very good. Values for the parameters were $\alpha =$ 31.6 ± 2.1 m^2 kg^{-1}, $R_{c0} = (2.1 \pm 0.2) \times 10^{11}$ m^{-1}, $\alpha_0 = (1.00 \pm 0.02) \times 10^9$ m kg^{-1} Pa^{-n} and $n = 0.8$ ± 0.17. For cell densities of 1.0 and 2.0 million cells/mL the same parameters can be used to fit the data. As can be seen, the cake is compressible. For example, in other studies, we determined that n is 0.26 for yeast cell filtration. Yeast cells have a cell wall which makes them far less compressible. The values of α_0 and n were used in Equation [3.5] $\alpha' = \alpha_0 \times \Delta p^n$ [3.5]
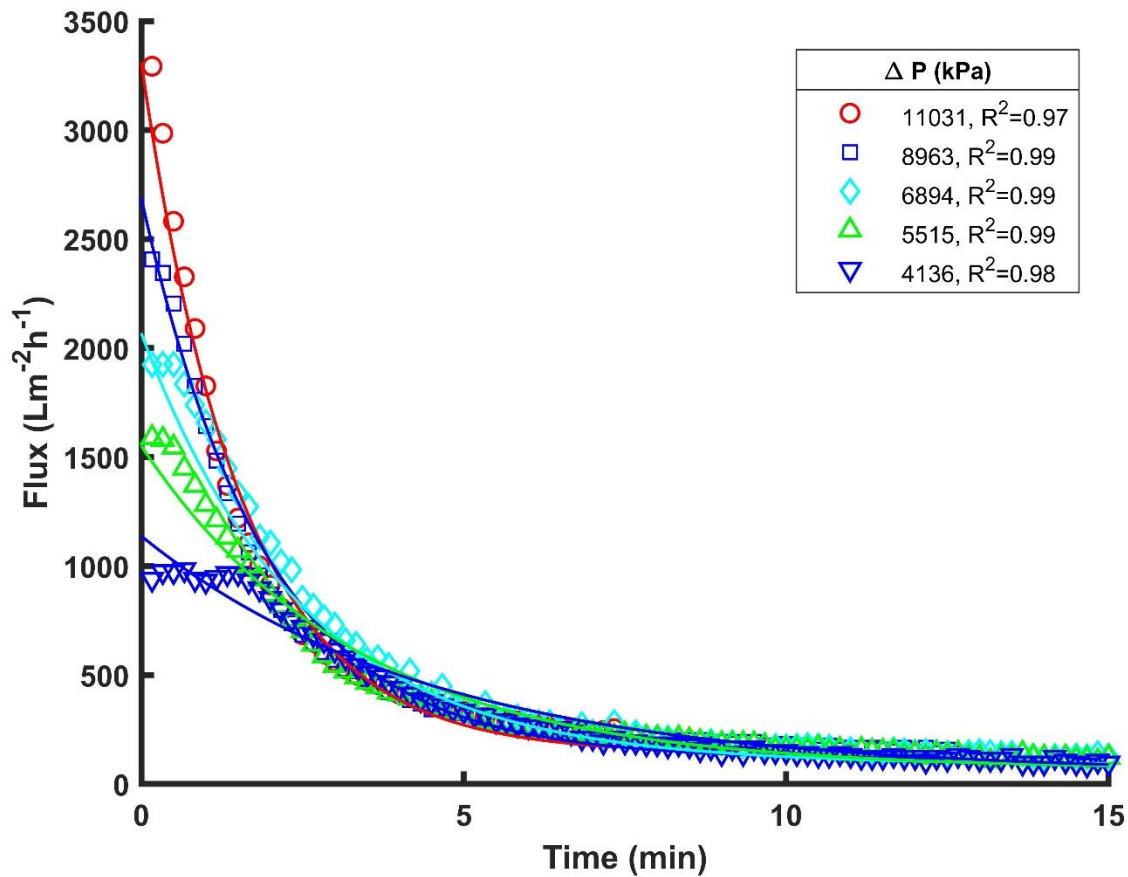
Figure 3.3. Variation of permeate flux with time for 5 different feed pressures (11, 9, 6.9, 5.5 and 4.1 kPa). The curves were obtained by fitting Equation [3.3]

3.4.2 TFF for determining resistance parameter

The average pressure drop for flow through the fiber lumen as a function of the flow rate is given in Figure 3.4 for three different initial feed pressures of 3.4 kPa (0.5 psi), 5.1 kPa (0.75 psi) and 6.9 kPa (1 psi) at 2000 s^{-1} shear rate. Average results for 3 repeat runs are given. The error bars given the range in the values obtained for three repeat runs. The slope gives $\frac{\mu \times R_{valve}}{A_{valve}}$. The TMP can then be calculated from Equation [3.12].

Based on the values of the resistance of the valve obtained from Figure 3.4 All equations are solved to obtain the permeate flux as a function of throughput as shown by the curves in Figure 3.5(a). Figure 3.5(b) gives the variation of TMP with throughput. In both cases, experimental data are shown by symbols. K, the attrition factor defined by Equation [3.8] $\frac{dm}{dt} = cQ_P - KQ_F m$ [3.8], was obtained by fitting the model to the experimental data. Figure 3.6 gives the variation of K with initial TMP. As can be seen, K increases with increasing TMP at the same wall shear rate. As the initial TMP increases, the thickness of the cake will increase due to more rapid convection of particulate matter to the membrane surface. However, a thicker cake will decrease the fiber lumen diameter thus increasing the shear stress on the cake surface. This will in turn tend to remove more particulate matter from the surface (higher value of K) and increase back diffusion suppressing further cake growth. In addition, a decrease in the fiber lumen diameter due to a thicker cake will lead to a decrease in permeate flux and therefore a lower induced drag force on particulate meter toward the membrane. Figure 3.6 may be used to obtain the value of K for a range of initial pressures enabling prediction of the variation of permeate flux and TMP with throughput for a wall shear rate of 2000 s-1.
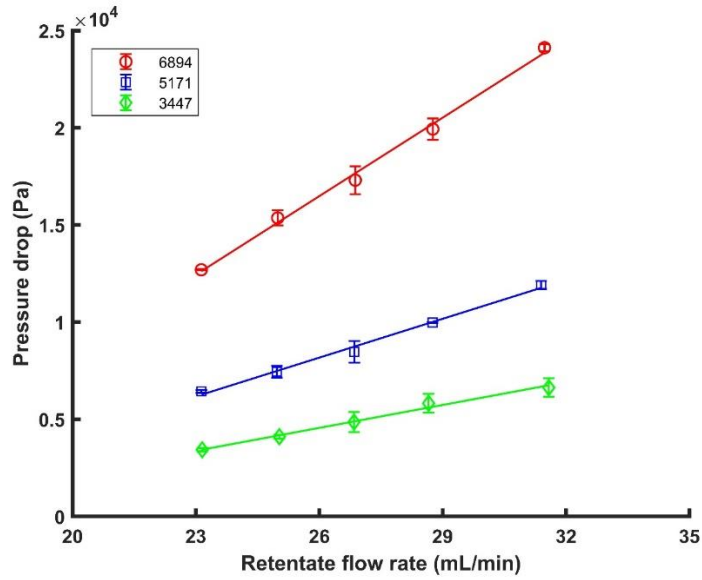
Figure 3.4 Variation of retentate flow rate with pressure drop for a range of initial feed pressure through the fiber lumen.
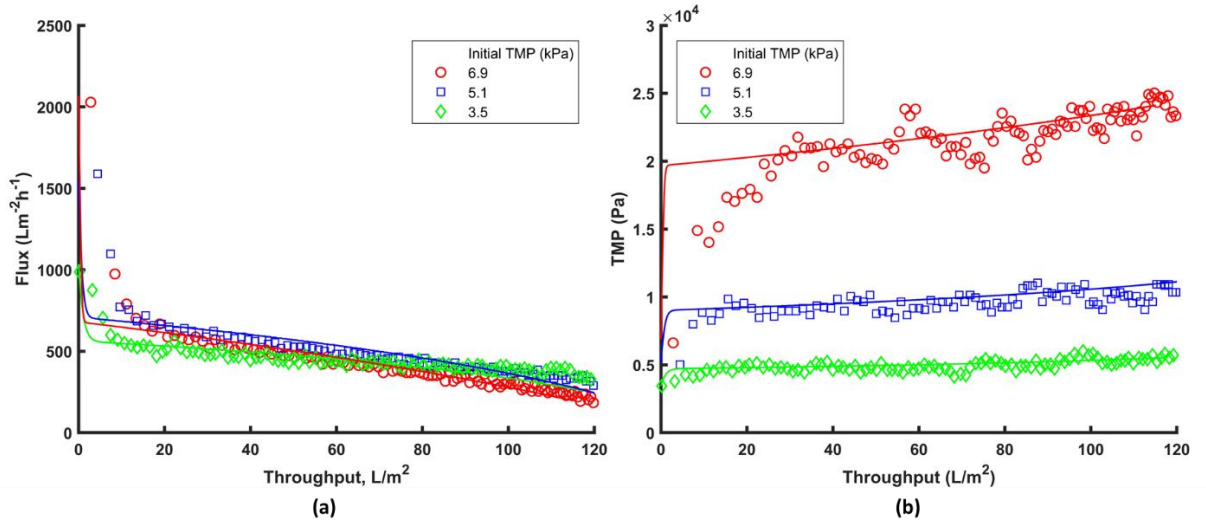
Figure 3.5 Variation of (a) flux and (b) TMP with throughput. Experimental data are given by symbols, curves show model fit. CHO cell density was 9 million/mL and the wall shear rate 2000 s^{-1}.
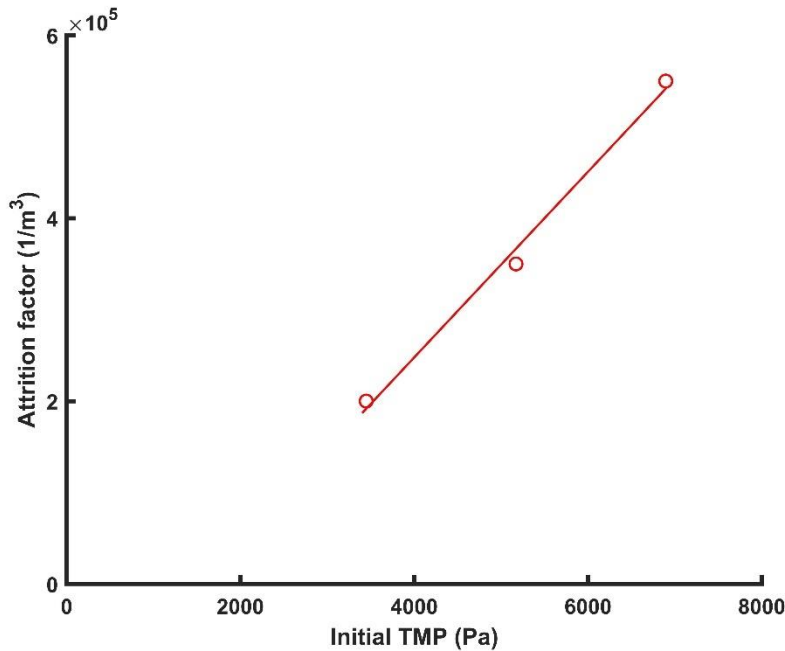
Figure 3.6 Variation of K with initial TMP

3.4.3 Comparison of TFF with and without reverse asymmetric hollow fibers

The performance of the BioOptimal™ MF-SL microfilter was compared to the UJP and UMP microfilters which contain symmetric hollow fibers. Since TFF is operated industrially under constant permeate flux conditions, our basis for comparison is the same initial flux. Figure 3.7 gives the variation of permeate flux as a function of throughput. The wall shear rate was 2,000 s^{-1}, the initial TMPs were 3.4 kPa (0.5 psi), 13 kPa (2 psi), 62 kPa (9 psi) for BioOptimal™ MF-SL, UJP, and UMP microfilters, respectively, and the initial permeate flux was 1100 Lm^{-2}h^{-1}.

The initial TMP for the UMP microfilter is higher than the larger nominal pore size UJP microfilter. However, the initial TMP for the UJP microfilter is higher than the BioOptimal™ MF-SL microfilter even though it has a large nominal barrier layer pore size than the BioOptimal™ MF-SL microfilter. These results indicate that the BioOptimal™ MF-SL

microfilter is a much higher permeability membrane. This is in agreement with the calculated

membrane resistance, R_m, for the microfilters.

As can be seen, the two symmetrical hollow fibers displayed rapid flux decline. The

throughput for the UMP microfilter which has a nominal pore size of 0.22 μm is lower followed

by the UJP microfilter which has a pore size of 0.65 μm. The BioOptimal™ MF-SL microfilter

displays a capacity and permeate flux that is significantly better than the two symmetric

membranes. The more open pore structure that faces the feed stream not only stabilizes the

rejected particulate matter but also acts as an inline secondary membrane that removes foulants

that could foul the barrier layer of the BioOptimal™ MF-SL microfilter filter.
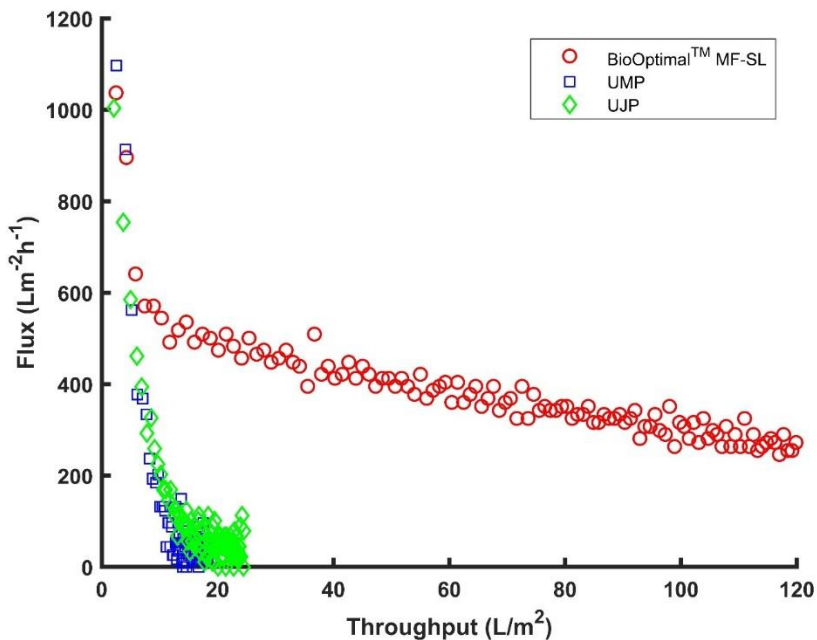
Figure 3.7 Variation of permeate flux with throughput for the BioOptimal™ MF-SL microfilter, UJP and UMP microfilters. The CHO cell density was 9 million/mL, wall shear rate 2000 s^{-1}, and initial flux 1100 Lm^{-2}h^{-1}.

The location of entrapment of particulate matter on and within the membrane was

determined by confocal laser scanning microscopy. Figure 3.8, 9 and 10 give images for the

BioOptimal™ MF-SL microfilter, UJP, and UMP microfilters, respectively. As can be seen from

Figure 3.8(a), significant DNA staining is observed to a depth of approximately 50 μm from the

inner membrane surface. However, no DNA is observed at the outer membrane barrier layer.

Figure 3.8(b) indicates significant host cell protein staining on the inner membrane surface and

to a depth of about 50 μm from the inner surface. However, some protein staining is detected

throughout the membrane structure and on the outer barrier layer. Since intact cells contain

proteins and DNA overlaying Figure 3.8 (a) and (b) indicate the location of intact cells as given

by Figure 3.8 (c). As can be seen, the more open structure of the BioOptimal™ MF-SL

microfilter that faces the feed stream helps stabilize rejected cells and cell debris. The secondary

membrane removes foulants. Figure 3.9 and 10 give analogous results for the UJP and UMP

microfilters. As can be seen, DNA and host cell proteins are trapped on the inner membrane

surface with little penetration into the membrane.
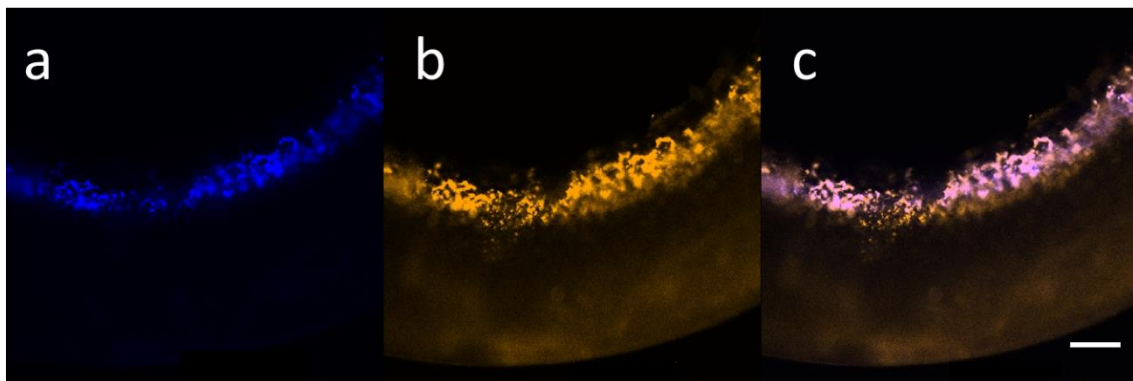
Figure 3.8 Confocal images of the BioOptimal™ MF-SL microfilter indicting the location of (a)
DNA, (b) protein and (C) overlay of DNA and protein binding. The scale bar represents 100 μm.
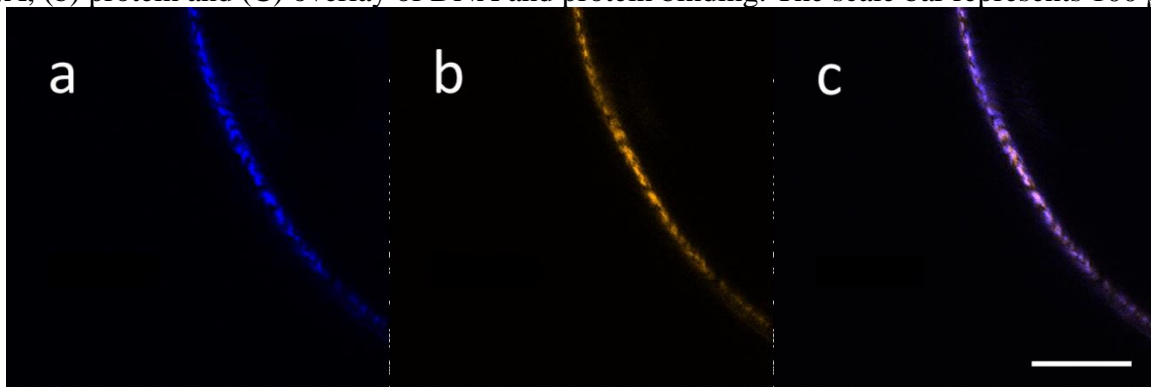
Figure 3.9 Confocal imaging of UJP microfilter indicting the location of (a) DNA, (b) protein and (C) overlay of DNA and protein binding. The scale bar represents 100 µm.
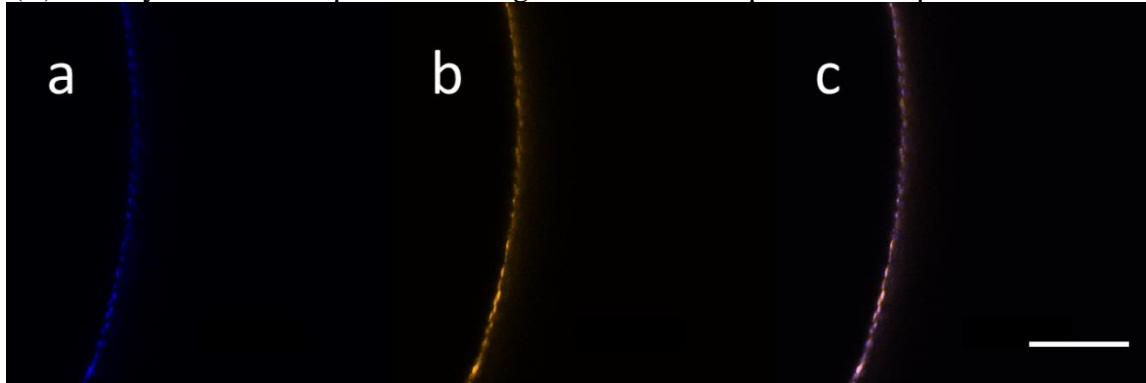
Figure 3.10 Confocal imaging of UMP microfilter indicting the location of (a) DNA, (b) protein and (C) overlay of DNA and protein binding. The scale bar represents 100 µm.

3.5   Discussion

The use of TFF for bioreactor clarification during fed batch operations requires minimizing membrane fouling in order to ensure an adequate permeate flux and throughput. If the permeate flux is too low, the clarification operation will take too long to complete from a practical perspective. Since in industrial practice, the permeate flux is normally controlled at a specific value it is essential to ensure the TMP does not reach unacceptably high values. In the case of the BioOptimal™ MF-SL microfilter, higher TMPs will lead to compaction of the internal cake which is undesirable. Consequently, only the feed flow rate is controlled. This leads to simplification of the external circuit used to run the BioOptimal™ MF-SL microfilter. As it is not practical to replace the microfilter during a batch clarification, adequate filter throughput is essential. The model we have developed here will enable estimation of both flux and throughput.

Bioreactor clarification operations must also result in adequate product recovery. The model we have developed here does not consider product recovery. In this work a CHO cell feed stream that does not produce a protein product was used. However in order to verify that little product rejection occurred, for a limited number of runs, the feed was spiked with BSA at 1, 5

and 10 g L^{-1} resulting in 99% recovery for a feed concentration of 1 and 5 g L^{-1} and 93% recover

for 10 g L^{-1}. In addition, a limited number of runs were spiked with a model IgG at 1.8, 5 and 10

g L^{-1}. The corresponding recoveries were 90.3, 95.4 and 95.5 % respectively. The results indicate

very good protein passage.

In a recent study, Pinto and Brower[25] investigated the performance of the UJP and

UMP microfilters for clarification during perfusion operations. They observed that the sieving

coefficient for the smaller nominal pore size UMP microfilter was superior to the larger nominal

pore size UJP microfilter. Scanning electron microscopy analysis of both membranes indicated

that the surface pore size of the UMP microfilter membrane was in the range 0.5 to 2.0 μm

(nominal pore size 0.2 μm) while the UJP microfilter membrane was 0.3-0.6 μm (nominal pore

size 0.65 μm). However, the membrane resistance calculated in this work was greater for the

UMP microfilter membrane compared to the UJP microfilter membrane. This result is in

agreement with the hydraulic permeability values calculated by Pinto and Brower of 3.08 x 10^{-3}

and 1.14 x 10^{-2} cm s^{-1} psi^{-1} for the UMP and UJP microfilter membranes, respectively. Pinto and

Brower indicate that this is due to the existence of a conical pore structure in the UMP

microfilter membrane. The reverse asymmetric membrane used here has a much more

pronounced conical pore structure. The results of Pinto and Brower, combined with the result

obtained here for BSA and IgG rejection, suggest that product rejection by the presence of a

stabilized internal cake layer will not be significant.

The model developed here does not explicitly included the effect of cell viability, density

of the feed stream as well as the wall shear rate (cross flow rate). Thus, it is important to

determine the model parameters over a limited range of these parameters in order to ensure

accurate estimation of the permeate flux and throughput. The model parameters determined here

were found to give an accurate estimation of permeate flux and throughput for cell densities between 8 and 12 million/mL. The cell viability was around 95%. Lower cell viabilities will lead to a greater amount of smaller particulate matter and hence a less permeable internal cake layer leading to lower permeate fluxes. For cell viabilities that vary by more than 5% from the 95% viability used here, the parameters should be determined at the lower cell viability. Increasing the wall shear rate will lead to an increase in the permeate flux. We operated the BioOptimal™ MF-SL microfilter at 2000 s^{-1} as recommended by the manufacture. The model parameters should be determined at the wall shear used in the actual runs. At wall shear rates up to 6,000 s^{-1}, where the Reynolds number is 1456 indicating lamina flow exists, we did not observe a decrease in cell viability during operation.

Today, TFF is of growing interest for perfusion operations where continuous clarification is essential. These operations run at much lower permeate fluxes over much longer times. Here we have focused on fed batch operations where microfilter performance must enable processing the entire batch in a relatively short time. In the case of perfusion operations, the model should be validated prior to use.

Here we have focused on bioreactor clarification for the production of protein based therapeutics. Purification of virus and virus like particles is of growing interest for virus vaccines and gene therapy applications. Purification of larger fragile virus particles e.g. measles virus is particularly challenging as they are easily degraded when subjected to an external pressure drop or shear stress.Use of a reverse asymmetric membrane may be beneficial as low TMPs are used. In earlier work[26] we showed that variation in TMP along the feed channel will reduce the resolving power of conventional tangential when used for virus purification. A more constant transmembrane pressure drop across the entire length of the hollow fiber may be

maintained by returning part of the permeate to the permeate side of the module resulting in co-current flow of the permeate. By creating an axial pressure drop along the permeate flow channel, the TMP is more nearly constant throughout the module. Thus, combining a reverse asymmetric membrane with a constant yet low transmembrane pressure drop across the entire hollow fiber may lead to new strategies for virus purification.

3.6   Conclusion

Our results indicate that by using a reverse asymmetric hollow fiber membrane, the membrane structure helps to stabilize a cake layer of rejected cells and cell debris. The secondary membrane that forms can remove foulants that could foul the barrier layer of the BioOptimal™ MF-SL microfilter. When compared to similar barrier layer pore sized symmetrical membranes, the permeate flux and throughput of the BioOptimal™ MF-SL microfilter are much higher. However, it is important that the BioOptimal™ MF-SL microfilter be run at a low TMP to prevent compression of the secondary membrane which will lead to reduced throughput and product recovery. For a given feed flow rate (wall shear rate), cell density and viability the model developed here can be used to estimate the throughput and TMP during operation for a range of initial TMPs. In order to estimate the model parameters, it is necessary to conduct a limited number of normal flow filtrations to determine the compressibility of the cake layer. In addition, two TFF runs should be conducted at the lowest and highest initial TMP of interest.

3.7   Acknowledgements

References

1.   Turner, R., et al., *Manufacturing of Proteins and Antibodies: Chapter Downstream Processing Technologies*, in *New Bioprocessing Strategies: Development and Manufacturing of Recombinant Antibodies and Proteins*. 2017, Springer International Publishing: Cham. p. 95-114.

2.   van Reis, R. and A. Zydney, *Membrane separations in biotechnology.* Current Opinion in Biotechnology, 2001. **12**(2): p. 208-211.

3.   Wang, S.B., et al., *Larger Pore Size Hollow Fiber Membranes as a Solution to the Product Retention Issue in Filtration‐Based Perfusion Bioreactors.* Biotechnology journal, 2019. **14**(2): p. 1800137.

4.   Stressmann, M. and C. Moresoli, *Effect of pore size, shear rate, and harvest time during the constant permeate flux microfiltration of CHO cell culture supernatant.* Biotechnology progress, 2008. **24**(4): p. 890-897.

5.   Defrance, L. and M. Jaffrin, *Comparison between filtrations at fixed transmembrane pressure and fixed permeate flux: application to a membrane bioreactor used for wastewater treatment.* Journal of Membrane Science, 1999. **152**(2): p. 203-210.

6.   Field, R.W., et al., *Critical flux concept for microfiltration fouling.* Journal of membrane science, 1995. **100**(3): p. 259-272.

7.   Frenander, U. and A.S. Jönsson, *Cell harvesting by cross‐flow microfiltration using a shear‐enhanced module.* Biotechnology and bioengineering, 1996. **52**(3): p. 397-403.

8.   Wang, S., et al., *Shear contributions to cell culture performance and product recovery in ATF and TFF perfusion systems.* Journal of biotechnology, 2017. **246**: p. 52-60.

9.   Karst, D.J., et al., *Characterization and comparison of ATF and TFF in stirred bioreactors for continuous mammalian cell culture processes.* Biochemical Engineering Journal, 2016. **110**: p. 17-26.

10.   Furey, J., *Scale-up of a cell culture perfusion process-A low-shear filtration system that inhibits filter-membrane fouling.* Genetic Engineering News, 2002. **22**(7): p. 62-62.

11.   Arunkumar, A., et al., *Investigation of single-pass tangential flow filtration (SPTFF) as an inline concentration step for cell culture harvest.* Journal of membrane science, 2017. **524**: p. 20-32.

12.   Arora, N. and R.H. Davis, *Yeast cake layers as secondary membranes in dead-end microfiltration of bovine serum albumin.* Journal of membrane science, 1994. **92**(3): p. 247-256.

13.   Kuberkar, V.T. and R.H. Davis, *Modeling of fouling reduction by secondary membranes.* Journal of Membrane Science, 2000. **168**(1-2): p. 243-258.

14.   Güell, C., P. Czekaj, and R. Davis, *Microfiltration of protein mixtures and the effects of yeast on membrane fouling.* Journal of Membrane Science, 1999. **155**(1): p. 113-122.

15.   Guerra, A., et al., *Low cross-flow velocity microfiltration of skim milk for removal of bacterial spores.* International Dairy Journal, 1997. **7**(12): p. 849-861.

16.   Gan, Q., *Beer clarification by cross-flow microfiltration—effect of surface hydrodynamics and reversed membrane morphology.* Chemical Engineering and Processing: Process Intensification, 2001. **40**(5): p. 413-419.

17.   Wickramasinghe, S.R., et al., *Understanding virus filtration membrane performance.* Journal of Membrane Science, 2010. **365**(1-2): p. 160-169.

18.   Chew, J.W., J. Kilduff, and G. Belfort, *The behavior of suspensions and macromolecular solutions in crossflow microfiltration: An update.* Journal of Membrane Science, 2020: p. 117865.

19.   Belfort, G., R.H. Davis, and A.L. Zydney, *The behavior of suspensions and macromolecular solutions in crossflow microfiltration.* Journal of membrane science, 1994. **96**(1-2): p. 1-58.

20.   Ho, C.-C. and A.L. Zydney, *A combined pore blockage and cake filtration model for protein fouling during microfiltration.* Journal of colloid and interface science, 2000. **232**(2): p. 389-399.

21.   Loh, S., et al., *Interplay among membrane properties, protein properties and operating conditions on protein fouling during normal-flow microfiltration.* Journal of Membrane Science, 2009. **332**(1-2): p. 93-103.

22.   Hermia, J., *Constant pressure blocking filtration laws: application to power-law non-Newtonian fluids.* Transactions of the Institution of Chemical Engineers, 1982. **60**(3): p. 183-187.

23.   Belter, P.A., E.L. Cussler, and W.S. Hu, *Bioseparations Downstream Processing for Biotechnology.* 1994, New Jersey: Wiley-Blackwell.

24.   Juang, R.-S., H.-L. Chen, and Y.-S. Chen, *Resistance-in-series analysis in cross-flow ultrafiltration of fermentation broths of Bacillus subtilis culture.* Journal of Membrane Science, 2008. **323**(1): p. 193-200.

25.   Pinto, N.D. and M. Brower, *Wide‐surface pore microfiltration membrane drastically improves sieving decay in TFF‐based perfusion cell culture and streamline chromatography integration for continuous bioprocessing.* Biotechnology and Bioengineering, 2020. **117**(11): p. 3336-3344.

26.   Grzenia, D.L., J.O. Carlson, and S.R. Wickramasinghe, *Tangential flow filtration for virus purification.* Journal of Membrane Science, 2008. **321**(2): p. 373-380.

Chapter 4.   Effect of shear rate and viability on the cell clarification

Summary

Tangential flow filtration sweeps the foulants on the membrane surface, keeping the membrane clear to perform its separating function. Therefore, it has been widely used in complex feed streams such as cell clarification. However, high cell density coupled with high product titer causes flux decay and even the failure of the filter. Here reverse asymmetric hollow fiber membrane with a unique membrane design was investigated. The fouling of the filter has shown a different pattern due to this special membrane structure from the previous study. The effect of shear rate and viability on cell clarification is studied for process optimization. Our results suggest that the viability below 90% could cause a low flux due to the changes in the cell diameter and accumulation of process-related impurities. A 3000 1/s shear rate is recommended, considering the efficiency of the filtration and the damage to the cell. An empirical model has been developed to describe the variation of flux and transmembrane pressure drop. The model could predict the flux with different shear rates and help to optimize the shear rate and size the filter.

4.1   Introduction

Membrane-based separations are widely used in the biopharmaceutical industry. Due to its low energy cost, easy scale-up, and simple operation, membrane-based separations are an effective method for cell harvesting, virus filtration, and product formulation. Cell harvesting is a critical process because cell density has increased over the years. A successful cell harvesting could extend the lifetime of other expensive separation resources, such as the protein A columns. The continuous disk-stack centrifuge is widely adopted as a cell clarification step for cell

clarification. Still, it is always coupled with tangential flow filtration because centrifugation cannot remove sufficient impurities from the effluent[1]. Therefore, multiple operations are required. Alternatively, depth filtration reduces the particle content by multiple principles. It is efficient in a complex feed stream where spent medium, viruses, host cells, microcarriers, cell debris, HCPs, and DNA are involved. However, due to concentration gradients, further flux reduction occurs in all filtration processes. The fouling of filters causes an increase in the processing time and a decrease in the sieving and yield.

During cell clarification, alternate tangential flow(ATF) filtration is introduced to reduce the fouling. ATF perfusion is featured by the backwash of the filter during the exhausting cycle. Several studies have demonstrated the ATF perfusion system's feasibility in supporting a high cell density at 40-100 $\times$ 10^6 cells/mL. Yet, unpredictable product retention and membrane fouling still exist[2]. In addition, the equipment for ATF is rather complex, including an additional vacuum pump, diaphragm pump, ATF controller, and the tubing/lines between them. The complexity increases the rate of process failures and difficulties in scaling up. Another process development highlights the tangential flow depth filtration (TFDF) by Spectrum Labs, which uses special hollow fiber modules with thicker fiber walls and a larger pore size distribution[3]. Here, the fibers act as depth filters, focusing on the entrapment of cell debris instead of forming a fouling gel layer on the inner surface of the fiber. Another manufacturer offering a similar filter for perfusion is BioOptimal^{TM} MF-SL, designed specifically for cell culture clarification applications. These filters enable biopharmaceutical manufacturers to improve the efficiency and the effectiveness of their protein harvest step. The key features of BioOptimal^{TM} MF-SL include high throughput and fast processing times, excellent filter performance even with high-density cell cultures, and high clarity of filtrate, even with highly

turbid cell cultures. The feed is introduced inside the hollow fibers. The hollow fibers are asymmetric, and the inside surface has a much larger pore size than the outer membrane surface. The outside membrane surface has an average pore size of 0.4 μm, while the inner surface contains 40 μm pores. Therefore BioOptimal^{TM} MF-SL can be considered as a hybrid TFF-depth filter.

The strategy to reduce the fouling includes optimizing cell culture and the cell clarification shear stress. Cell viability is critical in the characterization of the cell culture. Lower viability introduces more process-related impurities, such as host cell DNA, host cell proteins, and other cellular components in the cell suspension, contributing to the fouling of hollow fiber membranes[4]. Jin et al. found cell viability generated the most significant changes in the HCP profile. The difference in the viability is even larger than the cell line[5]. Plenty of those HCPs have an enzymic domain and are ready to interface with other proteins. The resulting aggerate of the proteins causes the membrane's fouling and affects the final product's function. Parau et al. showed the DNA concentration in the feed increases with lower viability, affecting the retention of DNA in the depth filter[6]. There is a delayed DNA breakthrough when the viability is high. The HCP breakthrough is not affected by cell culture viability or filter type and happens immediately. Although the lower viability challenges filtration, limited studies provide flux decay data in different viabilities.

The shear rate determines the efficiency of the tangential flow to remove the excess foulant deposition on the membrane surface. To optimize the process, the shear rate must be high enough to swipe the cake layer but low enough to reduce the shear stress for the cells. The typical shear stress for cell clarification is 2000-3000 1/s. Stressmann et al. reported that increasing the shear rate caused an unexpected increased initial fouling. However, the

irreversible fouling was not reduced. Although the smallest cake deposit is predicted at a higher shear rate, the differences can be ignored [7]. These results indicate high shear rate may help in short filtration. Therefore the choice of the shear rate needs to be considered systematically and largely case-dependent.

Previous studies have shown that BioOptimal™ MF-SL works well in HCPs, DNA, and solids removal, achieving high product transmission[8]. A mathematical model was developed based on Darcy's law, which could help size the BioOptimal™ MF-SL for different processes[9]. Confocal imaging was able to visualize the fouling caused by CHO cells which showed a different fouling pattern than the screen-type filter[10]. However, the study on the process optimization of BioOptimal™ MF-SL is scarce. This study investigates the effects of cell viability and shear rate on the cell clarification process using BioOptimal™ MF-SL. The results could provide insights into the process design and development of downstream purification.

4.2 Materials and methods

4.2.1 Materials

All reagents were biotechnology grade or higher unless specified. FreeStyle™ CHO-S cells were obtained from ThermoFisher (Waltham, MA, USA). Phosphate buffered saline was purchased from MilliporeSigma (Billerica, MA, USA). CHOgro® Expression Media, and poloxamer 188 solution, 10% w/v in cell culture grade water were purchased from Mirus Bio (Madison, WI, USA). Pressure sensors and a peristaltic pump were obtained from SciLog (Oxnard, CA, USA). Sodium hydroxide, sodium hypochlorite, a digital hotplate stirrer, and a pressure gauge were purchased from VWR (Radnor, PA, USA). An electronic scale (PL602-S) was purchased from Mettler Toledo (Columbus, OH, USA). All the rubber tubing used to deliver

fluid was purchased from Masterflex (Vernon Hills, IL, USA). All water used in this work was obtained from a ThermoFisher 18MΩ Barnstead Smart2pure system (Schwerte, Germany). BioOptimal™ MF-SL filters with membrane surface area of 0.00041 m², pore size of 0.4 µm on the permeate side and 40 µm on the feed side were provided by Asahi Kasei Bioproces (Glenview, IL, USA). All the filters contained 1 hollow fiber.

4.2.2   Cell culture

FreeStyle™ CHO-S Cells were cultured using a shaking incubator. Culture conditions were: temperature of 37 °C and a CO_2 concentration of 8%. The cell culture medium consisted of CHOgro® Expression Media, supplemented at a final concentration of 8 mM L-glutamine, 0.3% poloxamer 188, and 0.5× penicillin-streptomycin. Initially, a 30 mL inoculum of CHO cells was grown in a 200 mL shaker flask. Once the cell density was higher than 8 million cells/mL and cell culture was scaled up to 200 mL in a 1L shaker flask by seeding a portion of culture to the fresh growth medium at a cell density of 1.5 million cells/mL.

4.2.3   TFF for determining resistance parameter

A peristaltic pump was used to pump the feed. Three pressure sensors were mounted on the feed (P_F) retentate (P_R) and permeate (P_P) lines of the filter, respectively. The transmembrane pressure (TMP) is defined as:

$$\text{TMP} = \frac{P_\text{F} + P_\text{R}}{2} - P_\text{P} \qquad [4.1]$$

Assuming laminar tube flow, the wall shear rate within the fiber is given by

$$\Upsilon = \frac{4Q_F}{\pi r^3} \qquad [4.2]$$

where Υ is shear rate (s⁻¹), Q_F is volumetric flow rate (m³ s⁻¹) and r is radius of the fiber lumen (m).

The feed volume was 50 mL and the cell density of 9 million cells/mL. The permeate was collected on a balance. The retentate was returned to the feed tank. Experiments were conducted using the BioOptimal™ MF-SL microfilter. Before each experiment, the DI water flux was determined at a TMP of 3.4 kPa (0.5 psi) for the BioOptimal™ MF-SL microfilter and was found to be 1100 $Lm^{-2}h^{-1}$.

4.2.4   Particle size distribution

Particle size distribution was determined by LS 13 320 Particle Size Analyzer with a universal Liquid module(Brea, CA, USA). The Run length is 60 seconds, with a pump speed of 33%. Each run starts with an auto rinse of the module, followed by a de-bubble process. After measurement of the background, the sample was loaded based on the standard obscuration.

4.2.5   Modeling

The modeling process and all the coefficients are the same as in Chapter 3. The modeling is briefly described below

Considering CHO cell feed streams are highly compressible, a correlation between the resistance of deposited CHO cells and the TMP is obtained from normal flow filtration data using a combined pore blockage and cake filtration model developed by Ho and Zydney [11]. Three parameters are pore blockage parameter α, the resistance of single cell, R_{c0} and specific cake layer resistance, α', determined by best fitting of the experimental data. The values obtained will be used in TFF.

The permeate flux during TFF is resistance-in-series model.

$$J = \frac{TMP}{\mu(R_m + R_c + R_P)} \qquad [4.3]$$

$$R_c = \frac{m}{A} * \alpha' \qquad [4.4]$$

where R_m and R_c are the membrane and cake resistance. m is the mass of deposited cake and A is the membrane area. R_p is the resistance due to concentration polarization which is ignored here. The growth of the cake during TFF depends upon the convection of particulate matter towards the membrane due to the permeate flow and back migration away from the membrane.

We assume the growth of the cake is given by the product of the permeate flow rate multiplied by the concentration of CHO cells in the feed. Suppression of cake formation is assumed to depend on the mass of cake already deposited, m, as well as the feed flow rate, Q_F, and a cake attrition factor, K, as given by

$$\frac{dm}{dt} = cQ_P - KQ_F m \qquad [4.5]$$

The concentration of CHO cells in the feed increases with time and is given by

$$c = \frac{c_0 v_0 - m}{v_0 - v} \qquad [4.6]$$

where c_0, v_0 are the initial concentration and volume of the feed, respectively.

In this work, the initial TMP was set via the retentate valve. The TMP was free to increase as the feed is concentrated. The pressure drop for flow through the fiber lumen (ΔP) must equal the TMP. These two pressure drops are related to the retentate and permeate flow rates Q_R and Q_P by Darcy's law as follow.

$$\text{TMP} = μ \times R_{valve} \times \frac{Q_R}{A_{valve}} = μ \times (R_c + R_m) \times \frac{Q_P}{A} \qquad [4.7]$$

$$Q_F = Q_R + Q_P \qquad [4.8]$$

R_{valve} is the resistance for flow through the valve and is the only unknown parameter, and is determined experimentally.

The attrition factor, k, which may be obtained from fitting the filtration with constant flux data. The permeate flux is obtained by combining and solving equations [4.3] - [4.8].

4.2.6　Poloxamer quantitation

To a 1.5-mL microcentrifuge tube, 250µL of standard or sample, 25µL of (trichloroacetic acid) TCA and 250µL of methanol were added. The capped tube was vortexed for 0.5 min and centrifuged at 12,000rpm for 5min. The supernatant was transferred to a separate microcentrifuge tube containing 250µL of cobalt-thiocyanate reagent and 250µL of ethyl acetate. The sample was mixed for approximately 0.5 min on a vortex mixer and centrifuged at 12,000rpm for 5min. The upper two layers were removed using a vacuum aspiration device. The pellet and tube wall were washed three times with 1mL of ethyl acetate. The washed sample was air-dried with the tube open in a fume hood for more than 15 min. One microliter of acetone was added to dissolve the dried pellet, and the tube was capped immediately. The tube was vortexed until the pellet was dissolved completely. The absorbance was measured at 328nm on an UV-Vis spectrophotometer

4.2.7　Bradford assay

100mg Coomassie Brilliant Blue G-250 was dissolved in 50ml 95% ethanol and 100ml 85% (w/v) phosphoric acid. Once the dye has completely dissolved, dilute to 1 liter with deionized water. Bradford reagent was filtrated just before use. Protein samples were mixed with Bradford reagent with a ratio of 1:30. The mixture was vortexed and incubated at room temperature for 5 minutes and then transferred to cuvettes and measured the absorbance at 595nm. The absorbance was calibrated with bovine serum albumin (BSA) from 0.1 g/L to 1 g/L using the same method.

4.2.8　DNA quantitation

DNA quantitation follows PicoGreen dsDNA quantitation reagent. On the day of the experiment, prepare an aqueous working solution of the PicoGreen® reagent by making a 200-

fold dilution of the concentrated PicoGreen® reagent solution in TE(200 mM Tris-HCl, 20 mM EDTA, pH 7.5). The lambda DNA standard can simply be diluted 50-fold in TE to make the 2 μg/mL working solution. To create a five-point standard curve from 1 ng/mL to 1 μg/mL(ie blank, 1 ng/mL, 10 ng/mL, 100 ng/mL, 1ug ng/mL), dilute the 2 μg/mL working solution with TE. Add 100 uL sample or standard into 96 wells plate. Then add 100 uL PicoGreen working solution. Mix well. Incubate for 5 minutes at room temperature, protected from light. Measure the sample fluorescence using a fluorescence microplate reader and standard fluorescein wavelengths (excitation ~480 nm, emission ~520 nm)

4.3   Results and discussions

4.3.1   Effect of the viability on filtration flux

Tangential flow filtration of CHO cells was conducted at viability ranging from 96% to 71%, with extreme viability of 0% as a control. The experimental conditions are cell density of 9.2 million, the shear rate of 2000 s^{-1}, feed volume of 50 mL, and initial TMP of 0.5 psi. Figure 4.1 gives the experimental data in symbols, and clearly, a positive correlation between flux and viability was observed. These results are not surprising because lower viability is introduced by extended culture time, so the cell lysis and accumulation of secreted protein create more process-related impurities. There are 30,000 genes in the CHO genome, and 2000 HCPs have been identified using liquid chromatography-tandem mass spectrometry[12, 13]. With such proteins accumulated, a lower viability cell culture is expected to associate with higher host protein concentration. Previous studies identified the most abundant HCP, and the results show a lot of those HCPs are enzymes. Because the enzymes easily interact with other proteins, those abundant HCPs have the potential to form large aggreges[14]. The interaction is more significant considering the higher HCP concentration in low viability cell culture, which blocks the

membrane rapidly. The HCP, DNA, and poloxamer concentrations are listed in Table 4.1. Clearly, the HCPs and DNA concentrations are higher with lower viability. The table shows that the HCP concentration in 71% viability is more than 2 times higher than that of 96% viability. However, permeate concentration is less than 2 times higher. Therefore, more HCPs are retained on the membrane in low viability samples. Residual DNA also shows more retention in low viability samples. Comparing to the impurities in the feed, the small increase of the HCPs and DNA in permeate in the same viability due to the lysing of the cell from the shear stress during the filtation.

It is also interesting that the poloxamer keeps constant retention for all the viability. Poloxamer 188 is a nonionic surfactant with an average molecular weight of 8.4 kDa. The molecule is small and easy to pass through the filter, and therefore the retention of poloxamer is low in all the experiments. In the cell culture process, The incorporation of poloxamer 188 into the plasma membrane could decrease the fluidity of cells and thus increase the cell resistance to shear stress[15]. The binding of poloxamer 188 with CHO cell accounts for the retention, providing the filter rejects all the cells.

In addition to raising the impurity's concentration, the size of the foulants is also suspected to be varied in different viability. The cell size decreases with a higher impeller speed and a lower liquid volume[16]. Those are the results of cell damage and the generation of cell debris. The volume distributions of cell diameter are shown in Figure 4.2. The cell size decreases when the viability is below 89%, consistent with previous studies[17]. A sudden drop in cell diameter at the end of the cultures is expected due to cell death[18]. The decrease of the particles would cause a change in the cake packing, introducing additional hydraulic resistance for the flux. The smaller particles also enhance the diffusion effect in addition to the sedimentation. The

packing of the foulant plays an important role in maintaining high flux. An example is the usage of the filter aid to stabilize the cake formed by fine particles. Our previous results showed that the opened pores in BioOptimal™ MF-SL microfilter help to stabilize the cake and therefore establish a secondary membrane. This secondary membrane removes foulants that could foul the barrier layer of the filter, allowing a higher flux than screen type filter. However the overal flux is expected to decrease with lower particle size.

For a unique membrane design like BioOptimal™ MF-SL, another issue that needs to be considered is that the smaller particle will penetrate the membrane matrix as the open pores face the feed stream. As more internal fouling occurs, the tangential flow cannot swipe out foulants, resulting in a lower flux. Viabilities higher than 89% have similar flux decay, consistent with the HCPs concentration and cell diameter distribution.
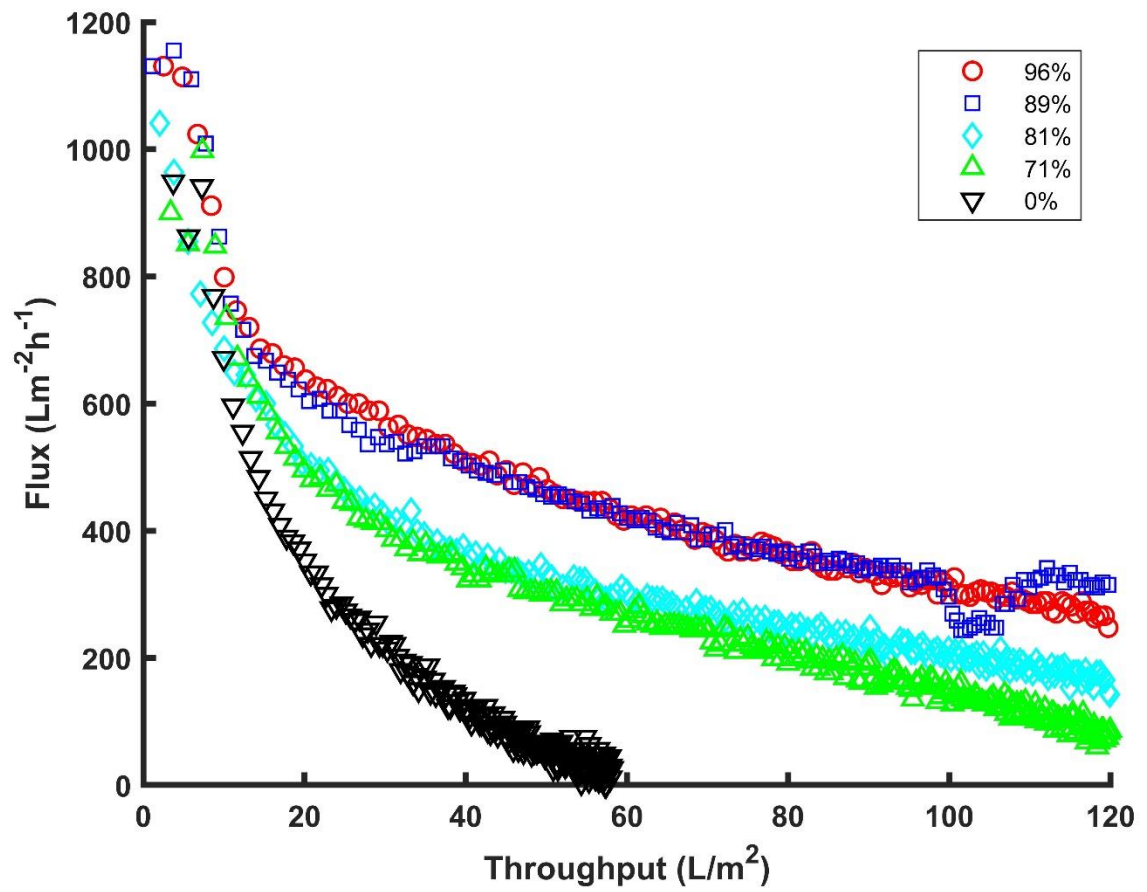
Figure 4.1 The flux decays with different viability.

Table 4.1 HCP, Poloxamer, DNA concentration in the feed(different viability)

Viability	HCP(ppm)		Poloxamer(ppm)		DNA(ng/mL)	
	Feed	Permeate	Feed	Permeate	Feed	Permeate
96.4%	366(±18)	460(±31)	3018(±124)	2538(±28)	595 (±21)	938 (±56)
89%	369(±5)	402(±39)	3092(±99)	2616(±61)	739 (±13)	1013 (±36)
81%	718(±55)	667(±8)	3101(±47)	2610(±5)	877 (±26)	1031 (±25)
71%	852(±15)	882(±29)	3094(±18)	2577(±32)	906 (±42)	1135 (±52)
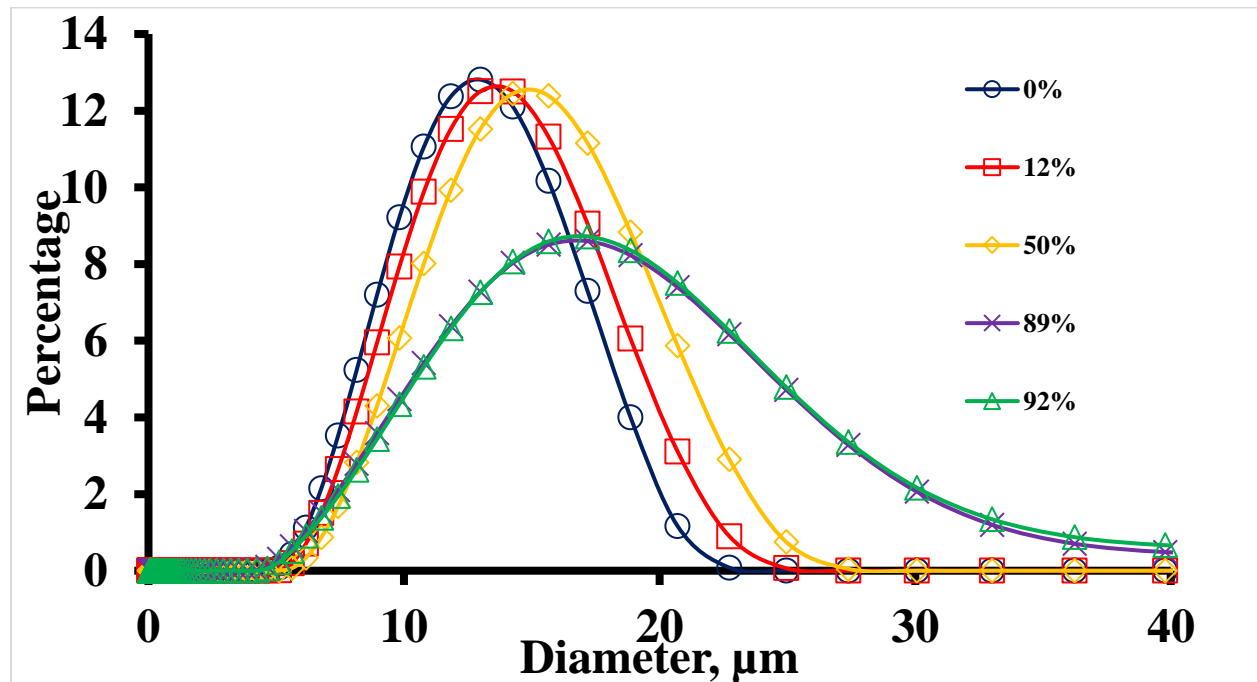
Figure 4.2 Size distribution of CHO cell with different viabilities

4.3.2   Effect of the viability on filtration flux

Tangential flow filtration of CHO cells was conducted at the shear rate ranging from 1000 1/s to 4000 1/s. The filtration conditions are cell density of 9 million, feed volume of 50 mL, and initial TMP of 0.5 psi. The flux decay and TMP increase are shown in Figure 4.3 and Figure 4.4. Flux is predicted using the model shown in the solid lines, and the experimental data are shown in the symbols. Because the TMP in BioOptimal™ MF-SL is low(around 1 psi), and low TMP is suggested by the manufacturer, only initial TMP is controlled. However, the increase of the TMP can be modeled by retentate flow. Figure 4.4 gives the increase of the calculated TMP in the solid lines, and the experimental data are shown in the symbols. BioOptimal™ MF-SL is similar to the depth filter, suggesting the thickness of the membrane is more than the normal tangential flow filter. High TMP compacts the membrane, limiting the flux.

The tangential flow filtration is featured by inhibiting the fouling process by continually sweeping the membrane surface. The higher tangential flow rate, represented by the shear rates, is expected to improve flux. However, the effect of the shear rates in this study is more significant than in a previous study using yeast cells[9]. The diameter of the yeast cells is around 3-4 μm, while the CHO cells are 13-15 μm. The deposition of CHO cells is more external compared to yeast cells(See yeast filtration in chapter 2, i.e. Figure 2.4, Figure 2.5). The excess external cake of CHO cell is stripped off at a higher tangential flow, resulting in higher flux.

In conclusion, the higher shear rate helps fouling reduction and especially important if the feed stream is CHO cell.. From the TMP increase profile, as shown in Figure 4.4, a Lower shear rate introduces high TMP with the filtration. High TMP compacts the membrane, limiting the flux. Therefore, the operation of BioOptimal™ MF-SL favors a high shear rate.

However, a higher tangential flow introduces shear stress on the cells and even causes cell death. Several mechanisms have been proposed to explain cell death in the presence of hydrodynamic shear: (1) turbulent eddy-cell interaction, (2) collisions between the cell and other cells or equipment surfaces, and (3) net laminar shear force exerted across a cell[19]. As the tangential flow in the lumen is in the laminar range, the latter two terms would cause damage to the cell during the filtration. As the shear rate from 3000 1/s to 4000 1/s doesn't improve the flux too much, a 3000 1/s shear rate is recommended.
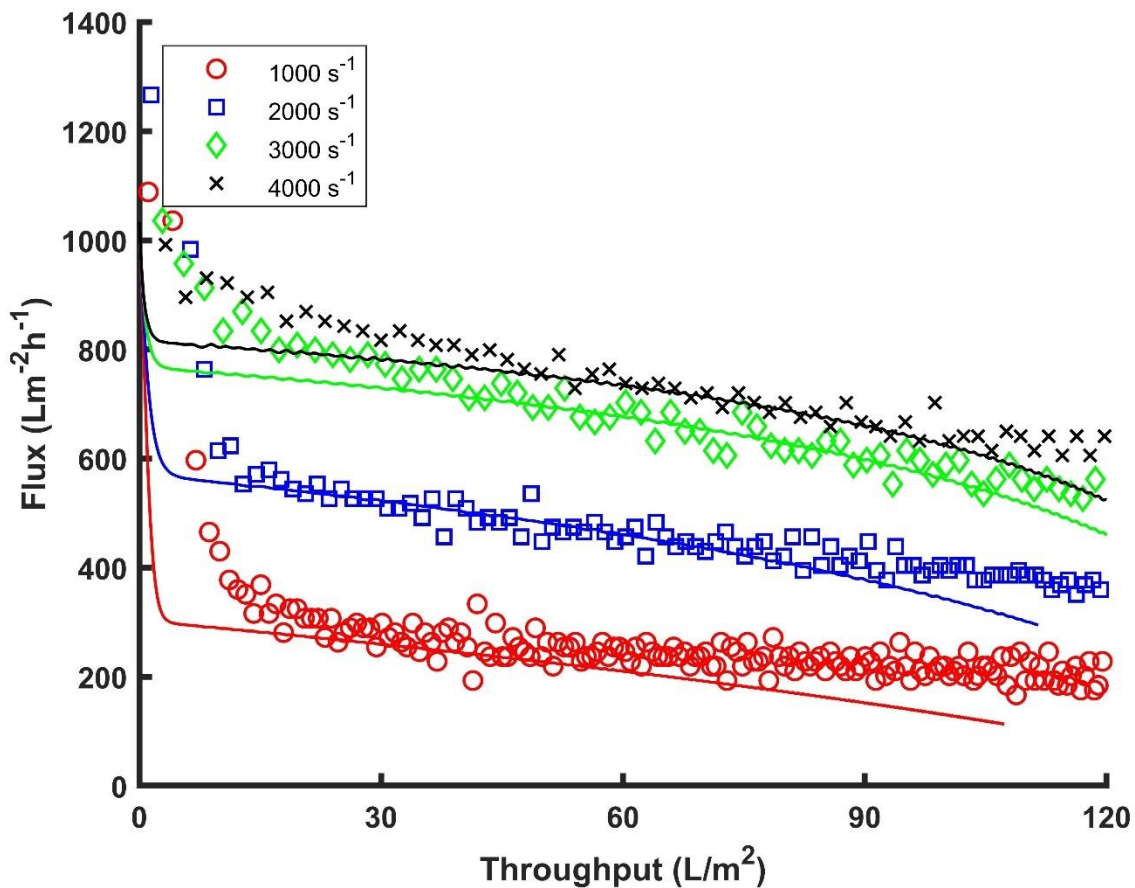
Figure 4.3 The flux decays with different shear rates
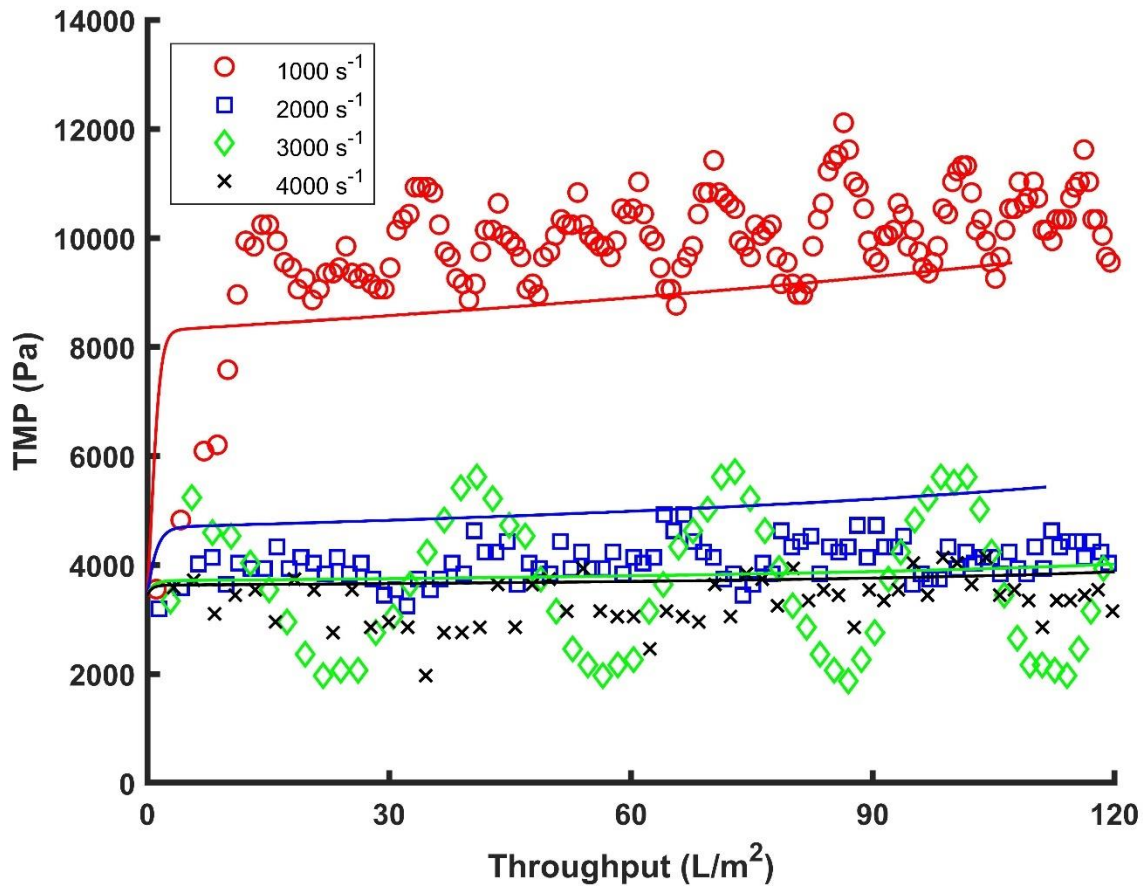
Figure 4.4 The TMP increases with different viability

4.4   Conclusion

Our results indicate that the viability of the cell culture and the shear rate significantly influence the tangential flow filtration flux. The lower viability affects the flux by increasing the impurities such as HCP and DNA. The permeability of the poloxamer is not affected by viability. Deceasing the cell diameter in low viability causes the cake's packing density, enhancing the hydraulic resistance. The shear rate is found to be more significant than yeast cells due to the properties of the foulants. The CHO cells are larger than the yeast cell. Therefore more external fouling is expected. For a given feed flow rate (wall shear rate), cell density, and viability, the model developed here can be used to estimate the throughput. Our results suggest that the feedstream should maintain a higher level of viability. A larger size of the foulants is preferred,

116

where the tangential flow rate could effectively sweep the growing cake. The effect of shear rate is significant in large foulant such as CHO cells. Choice of the shear rate should consider the lysing of the cell. As the shear rate from 3000 1/s to 4000 1/s doesn't improve the flux too much, a 3000 1/s shear rate is recommended.

4.5   Acknowledgements

Reference

1.   Roush, D.J. and Y. Lu, *Advances in primary recovery: centrifugation and membrane technology.* Biotechnology progress, 2008. **24**(3): p. 488-495.

2.   Kim, S.-C., et al., *Effect of transmembrane pressure on Factor VIII yield in ATF perfusion culture for the production of recombinant human Factor VIII co-expressed with von Willebrand factor.* Cytotechnology, 2016. **68**(5): p. 1687-1696.

3.   Hoffmann, D., et al., *Purification of new biologicals using membrane-based processes.* Current Trends and Future Developments on (Bio-) Membranes, 2019: p. 123-150.

4.   Azami, H., M.H. Sarrafzadeh, and M.R. Mehrnia, *Fouling in membrane bioreactors with various concentrations of dead cells.* Desalination, 2011. **278**(1-3): p. 373-380.

5.   Jin, M., et al., *Profiling of host cell proteins by two-dimensional difference gel electrophoresis (2D-DIGE): Implications for downstream process development.* Biotechnology and bioengineering, 2010. **105**(2): p. 306-316.

6.   Parau, M., et al., *Analysis of fouling and breakthrough of process related impurities during depth filtration using confocal microscopy.* Biotechnology Progress, 2022: p. e3233.

7.   Stressmann, M. and C. Moresoli, *Effect of pore size, shear rate, and harvest time during the constant permeate flux microfiltration of CHO cell culture supernatant.* Biotechnology progress, 2008. **24**(4): p. 890-897.

8.   Popova, D., et al., *Integrated economic and experimental framework for screening of primary recovery technologies for high cell density CHO cultures.* Biotechnology journal, 2016. **11**(7): p. 899-909.

9.   Zhang, D., et al., *Modeling tangential flow filtration using reverse asymmetric membranes for bioreactor harvesting.* Biotechnology Progress, 2021. **37**(1): p. e3084.

10.   Zhang, D., et al., *Modeling flux in tangential flow filtration using a reverse asymmetric membrane for Chinese hamster ovary cell clarification.* Biotechnology Progress, 2021. **37**(3): p. e3115.

11.   Ho, C.-C. and A.L. Zydney, *A combined pore blockage and cake filtration model for protein fouling during microfiltration.* Journal of colloid and interface science, 2000. **232**(2): p. 389-399.

12.   Park, J.H., et al., *Proteomic analysis of host cell protein dynamics in the culture supernatants of antibody-producing CHO cells.* Scientific reports, 2017. **7**(1): p. 1-13.

13.   Wang, X., A.K. Hunter, and N.M. Mozier, *Host cell proteins in biologics development: Identification, quantitation and risk assessment.* Biotechnology and bioengineering, 2009. **103**(3): p. 446-458.

14.   Liu, X., et al., *Identification and characterization of co-purifying CHO host cell proteins in monoclonal antibody purification process.* Journal of Pharmaceutical and Biomedical Analysis, 2019. **174**: p. 500-508.

15.   Guzniczak, E., et al., *Impact of poloxamer 188 (Pluronic F-68) additive on cell mechanical properties, quantification by real-time deformability cytometry.* Biomicrofluidics, 2018. **12**(4): p. 044118.

16.   Odeleye, A., et al., *On the fluid dynamics of a laboratory scale single-use stirred bioreactor.* Chemical engineering science, 2014. **111**: p. 299-312.

17.   Pan, X., et al., *Metabolic characterization of a CHO cell size increase phase in fed-batch cultures.* Applied microbiology and biotechnology, 2017. **101**(22): p. 8101-8113.

18.   Pan, X., et al., *Selection of chemically defined media for CHO cell fed-batch culture processes.* Cytotechnology, 2017. **69**(1): p. 39-56.

19.   Vickroy, B., K. Lorenz, and W. Kelly, *Modeling shear damage to suspended CHO cells during cross-flow filtration.* Biotechnology Progress, 2007. **23**(1): p. 194-199.

Chapter 5.   Proteomics analysis of host cell protein in the cell clarification

Summary

Chinese hamster ovary (CHO) cells are among the most common cell lines for therapeutic protein production. Host cell proteins (HCPs) are the most challenging impurities for downstream purification processes. In order to investigate the fouling during cell clarification, HCPs in the bioreactor, harvest, and stuck on the membrane were identified and quantified using different methods, including 2D SDS-PAGE, liquid chromatography/mass spectrometry(LC/MS). 2D SDS-PAGE could profile the distribution of the HCPs from the given process. Low abundancy HCPs could be identified in batch using proteomics workflow. A dataset was created using the identified HCPs and used to train the deep learning model. The model predicts unknown HCPs on fouling potential with an accuracy of 76%. The dataset of identified HCPs in this study provides insights into the characterization of membrane fouling, membrane selection, and process development.

5.1   Introduction

Therapeutic proteins are widely used to treat patients suffering from cancers, metabolic disorders, hematological disorders, and immunological diseases [1], showing the advantage of high specificity, high effectiveness, and multiple functions. These proteins are produced using microbial fermentation or cell cultures using mammalian cells. Among those available expression systems, Chinese hamster ovary (CHO) cells are the most prevalent mammalian cell factories due to their ability to synthesize human-like post-translational modifications, ease of maintenance in suspension cultures, and well-established standards of good manufacturing practice (GMP)[2, 3]. Cell densities above 100×10^6/mL with product titers of 10 g/L can be reached with perfusion bioreactors[4, 5]. While the cell density increases with more optimized

cell culture conditions and cell lines, more burden has been added to downstream processing. The purification of therapeutic proteins routinely begins with cell clarification, followed by Protein A chromatographic as the primary capture. Additional chromatographic polishing steps include cation exchange, anion exchange, or hydrophobic interaction for refinement. The process also includes two orthogonal steps for viral clearance: low pH viral inactivation after protein A chromatography and viral filtration after polishing chromatography. The final process step is frequently ultrafiltration/diafiltration to formulate and concentrate the product. During the downstream pipeline, the fouling of the membrane filter used for clarification and cell recycling has become a major limitation. The fouling reduces flux, throughput, and product recovery [6]. The major foulant in the cell culture consists of cell debris, host cell DNA, antifoam, product aggregates, and, importantly, host cell proteins (HCPs)[7]. The HCPs are process-related protein impurities produced by the host organism during biotherapeutic manufacturing and production. Despite the importance of HCP removal, the identity and dynamics of these proteins during cell culture and downstream processing are largely case-dependent [8]. The HCPs profile in the cell culture is critical not only because it may potentially cause the immune response in patients but also because the properties of the HCPs are similar to the product and, therefore, they are co-purified with biopharmaceutical drug products. The interaction between those difficult HCPs and products involves hydrophobic interaction, electrostatic repulsion, hydrogen bond, van der Waal's force, ionic interaction, and immunoglobulin-like domains[9]. The list of those difficult HCPs is reported during protein A chromatography[9], polishing chromatography[10], and in the final products[11]. Although the FDA does not specify an acceptable HCP level, HCP concentrations are typically reduced to 1-100 ppm for final mAb formulations[12]. Therefore, HCPs are expected to be removed by each operation unit in the downstream process as much as

possible. It has been demonstrated that HCPs clearance is a cumulative process and archived by different steps[13]. The reduction and profile of HCPs are reported intensively elsewhere. However, the removal of HCPs and fouling caused by HCPs during cell clarification has rarely been discussed. In addition, the interplay between the HCPs and the quality of the bioreactor stream, such as viability on filter fouling, is not well understood. This study aims to profile the HCPs removal during the cell clarification process and characterize the fouling potential of the HCPs in the cell culture. Previous studies on HCPs clearance focused on the 1) total HCP quantitation through unit operations. 2) visualization of the fouling locations using confocal laser scanning microscopy. 3) two-dimensional fluorescence difference gel electrophoresis to draw a picture of HCPs properties such as molecular weight and pI, and 4) proteomic study to identify the HCPs.

5.1.1   Total HCP quantitation through unit operations.

The current toolbox to measure/monitor total HCP concentration includes enzyme-linked immunosorbent assays (ELISA), the current gold-standard methodology. Gronemeyer et al. reported a significant increase in product titer corresponding with a nonlinear increase of HCP, which may also challenge the downstream process. Two-phase aqueous extraction has significantly reduced such HCP compared to centrifugation and filtration [14]. While ELISA assays offer high throughput, selectivity, and sensitivity, their major drawbacks are incomplete coverage of the HCP proteome by the polyclonal antibodies due to non or low immunoreactivity of HCPs[15]. In addition to the ELISA method, Capito et al. proposed alternative host cell protein quantification using Fourier transform mid-infrared spectroscopy (FT-MIR). The correlation between peak intensities and HCP concentrations measured by ELISA is found in the middle infrared range. Predicted HCP values agree with results obtained by an ELISA assay. FT-

MIR reduces exhaustive sample preparation steps and prevents dilution errors as the new method for HCP quantification. While similar to ELISA, those methods are used to quantify the total amount of HCP present, they cannot be used to define which HCPs are present. Therefore the information on HCP identity and individual properties is missing[16].

5.1.2 Confocal Laser Scanning Microscopy to visualize the fouling locations

Parau et al. investigated HCP and DNA breakthroughs during CHO cell clarification. The results show that the HCP breakthrough is immediate and not affected by cell culture viability or filter type, but DNA breakthrough correlates with low cell culture viability. Confocal imaging shows DNA is distributed evenly on the two layers of the membrane, but the cell debris and aggregates are only found on the first layer of the membrane. However, the mechanism of HCP fouling is not revealed, and only total HCP was quantified[17]. Zhang et al. compared the confocal imaging of three fouled membranes with different structures to identify the location of cell entrapment within and on the membrane. DNA and host cell proteins are trapped on the inner membrane surface with little penetration into the membrane for screen-type membrane. Significant host cell protein staining on the inner membrane surface and to a depth of about 50 μm from the inner surface is observed for reversed asymmetrical membrane. The limitation of confocal microscopy is that the HCPs are treated as a whole group. Therefore, the fouling mechanism cannot be differentiated based on the properties of a single HCP.

5.1.3 Two-dimensional fluorescence difference gel electrophoresis

Grzeskowiak et al. performed two-dimensional fluorescence difference gel electrophoresis for the CHO cells in different viability. The difference in cell viability has a greater influence on protein spot patterns than the difference in the cell clones. The HCP spot of low viability shows lower molecular weight than high molecular weight due to the degradation

of the protein. [18]. However, The disadvantage of 2D-DIGE is the labeling procedure. As a result, the physical properties such as solubility, hydrophobicity, and size are slightly altered. In addition, the assay will not detect non-immunoreactive or weakly immunoreactive proteins in the samples.

5.1.4 Proteomic study to identify the HCPs

Park et al. reported that 30 most abundant HCPs were found in batch and fed-batch cell cultures. Gene Ontology(GO) suggests that these HCPs are either in the cytoplasm or extracellular region and are secreted proteins[19]. Wilson et al. identified HCPs on different harvest days using LC/MS. HCPs increases with harvest day, and more intracellular HCPs are found due to the gradual breakdown of cells

Recently, combining those methods to characterize the HCPs and reveal the clearance efficiency has been more general. Those studies are compiled and summarized in Table 5.1

Table 5.1 A summary of methods to characterize the HCPs

Methods	Comments	Reference
2D SDS/PAGE, (MALDI-TOF/TOF) MS	Identification of co-elution resulting from non-specific binding of HCP	[20]
ELISA, 2D SDS/PAGE, (MALDI-TOF/TOF) MS	Identification of abundant HCP in the cell culture	[21]
ELISA, 2D SDS/PAGE, LC/MS	Characterization of co-purifying CHO host cell proteins	[22]
ELISA, LC/MS	The number of HCPs was reduced under mild hypothermia. However, the cell culture needs to be extended to reach normal cell density and yield	[23]
ELISA, 2-D DIGE	Cell viability generated the most significant changes on the HCP profile. The HCP species in production cell culture was found to be well-represented in null cell culture	[24]
ELISA, LC/MS	HCP in the approved therapeutics was determined. The commonly identified HCPs and their abundances are profiled. 2DE is limited in detecting	[11]

	proteins with extreme hydrophobicity, molecular weight, or isoelectric point.	
ELISA, 2D SDS-PAGE, LC/MS	The similarity in their cell-specific productivities for immunogenic HCPs and the total numbers and major populations of proteins was found in different CHO lineage, upstream process, and culture performance	[25].
2D SDS-PAGE, MALDI/ MS	37% of identified HCPs have previously been identified as potentially difficult to remove by downstream processes	[26]

The present study focuses on the HCPs fouling in the cell clarification. The filter used in this study is BioOptimal™ MF-SL, featured by its asymmetrical membrane structure. BioOptimal™ MF-SL is a commercially available hollow fiber module that contains a reverse asymmetric membrane. The inside surface has pores up to 40 μm in diameter, while the outside has 0.4 μm pores. Since the feed is pumped inside the fibers, the more opened membrane surface contacts the feed. The strategy of the study is directly extraction of the fouling after being used by backwashing the membrane. Then the backwashed solution was performed 2D SDS-PAGE together with MALDI/ MS, or SDS-PAGE followed by LC/MS. Two different feed streams with high viability(>95%) and low viability(20%) were also investigated in the filtration, backwash,

and identification. This study fills up the white area of the database for difficult HCPs in the cell clarification.

5.2   Materials and methods

5.2.1   Materials

All reagents were biotechnology grade or higher unless specified. FreeStyle™ CHO-S cell, bovine serum albumin, and formic acid were obtained from ThermoFisher (Waltham, MA, USA). CHOgro® expression media and poloxamer 188 solution, 10% w/v in cell culture grade water were purchased from Mirus Bio (Madison, WI, USA). Coomassie brilliant Blue G-250, coomassie brilliant blue R-250, bromophenol blue, glycerol were purchased from MilliporeSigma (Burlington, MA, USA). Pressure sensors and a peristaltic pump were obtained from SciLog (Oxnard, CA, USA). TRITON™ X-100, sodium hydroxide, sodium hypochlorite, methanol, agarose, phosphoric acid, ammonium bicarbonate, acetonitrile, sodium dodecyl sulfate, a digital hotplate stirrer, and a pressure gauge were purchased from VWR (Radnor, PA, USA). Trypsin/lys-C mix was purchased from Promega (Madison, WI, USA). Ethanol was purchased from Decon Labs(King of Prussia, PA, USA). Glacial acetic acid was obtained from Labchem(Zelienople, PA, USA). Tris and urea were obtained from Chem Impex(Wood Dale, IL, USA). Dithiothreitol (DTT) was purchased from Goldbio (St Louis, MO, USA). Chloroform was obtained from Alfa Aesar (Haverhill, MA, USA). Iodoacetamide (IAA) was obtained from BeanTown Chemical (Hudson, NH, US). Immobiline dryStrip pH 3-11NL, 7 cm, rehydration solution, cover fluid for IEF were purchased from Cytiva (Marlborough, MA, US). Precision plus protein™ unstained protein was obtained from Bio-Rad (Hercules, CA, USA). An electronic scale (PL602-S) was purchased from Mettler Toledo (Columbus, OH, USA). All the rubber tubings used to deliver fluid were purchased from Masterflex (Vernon Hills, IL, USA). All water

used in this work was obtained from a ThermoFisher 18MΩ Barnstead Smart2pure system (Schwerte, Germany). BioOptimal™ MF-SL filters with a membrane surface area of 0.00041 m^2, with a pore size of 0.4 μm on the permeate side and 40 μm on the feed side, were provided by Asahi Kasei Bioprocess (Glenview, IL, USA). The filters contained one hollow fiber.

5.2.2 Method

5.2.2.1 Cell culture

FreeStyle™ CHO-S Cells were cultured using a shaking incubator. Culture conditions were: temperature of 37 °C and a CO_2 concentration of 8%. The cell culture medium consisted of CHOgro® Expression Media, supplemented with a final concentration of 8 mM L-glutamine, 0.3% poloxamer 188, and 0.5× penicillin-streptomycin. Initially, 30 mL inoculum of CHO cells was grown in a 200 mL flask. Once the cell density was greater than 8 million cells/mL and cell culture was scaled up to 200 mL in a 1L shaker flask by seeding a portion of culture to the fresh growth medium at a cell density of 1.5 million cells/mL.

5.2.2.2 Tangential flow filtration (TFF) operation

A peristaltic pump was used to pump the feed. Three pressure sensors were mounted on the feed (P_F), retentate (P_R), and permeate lines (P_P of the filter, respectively. The transmembrane pressure (TMP) is defined as:

$$\text{TMP} = \frac{P_F + P_R}{2} - P_P \qquad [5.1]$$

Assuming laminar tube flow, the wall shear rate within the fiber is given by:

$$\Upsilon = \frac{4Q_F}{\pi r^3} \qquad [5.2]$$

where Υ is the shear rate (s^{-1}), Q_F is volumetric flow rate (m^3/s), and r is radius of the fiber lumen (m).

The CHO cells were freshly harvested from the incubator and directly loaded in to feed reservoir, and the feed volume was 50 mL, giving a throughput of 120 L/m^2 or higher loading with 500mL. The shear rate was set as $2,000s^{-1}$. The permeate was collected on a balance. The flux was calculated based on the change in permeate weight during a specified time. The retentate was returned to the feed tank. Experiments were conducted using the BioOptimal™ MF-SL filters. The TMP was not regulated based on manufacturer instruction. The experimental set-up is shown in Figure 5.1.
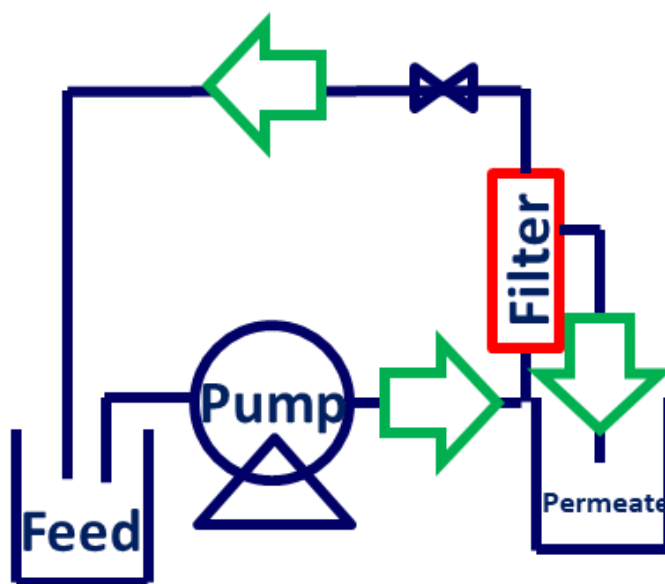

Figure 5.1 Experimental setup TFF, concentration mode, and controlled initial TMP.

5.2.2.3 Backwash

After filtration, the residual cell culture inside and outside the lumen was drained by gentle shaking. The lumen of the fiber was flushed with backwash solution at a slow flow rate(<10mL/min or <1 psi hydraulic pressure) to remove the residual cell or cell debris in the lumen. Then shell side of the filter was flushed with backwash solution for about 200 mL and finally filled with backwash solution. Backwash was performed by pumping the backwash solution from the shell side to the inside of the fiber. The extracted foulants are collected at the

lumen port. The backwash pressure was as high as possible but must be lower than membrane tolerance. For each backwash, the fouling was collected as three fractions.

5.2.2.4 Confocal imaging

DAPI was used to label DNA. It displays a blue fluorescent signal. MemBrite™ was used to label cell membrane proteins. It displays an orange fluorescent signal. A stock 5mg/mL DAPI solution was prepared in DI water. A concentration of 2μg/mL was used for all staining experiments based on screening experiments. The MemBrite™ staining solution was prepared according to the manufacturer's instructions.

After filtration, the module was opened, and the fouled hollow fiber was soaked in PBS to remove unbound cells and cell debris. Next, the fiber was incubated with 4% paraformaldehyde for 20 min, then washed again with PBS buffer. The fiber was then incubated with 0.5% Triton-X 100 for 10 min and washed again with PBS buffer. The fiber was quickly dipped into liquid nitrogen and sectioned into small pieces. The fiber samples were first incubated with DAPI for 30 min in the dark and washed twice with PBS to remove excess dye. Next, MemBrite™ labeling was carried out. The fiber samples were incubated in a pre-staining solution (provided by MemBrite™ dye kit) for 5 min at 37 °C followed by incubation in the staining solution (provided by MemBrite™ dye kit) for 5 min at 37 °C. After incubation, the fiber sections were washed twice with PBS buffer to remove excess dye. The fibers were mounted on slides and then imaged with a Leica TCS SP5 Confocal Laser Scanning Microscope (Buffalo Grove, IL, USA). The excitation/emission wavelength for DAPI is 405/461, and MemBrite™ 594/615 nm.

5.2.2.5 Bradford Assay

100mg Coomassie Brilliant Blue G-250 was dissolved in 50ml 95% ethanol and 100ml 85% (w/v) phosphoric acid. Once the dye has completely dissolved, dilute to 1 liter with deionized water. Bradford reagent was filtrated just before use. Protein samples were mixed with Bradford reagent with a ratio of 1:30. The mixture was vortexed and incubated at room temperature for 5 minutes and then transferred to cuvettes and measured the absorbance at 595nm. The absorbance was calibrated with bovine serum albumin (BSA) from 0.1 g/L to 1 g/L using the same method.

5.2.2.6 Protein precipitation

According to the concentration measured by the Bradford assay, starting volume for precipitation was calculated so that the total mass of the HCPs was 200 µg. In a 2 mL tube, DI water was added to the sample to 800 µL. Then 800µL methanol and 200µL chloroform were added into the tube, vortex well. The mixture was spined for 3 min at 14,000 g. The top aqueous layer was carefully pipetted off. Protein exists between layers and may be visible as a thin wafer. This interface protein layer was retained and added with 1.6 mL of methanol. Vortex well. The mixture was spined for 4 min at 14,000 g, and the top aqueous layer was carefully pipetted off without disturbing the pellet. The pellet was dried at room temperature. The pellet was then resuspended in 20 µL 8M urea, 20 mM Dithiothreitol (DTT) solution.

5.2.2.7 SDS-PAGE

The precast gel cassette was loaded and assembled in the electrophoresis cells and filled with running buffer (250 mM Tris, 1.92 M glycine, 1% SDS, pH 8.3). The resuspended mixture, spiked with 1 µg BSA as internal standard, was mixed with loading buffer(62.5 mM Tris-HCl, pH 6.8, 25% glycerol, 2% SDS, 0.01% bromophenol blue), then incubated in boiling water for 5

minutes, and loaded in the wells of the gel. The SDS-PAGE was run at 150 V constant voltage for about one and a half-hour. The gel was then taken down and stained with a Coomassie blue staining solution(0.1% Coomassie brilliant blue R-250, 40% methanol, 10% glacial acetic acid, and 50% DI water) overnight. Then the gel was incubated with destaining solution(20% methanol, 10% glacial acetic acid, and 70% DI water.) until the background was acceptably clear.

5.2.2.8 2D SDS-PAGE

The sample from precipitation (up to 30μL for 7cm Immobiline DryStrip) was mixed with rehydration solution (up to 120 μL, total volume), and transferred into an Immobilized pH gradient (IPG) holder. The IPG strip was positioned in the holder, and Immobiline DryStrip cover fluid was applied, proceeding with the rehydration overnight. IEF was performed in Ettan IPGphor 3 platform with the following steps: 300V hold 30 min; Gradient to 1000V 30 min; Gradient to 5000V 1 hour 20 min; 5000V hold 20 min. After IEF, strip was incubated the in reducing SDS equilibration buffer (6 M urea, 75 mM Tris-HCl pH 8.8, 29.3% glycerol, 2% SDS, 0.002% bromophenol blue, DTT 100 mg per 10 ml) for 15 min, and then incubated the strip in alkylation SDS equilibration buffer (6 M urea, 75 mM Tris-HCl pH 8.8, 29.3% glycerol, 2% SDS, 0.002% bromophenol blue, IAA 250 mg per 10 ml) for 15 min. The strip was then positioned on the top of SDS-PAGE gel together with 10 μL protein standard marker on the filter paper beside the strip. Strip and protein marker was sealed with sealing buffer(25 mM Tris base, 192 mM glycine, 0.1% SDS, 0.5% agarose, 0.002% bromophenol blue). The vertical SDS-PAGE was performed with 80 volts constant voltage in the first 30 min and then 100 volts to the end. After SDS-PAGE, the gel can be stained by Coomassie blue reagent and then destained with the solution described above.

5.2.2.9 LC/MS and MALDI/MS

The vertical lane of gel was chopped into 1 mm^3 pieces and transferred into 4 sterile microcentrifuge tubes. Those 4 tubes dices serve as fractions in order to enhance HCP detection. The dices were washed with 500 µL 25 ammonium bicarbonate. Then, the dices were washed with 500 µL of wash solution (50mM ammonium bicarbonate, 100% acetonitrile, 1:1 ratio) and incubated at room temperature until the Coomassie dye was completely removed with gentle agitation. Then the solution was pipetted off. The gel dices were dehydrated in 300 µL 100% acetonitrile for 5 min vortex. When the gel was completely dry at room temperature and acetonitrile was pipetted off. The gel pieces were rehydrated in 300 µL reduction solution (10 mM DTT, 25 mM ammonium bicarbonate) for 30 min at 56 C. Then the reduction solution was discarded, and 400 alkylation solution was added (25 mM iodoacetamide, 25 mM ammonium bicarbonate) and incubated for one hour in the dark at room temperature. After the alkylation solution was discarded with a pipette, 500 µL of wash solution (25 mM ammonium bicarbonate) was added and incubated at room temperature for 15 minutes with gentle agitation. Then the wash solution was pipetted off, and the gel was dehydrated in 400 µL 100% acetonitrile for 5 min, vortex. Discard acetonitrile and completely dry gel at room temperature. The dry gel was mixed with a trypsin digestion solution (10 ng/µL, 25 mM ammonium bicarbonate), incubated at 4 C for 30 minutes. Then 200 µL 25 mM ammonium bicarbonate was added to the top of the tube and incubated at 37 C overnight. Then the supernatant (containing tryptic peptides) was then transferred to a sterile centrifuge tube. Meanwhile, 300 µL of extraction solution (60% acetonitrile, 40% water, 5% formic acid) was added to gel pieces and vortex every 10 min for 3 times. Then the extraction solution was transferred and combined with the tryptic peptides supernatant from the last step.

5.2.2.10   Protein properties retrieval

The properties of these HCPs were then retrieved from the open-sourced

database(https://www.uniprot.org and https://www.expasy.org). The corresponding intensity

from the feed normalized the mass spectrum intensity of the backwash and the permeate. We

define the fouling index as 1 if the intensity of normalized backwash is higher than that in the

permeate or 0 if the intensity of normalized backwash is lower than that in the permeate. The

protein properties investigated include molecular weight (MW), isoelectric point (pI), protein

instability index, hydrophobicity index (GRAVY), aliphatic index (thermal stability), Rg/Rh

ratio, and subcellular locations.

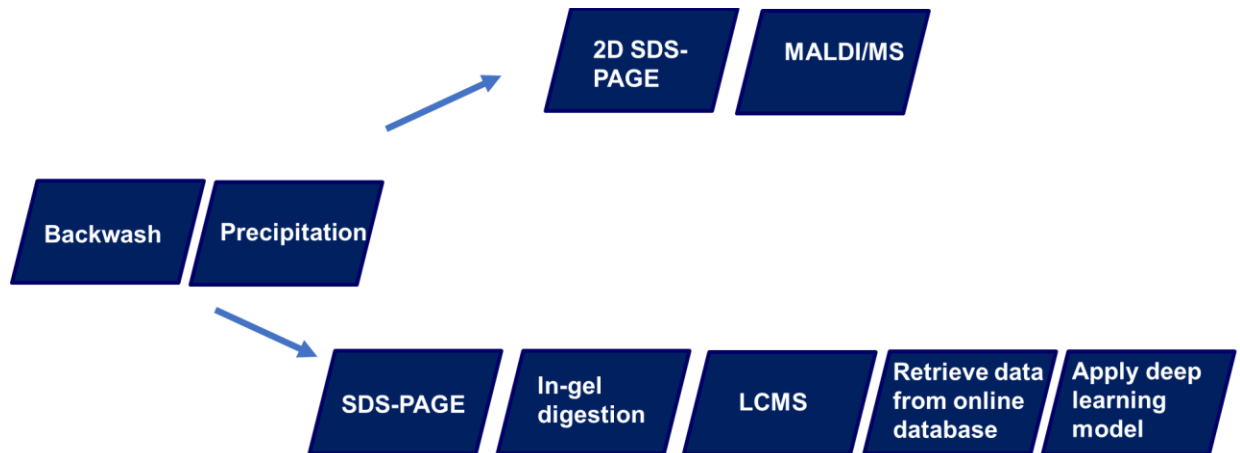5.2.2.11   The workflow of the proteomics study of the HCPs foulants

Figure 5.2 The workflow of the proteomics study of the HCPs foulants
        The workflow starts with the backwash samples, including the feed, permeate, backwash.

Bradford assay measures the concentration of the HCPs in the samples. The total concentration

of HCPs in each sample is required to be the same when SDS-PAGE and LC/MS are performed.

The goal of precipitation is to increase the concentration of the HCPs. A higher concentration

improves the LC/MS detection, especially for trace HCPs. Precipitation also normalizes the

concentration difference of the samples. After precipitation, the resuspended solution can be

carried out with 2D SDS-PAGE or SDS-PAGE for total HCPs detection by LC/MS. SDS-PAGE

133

achieves primary separation of the HCPs, and removes small particles, salts, and other soluble

impurities, therefore reducing the burden for LC/MS. LC/MS gives the total mass spectrum

count and can be followed by a deep learning model and other analyses.

5.3 Results and discussions

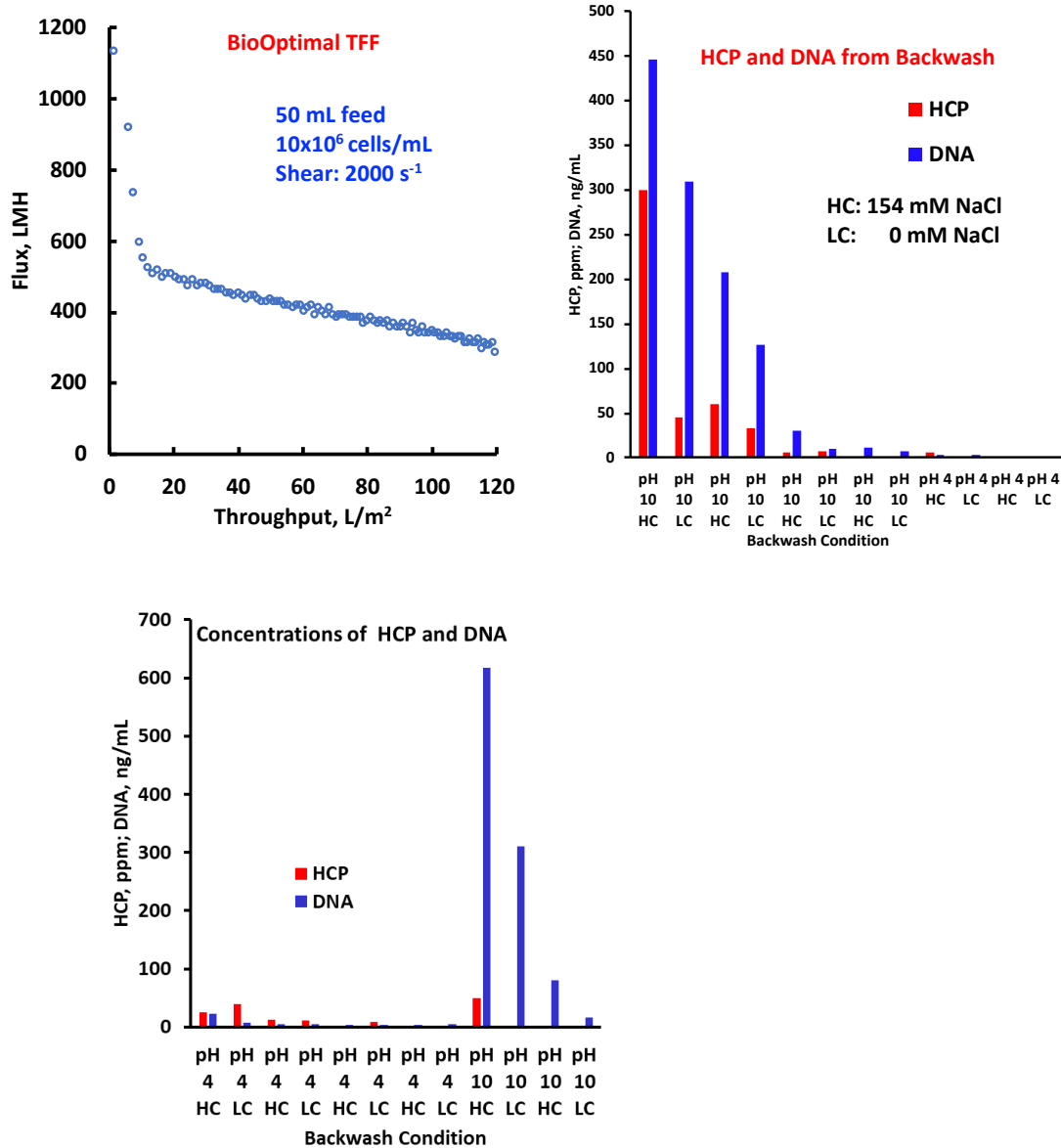### 5.3.1 Optimization of backwash conditions

Figure 5.3 Flux decay as a function of throughput during CHO harvesting using BioOptimal TM MF-SL (left); The HCP and DNA concentrations with repeated backwash using high conductivity (HC) and low conductivity (LC) phosphate buffers at pH 10 and pH 4 (right). The

HCP and DNA concentrations with repeated backwash using low conductivity (LC) and high conductivity (HC) phosphate buffers at pH 10 and pH 4 (bottom).

For CHO cell filtration, a rapid flux decay at the beginning of the filtration is followed by a steady slow flux decline, as shown in the left panel of Figure 5.3. The fouled filter was then backwashed with alternating high and low conductivity (HC, LC) buffers at pH 10 and then at pH 4 to extract foulants from the filter for subsequent analysis. As seen from the right panel of Figure 5.3, the HCPs and DNA are extracted effectively during backwash at pH 10. After the third HC and LC cycle, the extracted total HCP concentration is reduced to less than 20 ppm, whereas the DNA concentration is reduced to less than 10 ng/mL. The second washing strategy reverses the order with repeated pH 4 washing followed by pH 10. The fouling in the HCPs and DNA still comes with a high pH washing solution. It can be seen that pH 10 washing is more effective in releasing the foulants than washing at pH 4. This work demonstrates the establishment of high pH as an effective method for releasing foulants from the fouled filter.

After two sets of backwashing studies, the TMPs measured by DI water filtration for the clean and fouled filters are plotted in the Figure 5.4. It can be seen that the TMPs are higher for the filters even after repeated washing.
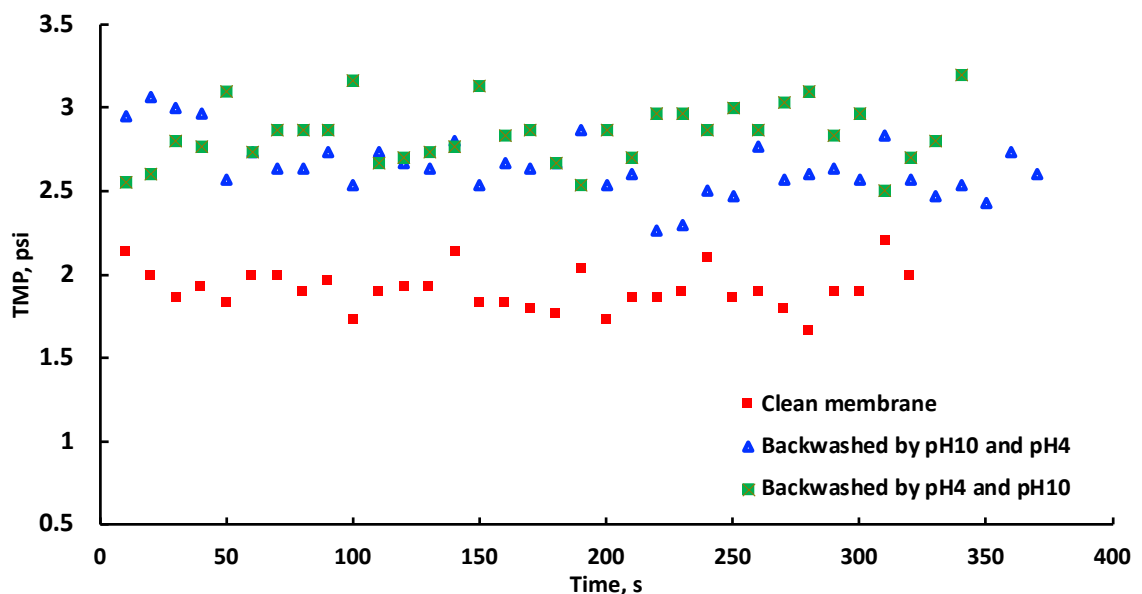

135

Figure 5.4 Flux recoveries after backwash

In order to further investigate the characteristics of the residue foulants on the membrane even after repeated washing at different pH and conductivity, confocal imaging of the fouled filter stained for both DNA (blue) and protein (orange) was conducted, as shown in Figure 5.5. The signals are very weak compared to a fouled membrane (See Figure 3.8 in chapter 3). Considering the pressure difference is very small (about 1 psi), the residual foulants on the membrane appear to be relatively small.

High pH solution is widely used in fouled membrane cleaning[27]. Studies have recommended high pH values cleaning agents with trisodium phosphate, sodium tripolyphosphate, and EDTA [28]. Still, cleaner with too many strong chemicals would cause lysing of the cell, further creating foulant artificially. The CHO cells were incubated in different buffers at room temperature for 30 min. The released HCPs and DNA concentrations are determined using Bradford and Picogreen assays, respectively. The buffer conditions that lead to enhanced release of HCPs and DNA and the appearance of the floc are studied. It was found that CHO cells are stable in PBS buffer in the pH range of 4-10. CHO cells are not stable in Tris buffer at pH above 9 where flocs of CHO were observed. In this study, a relatively mild buffer, 20 mM phosphate, pH 10, was used to extract the foulants.
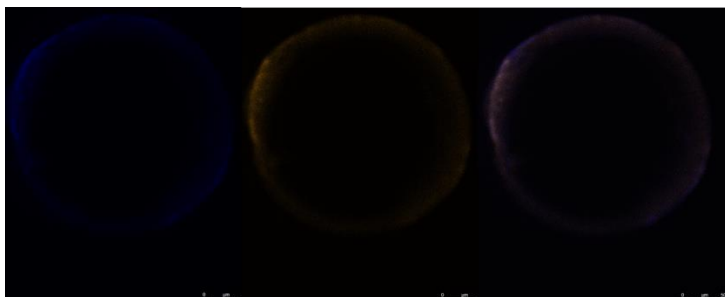
Magnification: 50 times
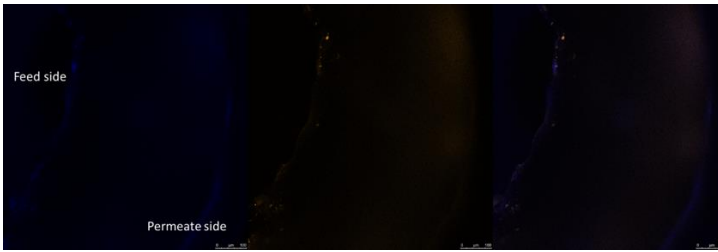
Magnification: 200 times

Figure 5.5 Confocal imaging of fouled filter after repeated washing by pH 10 and pH 4. The blue color represents DNA, and the orange color represents a protein.

5.3.2 CHO cell filtration with different cell viability
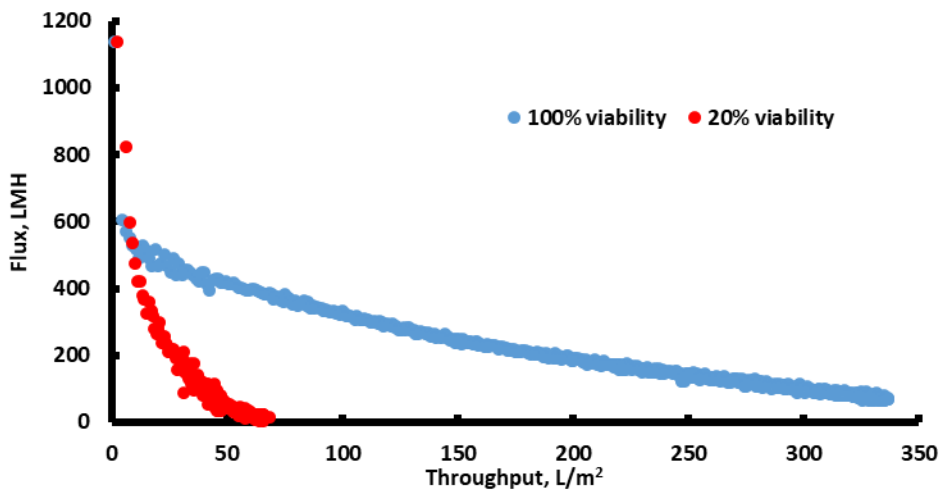
Figure 5.6 Flux decay with different viability

In order to better understand the fouling propensity of the HCPs, different operation conditions and cell viabilities are needed. Here CHO cells were grown to about 12 millions/mL with 100% and 20% viability, and feed volumes of 500 mL were investigated. Figure 5.6 shows the flux decay of the two sets of experiments at 100 and 20% cell viability. The flux decay is consistent with a higher concentration of HCPs and DNA shown below.

Table 5.2 The HCP and DNA concentrations in the feed, permeate, backwash 1, backwash 2 and backwash 3 for the CHO filtration at 100% and 20% viability. The backwash was performed under phosphate buffer at pH 10 with 150 mM NaCl..

		Feed	Permeate	Backwash 1	Backwash 2	Backwash 3
Viability 100%	HCP (ppm)	360	318	343	37	0
	DNA (ng/mL)	1086	1156	1112	667	303
Viability 20%	HCP (ppm)	2461	1841	381	0	0
	DNA (ng/mL)	1577	1718	1264	375	214

Viability has the most important contribution to fouling[17, 18]. As shown in the table, the HCP concentration of 20% viability is 7 times higher than that of 100% viability. However, permeate concentration is only 6 times higher. Clearly, more HCPs were retained on the membrane in low viability samples. Residual DNA is also increased in low viability samples, while a high concentration is found in permeate due to the lysing of the cell from the shear stress. Shen et al. investigated the size of residual DNA in the cell culture [29]. The medium length of residual DNA was 200 bp or 123 kDa, which was the same molecular weight range as most HCPs. However, the shape of DNA is linear and is ready to penetrate the membrane. Compared to the HCPs in the same molecular weight, DNA is more permeable. DNA is eluted gradually through the fractions during the backwash because it is trapped in the membrane matrix. The membrane structure of BioOptimal[TM] MF-SL is similar to the depth filter, and this entrapment is more significant than a screen-type filter. The visualization of DNA fouling in BioOptimal can be found in the previous study[30].

138

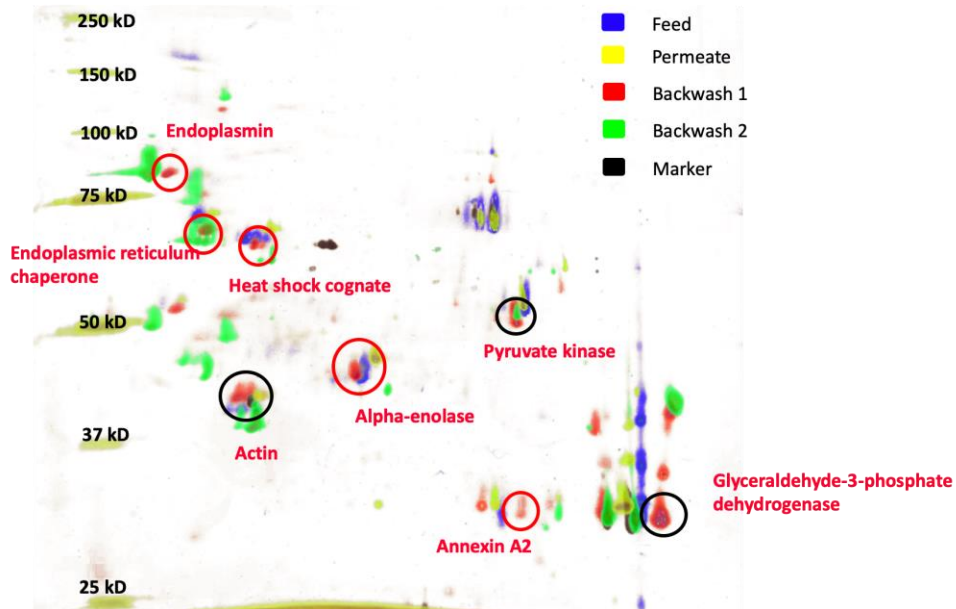### 5.3.3 Proteomics study of the HCPs foulants

Figure 5.7 2D SDS PAGE (vertical, MW; horizontal, pI) to identify HCPs in the feed, permeate and extract samples from the fouled membrane.

Table 5.3 Identified HCPs from both gel electrophoresis and MALDI-MS. The corresponding spots on the 2D electropherogram are shown in the Figure above.

2D IEF SDS PAGE	MALDI-MS	Identified Host Cell Proteins
(pI, MW in kD)	(pI, MW in kD)	
5.1, 43	5.2, 42	Actin, cytoplasmic 1
7.3, 51	7.9, 58	Pyruvate kinase PKM
8.5, 36	9.2, 36	Glyceraldehyde-3-phosphate dehydrogenase
<5.1, 90	4.6, 92	Endoplasmin
~5.1, 75	4.9, 72	Endoplasmic reticulum chaperone BiP
~5.1, 70	5.2, 71	Heat shock cognate
5.7, 47	6.4, 47	Alpha-enolase
7.9, 36	8.5, 39	Annexin A2

In order to analyze and identify the extracted HCP, 2D SDS PAGE gel electrophoresis

was performed. Figure 5.7 shows the 2D SDS PAGE gel of the feed, the permeate, backwash 1

(~280 ppm), and backwash 2 (~60 ppm) samples at pH 10 and high conductivity elution. The

horizontal dimension is the isoelectric point (pI) distribution, and the vertical dimension is the

molecular weight (MW) distribution. It can be seen that 2D SDS PAGE separates the HCPs based on their pI and MW for these samples with high resolution. In addition, MALDI-MS is performed with in-gel digestion to identify these released foulants further. For the abundant 8 spots on 2D SDS PAGE, the pI and MW from MALDI-MS identification match well with the 2D gel, as shown in Table 5.3. Good agreement is obtained between the two MALDI MS and 2D SDS PAGE.

Abundant HCPs are found in the pI around 5, consistent with previous studies[11]. The main HCPs locate in the left-bottom corner, which is consistent with Jin et al.'s observation [24]. The HCPs in the backwash samples also prevail in this trend, where the top right corner is abundant in feed and permeate, and the bottom right corner is abundant in feed and backwash. HCPs of backwash fraction 2 in acidic molecular weight 50kDa area are not found in other samples. The identified HCPs in the list are the abundant spots from backwash fraction 1, indicating the filter rejects those HCPs. Interestingly, the list covers serval problemic HCPs from previous research, such as the actin, glyceraldehyde-3-phosphate dehydrogenase, heat shock 70 kDa protein, and pyruvate kinase, which easily interacts with mAbs. The majority of those HCPs have a catalytic function, suggesting active enzymic interaction with these mAbs, or other HCPs [22]. The resulting interaction between HCPs contributes to forming large aggregates, which are more likely to foul the filter. In addition, the retention of those HCPs may trap the permeation of mAbs, which causes a decrease in the sieving.

Compared to 2D SDS-PAGE in different viabilities, more HCPs species have low viability in the backwash's bottom right corner of the feed and center area. These results indicate low viability cell culture has a higher potential to foul the membrane and cause the low sieving for the mAbs. Since the individual HCP concentration in the feed solution is relatively low, LC-

MS/MS will be used for low-concentration HCPs, and multiple HCP will be detected in one batch.
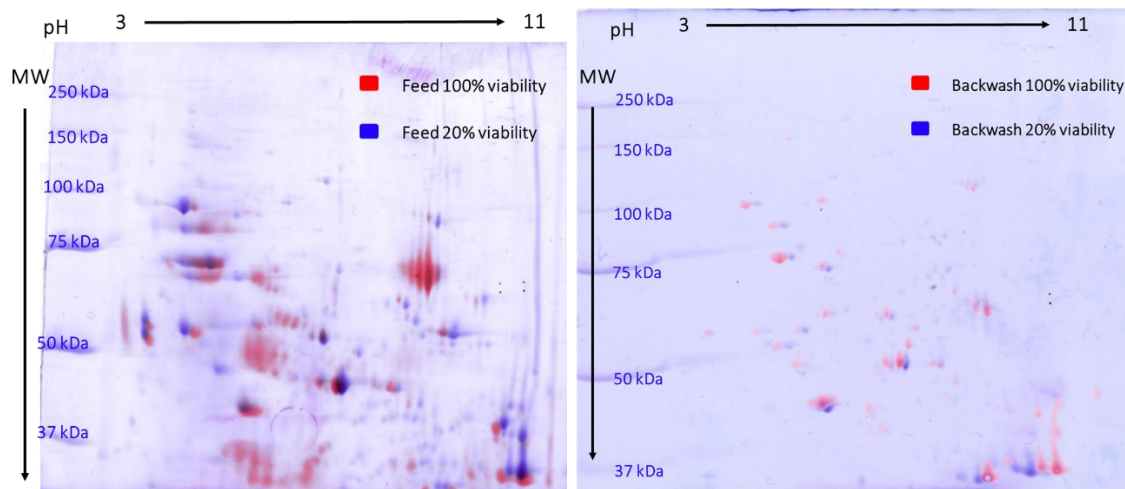

Figure 5.8 2D SDS PAGE of feed and backwash in 100% viability and 20% viability.

5.3.4 LCMS identification and model prediction

2D SDS PAGE followed by MALDI-MS has identified the abundant HCP. However, the low concentration HCPs in the sample are not quantitively determined. Here, LC/MS are performed with the extracted HCPs. The deep learning model is used to identify and predict the HCPs that are more fouling. The fouling index to be predicted is 0 if the mass spectrum count in the backwash is higher than permeate, 1 if the mass spectrum count in the backwash is lower than permeate. The model has three layers. The hidden layer has 30 nodes, and the output layer has 1 node, as shown in Figure 5.9. A total of 80% of the dataset is used to train the model, and the remaining 20% is used to test the model. 20% of the training dataset is used to validate the model during the training. The model is trained by 200 epochs and optimized by mean square displacement (MSD). Protein properties investigated include molecular weight (MW), isoelectric point (pI), protein instability index, hydrophobicity index (GRAVY), aliphatic index (thermal stability), Rg/Rh ratio, and subcellular locations. The accuracy is about 76% for unknown HCPs

as the prediction. A better choice of more related properties and values of the properties that

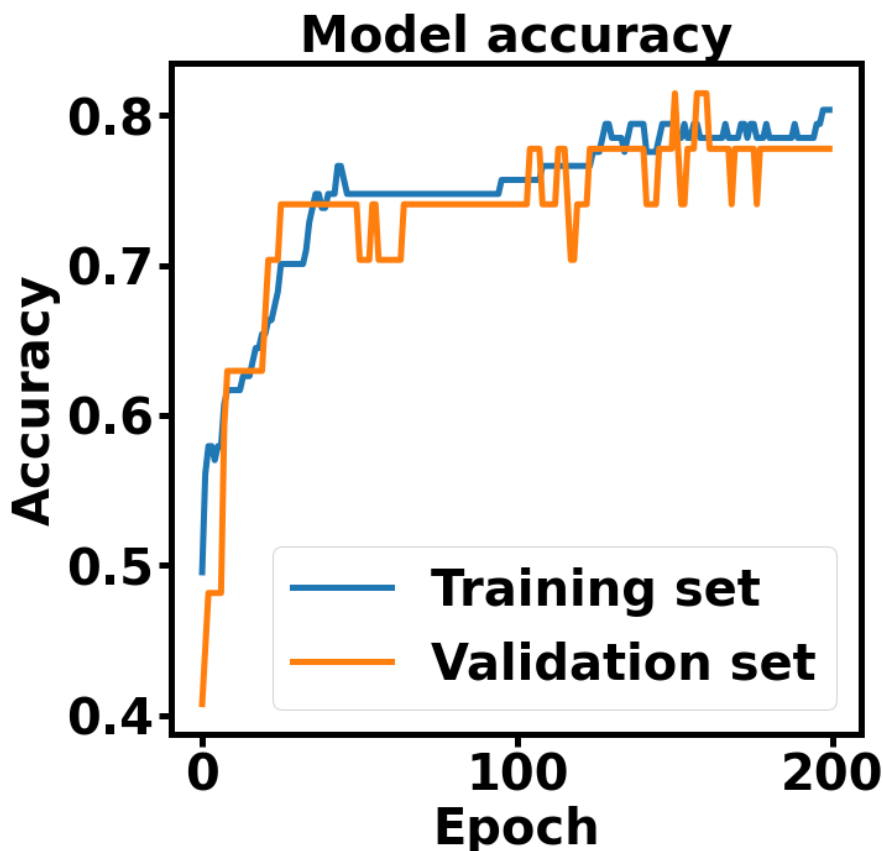reflects the real conditions may help to improve the prediction accuracy.

Figure 5.9 Accuracy of deep learning model, trained by culture in normal viability

5.4   Conclusion.

Proteomics analysis was applied to characterize the fouling during the cell clarification

process using a reverse asymmetric membrane. The phosphate buffer, pH 10 was found to be

efficient for foulants extraction. 2D SDS-PAGE followed by MALDI/MS identified the most

abundant HCPs in the extraction. The HCPs are found intensively in the bottom-left diagonal of

the gel. The rejection of those HCPs on the membrane is due to their enzymatic properties. Since

the individual HCP concentration in the feed solution is relatively low, LC-MS/MS is used for

low-concentration HCPs. The list of identified HCPs forms a dataset, including the properties

such as include molecular weight (MW), isoelectric point (pI), protein instability index,

hydrophobicity index (GRAVY), aliphatic index, Rg/Rh ratio, and subcellular locations. The

dataset is used to train a deep learning model, and an accuracy of about 76% is achieved to

predict the fouling potential. This deep learning model can be used to predict the fouling of

protein providing the amino acid sequence. The dataset of identified HCPs in this study provides

insights into the characterization of membrane fouling, membrane selection, and process

development.

5.5 Acknowledgements

Reference

1.   Usmani, S.S., et al., *THPdb: Database of FDA-approved peptide and protein therapeutics.* PloS one, 2017. **12**(7): p. e0181748.

2.   Xu, N., et al., *Comparative proteomic analysis of three Chinese hamster ovary (CHO) host cells.* Biochemical engineering journal, 2017. **124**: p. 122-129.

3.   Lakshmanan, M., et al., *Multi-omics profiling of CHO parental hosts reveals cell line-specific variations in bioprocessing traits.* Biotechnology and bioengineering, 2019. **116**(9): p. 2117-2129.

4.   Gimenez, L., et al. *Overcoming the clarification challenges of high cell density culture*. in *BMC Proceedings*. 2015. BioMed Central.

5.   Bielser, J.-M., et al., *Perfusion mammalian cell culture for recombinant protein manufacturing–A critical review.* Biotechnology advances, 2018. **36**(4): p. 1328-1340.

6.   Bolton, G.R. and A.J. Apostolidis, *Mechanistic modeling of the loss of protein sieving due to internal and external fouling of microfilters.* Biotechnology Progress, 2017. **33**(5): p. 1323-1333.

7.   Guiochon, G. and L.A. Beaver, *Separation science is the key to successful biopharmaceuticals.* Journal of Chromatography a, 2011. **1218**(49): p. 8836-8858.

8.   Hogwood, C.E., D.G. Bracewell, and C.M. Smales, *Host cell protein dynamics in recombinant CHO cells: impacts from harvest to purification and beyond.* Bioengineered, 2013. **4**(5): p. 288-291.

9.   Goey, C.H., S. Alhuthali, and C. Kontoravdi, *Host cell protein removal from biopharmaceutical preparations: Towards the implementation of quality by design.* Biotechnology advances, 2018. **36**(4): p. 1223-1237.

10.   Joucla, G., et al., *Cation exchange versus multimodal cation exchange resins for antibody capture from CHO supernatants: Identification of contaminating Host Cell Proteins by mass spectrometry.* Journal of Chromatography B, 2013. **942**: p. 126-133.

11.   Molden, R., et al. *Host cell protein profiling of commercial therapeutic protein drugs as a benchmark for monoclonal antibody-based therapeutic protein development.* in *Mabs.* 2021. Taylor & Francis.

12.   Chiu, J., et al., *Knockout of a difficult-to-remove CHO host cell protein, lipoprotein lipase, for improved polysorbate stability in monoclonal antibody formulations.* Biotechnology and bioengineering, 2017. **114**(5): p. 1006-1015.

13.   Zhu-Shimoni, J., et al., *Host cell protein testing by ELISAs and the use of orthogonal methods.* Biotechnology and bioengineering, 2014. **111**(12): p. 2367-2379.

14.   Gronemeyer, P., R. Ditz, and J. Strube, *DoE based integration approach of upstream and downstream processing regarding HCP and ATPE as harvest operation.* Biochemical Engineering Journal, 2016. **113**: p. 158-166.

15.   Mörtstedt, H., et al., *Improved identification of host cell proteins in a protein biopharmaceutical by LC–MS/MS using the ProteoMiner™ Enrichment Kit.* Journal of Pharmaceutical and Biomedical Analysis, 2020. **185**: p. 113256.

16.   Capito, F., et al., *Host cell protein quantification by fourier transform mid infrared spectroscopy (FT-MIR).* Biotechnology and Bioengineering, 2013. **110**(1): p. 252-259.

17.   Parau, M., et al., *Analysis of fouling and breakthrough of process related impurities during depth filtration using confocal microscopy.* Biotechnology Progress, 2022: p. e3233.

18.   Grzeskowiak, J.K., et al., *2-D DIGE to expedite downstream process development for human monoclonal antibody purification.* Protein expression and purification, 2009. **66**(1): p. 58-65.

19.   Park, J.H., et al., *Proteomic analysis of host cell protein dynamics in the culture supernatants of antibody-producing CHO cells.* Scientific reports, 2017. **7**(1): p. 1-13.

20.   Levy, N.E., et al., *Identification and characterization of host cell protein product-associated impurities in monoclonal antibody bioprocessing.* Biotechnology and bioengineering, 2014. **111**(5): p. 904-912.

21.   Tait, A.S., et al., *Host cell protein dynamics in the supernatant of a mAb producing CHO cell line.* Biotechnology and Bioengineering, 2012. **109**(4): p. 971-982.

22.   Liu, X., et al., *Identification and characterization of co-purifying CHO host cell proteins in monoclonal antibody purification process.* Journal of Pharmaceutical and Biomedical Analysis, 2019. **174**: p. 500-508.

23.   Goey, C.H., et al., *Cascading effect in bioprocessing—the impact of mild hypothermia on CHO cell behavior and host cell protein composition.* Biotechnology and Bioengineering, 2017. **114**(12): p. 2771-2781.

24.   Jin, M., et al., *Profiling of host cell proteins by two-dimensional difference gel electrophoresis (2D-DIGE): Implications for downstream process development.* Biotechnology and bioengineering, 2010. **105**(2): p. 306-316.

25.   Yuk, I.H., et al., *More similar than different: Host cell protein production using three null CHO cell lines.* Biotechnology and bioengineering, 2015. **112**(10): p. 2068-2083.

26.   Valente, K.N., A.M. Lenhoff, and K.H. Lee, *Expression of difficult-to-remove host cell protein impurities during extended Chinese hamster ovary cell culture and their impact on continuous bioprocessing.* Biotechnology and Bioengineering, 2015. **112**(6): p. 1232-1242.

27.   Madaeni, S.S., T. Mohamamdi, and M.K. Moghadam, *Chemical cleaning of reverse osmosis membranes.* Desalination, 2001. **134**(1-3): p. 77-82.

28.   Al-Amoudi, A., et al., *Cleaning results of new and fouled nanofiltration membrane characterized by zeta potential and permeability.* Separation and purification technology, 2007. **54**(2): p. 234-240.

29.   Shen, X., et al., *Size analysis of residual host cell DNA in cell culture-produced vaccines by capillary gel electrophoresis.* Biologicals, 2013. **41**(3): p. 201-208.

30.   Zhang, D., et al., *Modeling flux in tangential flow filtration using a reverse asymmetric membrane for Chinese hamster ovary cell clarification.* Biotechnology Progress, 2021. **37**(3): p. e3115.

Chapter 6.   Proteomics analysis of host cell protein in the perfusion cell culture

Summary: Alternating tangential flow (ATF) based perfusion cell culture is the continuous form of the bioreaction and is employed for the production of biopharmaceuticals. Its high cell density, mild shear rate, and long-term expression have made widely research interest. Here the fouling of ATF filter during industrial perfusion and in-house perfusion has been analyzed using liquid chromatography/mass spectrometry (LC/MS). The results show the molecular weight and pI distribution of HCPs show different across the companies, i.e Amgen, Biogen and MilliporeSigma. The overall molecular weight distribution in Amgen is higher than in Biogen and MilliporeSigma. In pI distributions, there are two major peaks in the backwash samples from all the companies. The first peak in Biogen shows a more acidic trend, while Amgen shows a basic trend. The perfusion run at the University of Arkansas compared the fouling in three different filters. The results showed that the pore size and membrane materials affect the fouling of the filter, and pI distribution is more sensitive to the condition.

6.1   Introduction

In biopharmaceutics manufacturing, suspension culture technologies improve product titer dramatically[1]. Today the industry standard for producing stable proteins such as monoclonal antibodies (mAbs) is a fed-batch process in stirred tank bioreactors of up to 20 kL[2]. However, mixing difficulties, large footprint, and slow product transition has limited the development of the fed-batch process. These limitations are addressed by the recent advances in perfusion technologies[3]. The perfusion allows the manufacturer to use a smaller bioreactor in the continuous mode, with high cell density and extended culture period. The perfusion cell culture is featured in its cell retention device. Tangential flow filters and alternating tangential

147

flow filters are compatible with perfusion bioreactors, although the ATF filter attracts more attention.

In ATF perfusion cell culture, the hollow fibers are pressurized and exhausted alternatively, where the membrane is backwashed repeatedly. Therefore, the ATF perfusion is considered a mild process compared to TFF[4]. However, with high cell density achieved in perfusion cell culture, the fouling of ATF filter results in low product titer, sieving, and product quality. A better understanding of the fouling in the perfusion will provide insights into membrane selection, cell line development, and process optimization.

Cell culture includes process-related impurities such as cell debris, whole cells, host cell protein(HCPs), host cell DNA, poloxamer, and antifoam[2, 5]. The cell retention device in the perfusion is easy to foul because those impurities are boosted due to the extended bioreaction. The cell density in the perfusion cell culture is normally higher than 20 million per mL[6]. Therefore, the cell debris, host cell DNA generated, and poloxamer used in the perfusion are higher than in batch mode[6]. In addition to the process-related impurities, the production and viscosity of the cell culture also increase[7]. Clincke et al. report their system can reach a maximal cell density of 1.3×10^8 cells/mL followed by the vacuum capacity failing to pull the highly viscous fluid[7]. Due to the dilution of the fresh medium, the transient concentration of mAbs is lower than batch mode, typically less than 2 g/L[3, 8]. However, the accumulated mAbs are much higher than in batch mode. Product concentration in fed-batch is 2.5 times greater than perfusion, while average productivity in perfusion is 7.5 times greater than fed-batch[3]. Using 10L WAVE Bioreactor, a total of 93 g of mAbs is harvested after 47 days from the study of Clincke et al. [9]. Those impurities, products, and physical changes of the culture limit the application of perfusion.

Host cell proteins (HCPs) are endogenous proteins derived from the host cells used for bioproduction [10]. HCPs could be generated from cell debris, secreted protein, and cell lysate. More than 6,000 HCPs have been found in the CHO cell proteome, and many HCPs are released to cell culture fluid (CCF) as the results of secretion and cell lysis caused by either normal cell death or shear stress during harvest[11]. HCPs form a major class of process-related impurities because they can potentially cause the patient's immune response. Second, HCPs consist of thousands of proteins. Each protein has a various molecular weight, isoelectric point, and hydrophobicity; therefore, the peripeties of HCPs need to be studied and determined case by case. Third, the HCPs are normally co-purified with biopharmaceutics, for example, monoclonal antibodies. Final recombinant mAb products must be clear of impurities and typical target levels of impurities are <100 ppm of HCP. Therefore, the present of HCPs cannot be ignored.

HCP level in the harvested cell culture from a particular production platform depends on the cell culture process and harvest conditions. Cell viability plays an important role at the HCP level. Low viability cell culture involves more cell debris, cells with fewer diameters, and high HCPs due to lysing of the cells, applying more burden on the downstream purification steps. Removal of HCPs occurs at the beginning of the purification, i.e., cell clarification, and is expected in each unit operation.

In this study the fouling of the filters from industrial perfusion bioreaction is analyzed. The fouling HCPs are identified using LCMS and compared across the companies. Three additional perfusions are performed at the University of Arkansas. Three filters have been tested in 2 weeks of perfusion. The Repligen and UMP have been studied in perfusion cell culture elsewhere[3, 12]. However, the application of BioOptimal^{TM} MFSL in perfusion mode has not been reported. The information on the filters is shown in the table below

Table 6.1 Information on the filters used in the perfusion cell culture

	Repligen	**Asahi**	**Asahi**
Model	F2:RF02PES	UMP	BioOptimal MFSL
Pore size (µm)	0.2	0.2	0.4-40
Membrane area (m2)	0.13	0.1	0.1
Materials	PES	PVDF	PSF
Module	Hollow fiber	Hollow fiber	Hollow fiber

6.2   Materials and methods

6.2.1   Perfusion cell culture

An IgG-producing CHOZN cell line was used in all the experiments. EX-CELL®

Advanced HD Perfusion Mediumwere used for the perfusion cell culture. The cells were firstly

expanded in shake flasks at 37°C, 120 rpm and 5% of CO_2, and then were transferred to a

Sartorius BioStat A plus with a starting cell density of 1 million viable cells per milliliter in 1.5 L

working volume. Repligen alternating tangential flow-2 (ATF-2) filtration system was used for

perfusion system set-up. Set points for pH, temperature and DO were 7, 37°C and 40%.

Perfusion was initiated one day after inoculation at 1 reactor volume per day (RV/day). The

perfusion rate was then increased to 1 RV/day on the following day (day 1) and further increased

to 1.5 RV/day when the cell density approached a value of 10 million viable cells per milliliter.

After that, the perfusion rate was maintained at 1.5 RV/day. The perfusion run was performed for

14 days. Three runs were conducted in house using three different hollow fiber modules as given

in Table 6.1

Proprietary industrial perfusions were performed onsite in Amgen, Biogen, and

MilliporeSigma. Four runs at Biogen and Amgen used similar though not identical conditions

respectively. However all runs were conducted in ATF mode. The five runs conducted at

MilliporeSigma used not only slightly different conditions but also TFF and ATF was investigated. Fouled filter in Amgen and Biogen. Bioreactor, permeate, and backwash samples were shipped to the University of Arkansas with dry ice. The filter from the MilliporeSigma was flushed with PBS buffer onsite right after the perfusion. Then the filter was drained and shipped to the University of Arkansas at 4 °C. The filter was carried out with backwash after being received. All the backwash samples from the 3 companies were performed using the in-gel digestion method. The digested peptides were submitted to LC/MS..

6.2.2   The workflow of the proteomics study of the HCPs foulants

Figure 6.1The workflow of the proteomics study of the HCPs foulants
        The workflow starts with the backwash samples, including the feed, permeate, backwash. Bradford assay measures the concentration of the HCPs in the samples. The total concentration of HCPs in each sample is required to be the same when SDS-PAGE and LC/MS are performed. The goal of precipitation is to increase the concentration of the HCPs. A higher concentration improves the LC/MS detection, especially for trace HCPs. Precipitation also normalizes the concentration difference of the samples. After precipitation, the resuspended solution can be carried out with SDS-PAGE for total HCPs detection by LC/MS. Amgen samples are treated with protein A due to the excess mAbs, which disturb the HCP identification. SDS-PAGE achieves primary separation of the HCPs, and removes small particles, salts, and other soluble impurities, therefore reducing the burden for LC/MS. LC/MS gives the total mass spectrum count and can be followed by other analyses.

6.2.3 Fouling extraction

After filtration, the residual cell culture inside and outside the lumen was drained by gentle shaking. The lumen of the fiber was flushed with backwash solution at a slow flow rate(<10mL/min or <1 psi hydraulic pressure) to remove the residual cell or cell debris in the lumen. Then shell side of the filter was flushed with backwash solution for about 200 mL and finally filled with backwash solution. Backwash was performed by pumping the backwash solution from the shell side to the inside of the fiber. The extracted foulants are collected at the lumen port. The backwash pressure was as high as possible but must be lower than membrane tolerance. For each backwash, the fouling was collected as three fractions.

6.2.4 Protein precipitation

According to the concentration measured by the Bradford assay, starting volume for precipitation was calculated so that the total mass of the HCPs was 200 µg. In a 2 mL tube, DI water was added to the sample to 800 µL. Then 800µL methanol and 200µL chloroform were added into the tube, vortex well. The mixture was spined for 3 min at 14,000 g. The top aqueous layer was carefully pipetted off. Protein exists between layers and may be visible as a thin wafer. This interface protein layer was retained and added with 1.6 mL of methanol. Vortex well. The mixture was spined for 4 min at 14,000 g, and the top aqueous layer was carefully pipetted off without disturbing the pellet. The pellet was dried at room temperature. The pellet was then resuspended in 20 µL 8M urea, 20 mM Dithiothreitol (DTT) solution.

6.2.5 Protein A chromatography

All chromatography experiments were performed using 1mL pre-packed HiTrap Protein A HP antibody purification columns(Cytiva, Marlborough, MA, USA) using an ÄKTA FPLC (GE Healthcare Bio-Sciences Corp, Chicago, IL, USA).and at a linear flow rate of 1 mL/min.

The washing buffer contains 0.02 M sodium phosphate, pH 7.0, and the elution buffer contains 0.1 M sodium citrate, pH 3.0 were filtered before use. 0.5 mL filtered samples solution containing HCPs and mAbs was loaded onto the membrane at a flow rate of 1 mL/min. Unbound proteins(HCPs) were then washed from the columns using the washing buffer for 10 min at 1 mL/min, followed by elution with elution buffer at a flow rate of 1 mL/min for 10 min. The runs ended when the UV absorbance at 280 nm reached a constant. The peak during the washing was monitored and collected based on the UV absorbance.

6.2.6   SDS-PAGE

The precast gel cassette was loaded and assembled in the electrophoresis cells and filled with running buffer (250 mM Tris, 1.92 M glycine, 1% SDS, pH 8.3). The resuspended mixture, spiked with 1 μg BSA as internal standard, was mixed with loading buffer(62.5 mM Tris-HCl, pH 6.8, 25% glycerol, 2% SDS, 0.01% bromophenol blue), then incubated in boiling water for 5 minutes, and loaded in the wells of the gel. The SDS-PAGE was run at 150 V constant voltage for about one and a half-hour. The gel was then taken down and stained with a Coomassie blue staining solution(0.1% Coomassie brilliant blue R-250, 40% methanol, 10% glacial acetic acid, and 50% DI water) overnight. Then the gel was incubated with destaining solution(20% methanol, 10% glacial acetic acid, and 70% DI water.) until the background was acceptably clear.

6.2.7   LC/MS

The vertical lane of gel was chopped into 1 mm^3 pieces and transferred into 4 sterile microcentrifuge tubes. Those 4 tubes of dices serve as fractions in order to enhance HCP detection. The dices were washed with 500 μL 25 ammonium bicarbonate. Then, the dices were washed with 500 μL of wash solution (50mM ammonium bicarbonate, 100% acetonitrile, 1:1

153

ratio) and incubated at room temperature until the Coomassie dye was completely removed with gentle agitation. Then the solution was pipetted off. The gel dices were dehydrated in 300 µL 100% acetonitrile for 5 min vortex. When the gel was completely dry at room temperature and acetonitrile was pipetted off. The gel pieces were rehydrated in 300 µL reduction solution (10 mM DTT, 25 mM ammonium bicarbonate) for 30 min at 56 C. Then the reduction solution was discarded, and 400 alkylation solution was added (25 mM iodoacetamide, 25 mM ammonium bicarbonate) and incubated for one hour in the dark at room temperature. After the alkylation solution was discarded with a pipette, 500 µL of wash solution (25 mM ammonium bicarbonate) was added and incubated at room temperature for 15 minutes with gentle agitation. Then the wash solution was pipetted off, and the gel was dehydrated in 400 µL 100% acetonitrile for 5 min, vortex. Discard acetonitrile and completely dry gel at room temperature. The dry gel was mixed with a trypsin digestion solution (10 ng/µL, 25 mM ammonium bicarbonate), incubated at 4 C for 30 minutes. Then 200 µL 25 mM ammonium bicarbonate was added to the top of the tube and incubated at 37 C overnight. Then the supernatant (containing tryptic peptides) was then transferred to a sterile centrifuge tube. Meanwhile, 300 µL of extraction solution (60% acetonitrile, 40% water, 5% formic acid) was added to gel pieces and vortex every 10 min for 3 times. Then the extraction solution was transferred and combined with the tryptic peptides supernatant from the last step.

6.3 Results and discussions

6.3.1 SDS-PAGE

After extraction and protein precipitation, SDS-PAGE was performed as shown in Figure 6.2-Figure 6.5. The Biogen and MilliporeSigma samples contain two main bands that belong to the mAbs. The Amgen samples have more intensive mAbs that affect the HCP identification.

Therefore the samples are treated with protein A. SDS-PAGE shows that HCPs cover the MW

range from 250 kDa to less than 25 kDa. Some HCPs'MW is closed to the heavy chains and light

chains of the mAbs. The medium length of residual DNA was 200 bp or 123 kDa, which was the

same molecular weight range as most HCPs. SDS-PAGE serves as a preliminary separation and

fractionation to eliminate those impurities, leaving the HCPs in the samples. SDS-PAGE

improves the later LCMS detection in our preliminary study using in-solution digestion where

SDS-PAGE is not involved.
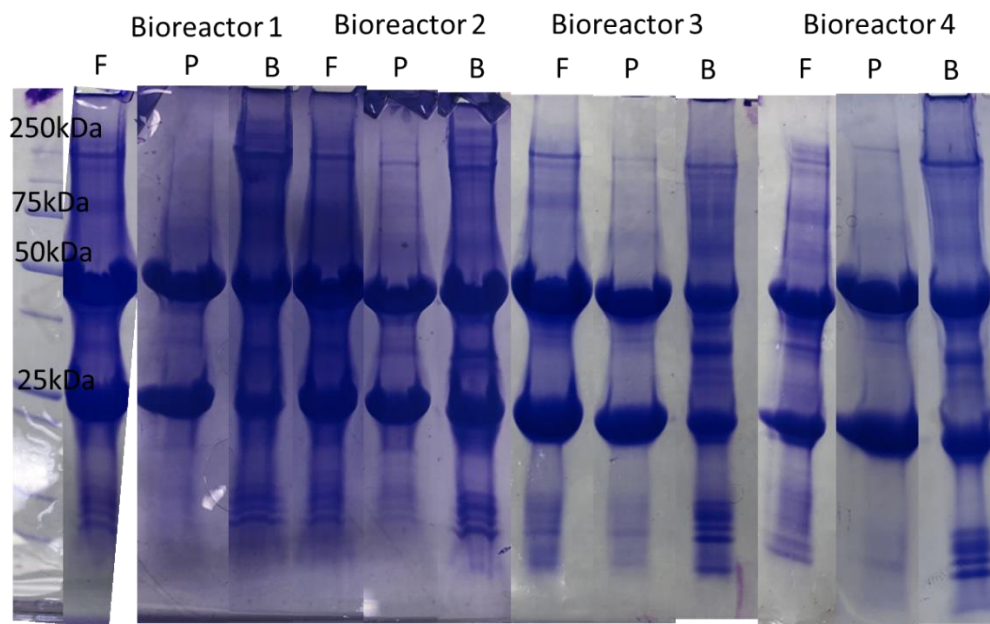
Figure 6.2 SDS-PAGE of samples from Biogen, F represents the feed sample, P represents permeate sample, B represents the backwash sample.
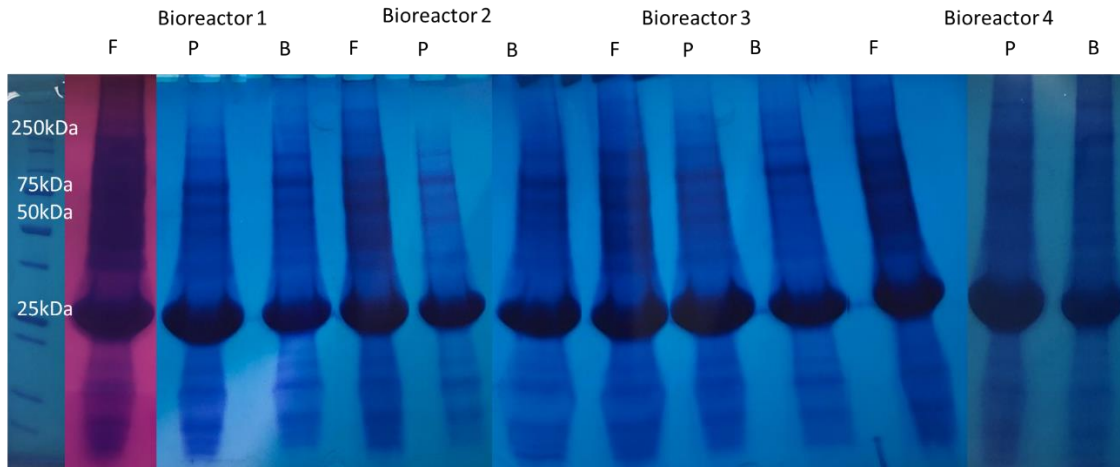
Figure 6.3 SDS-PAGE of samples from Amgen, F represents the feed sample, P represents permeate sample, B represents the backwash sample.
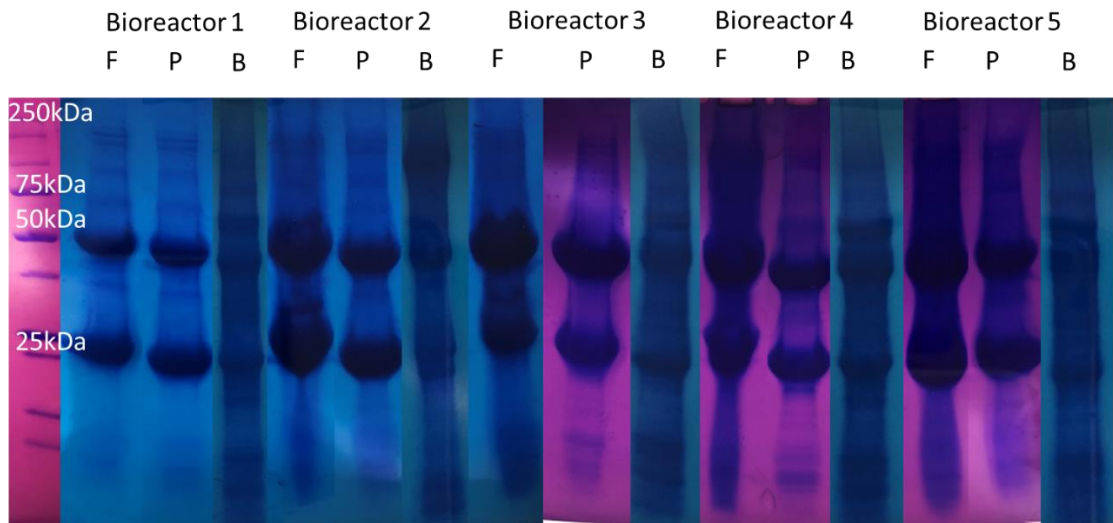

Figure 6.4 SDS-PAGE of samples from MilliporeSigma, F represents the feed sample, P represents permeate sample, B represents the backwash sample.
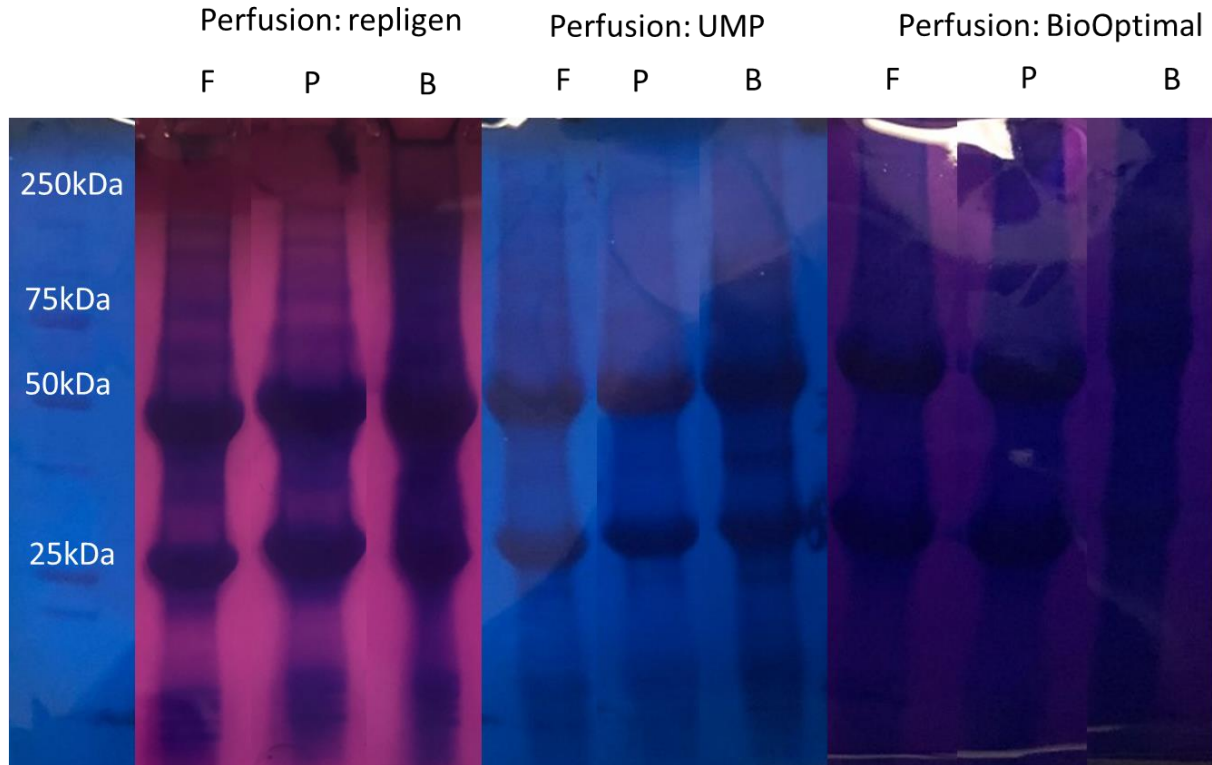
Figure 6.5 SDS-PAGE of samples from perfusion cell culture in University of Arkansas, F represents the feed sample, P represents permeate sample, B represents the backwash sample

6.3.2 Molecular weight distribution

The y axis shows the fraction of the HCPs in the corresponding molecular weight. The solid line represents the backwashes in the Biogen. The higher the curve means more HCPs are found at that MW. The dashed line represents the backwashes in the Amgen, and the dotted line represents the backwashes in the MilliporeSigma. Different color represents the samples from the different bioreactor. From the backwash distribution with molecular weight, it is clear that Biogen and Millipore sigma show a similar trend. However, the peak of MilliporeSigma is higher than Biogen, indicating the MilliporeSigma backwash is dominated by low molecular weight HCPs. The overall molecular weight distribution in Amgen is higher than in other companies.
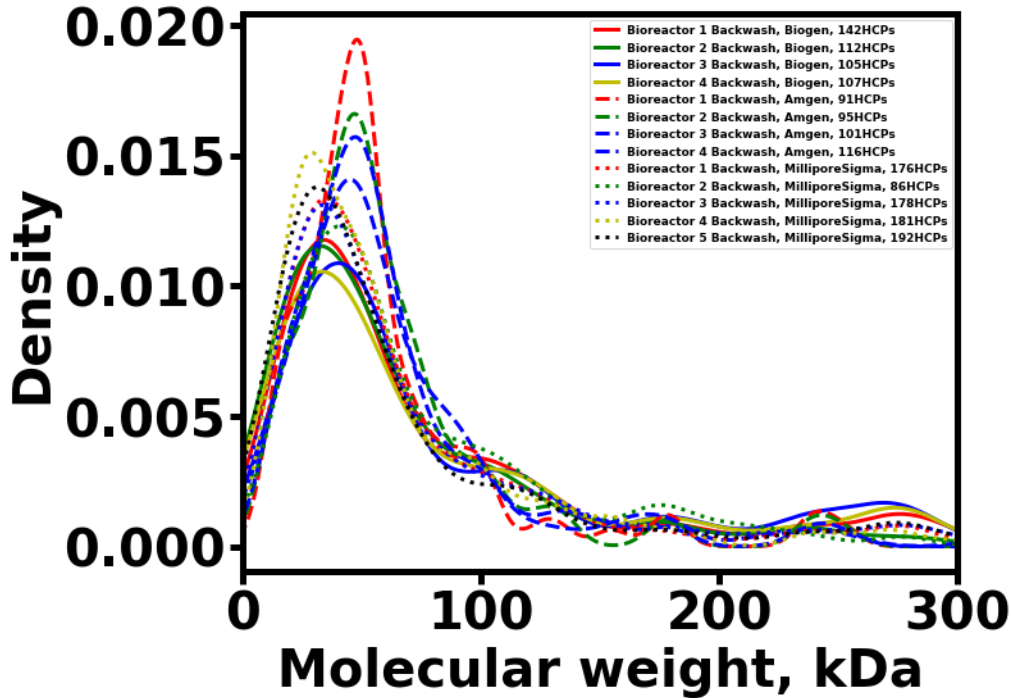
157

Figure 6.6 Molecular weight distribution across companies

6.3.3 pI distribution

The y axis shows the fraction of the HCPs in the corresponding isoelectric point. The higher the curve means more HCPs are found at that pI. There are two major peaks in the backwash samples from all the companies. The first peak covers the pI from 5-6, and the second covers the pI at about 8. The first peak is board, suggesting more variation and sensitivity of pI in this area. The first peak in Biogen shows a more acidic trend, while Amgen shows a basic trend. The distribution of MilliporeSigma shows the trend in between: Bioreactor 4 (yellow dotted) is more basic, but Bioreactor 2 (green dotted) is more acidic
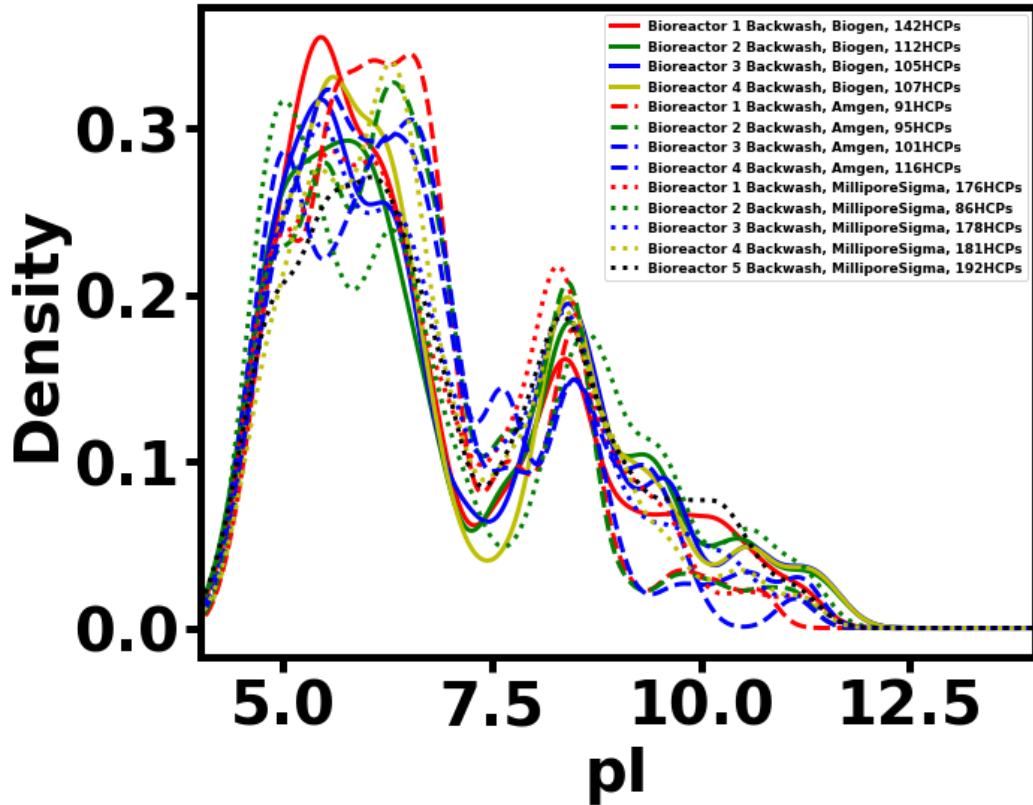
Figure 6.7 pI distribution across companies

6.3.4 Common HCP distributions

The distributions of those properties are also plotted for the common HCPs in all the industrial bioreactors. The common HCPs mean the HCPs are found in all the bioreactors. Therefore, the noise of the distribution is reduced. The distributions of the common HCPs with respect to those properties are shown in Figure 6.8 and Figure 6.9

The trends in all HCPs are also found in the common HCPs distribution. The Amgen HCPs show a higher molecular weight than Biogen and MilliporeSigma. The MilliporeSigma distribution shows the least molecular weight in all companies. This trend is consistent with all HCP distributions

The distribution of pI in common HCPs confirms the Biogen first peak shows an acidic trend and Amgen first peak shows a basic trend. The MilliporeSigma distribution is similar to Amgen, although more HCPs are found in pI of about 10
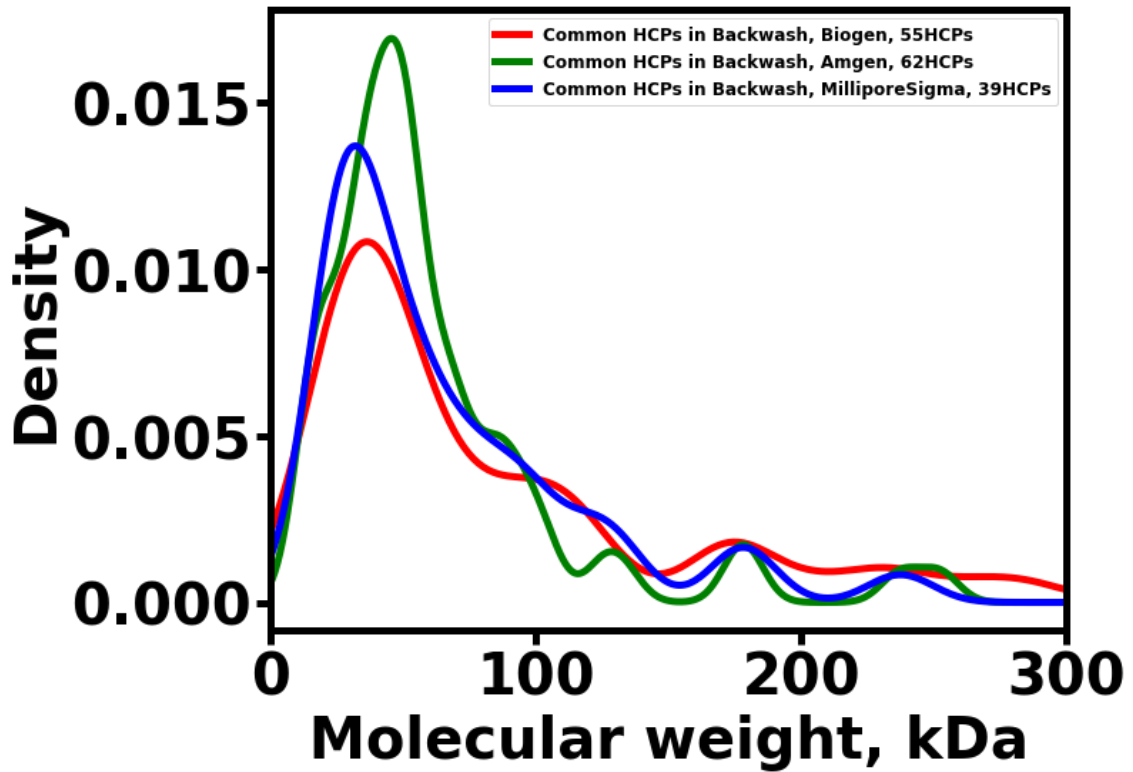

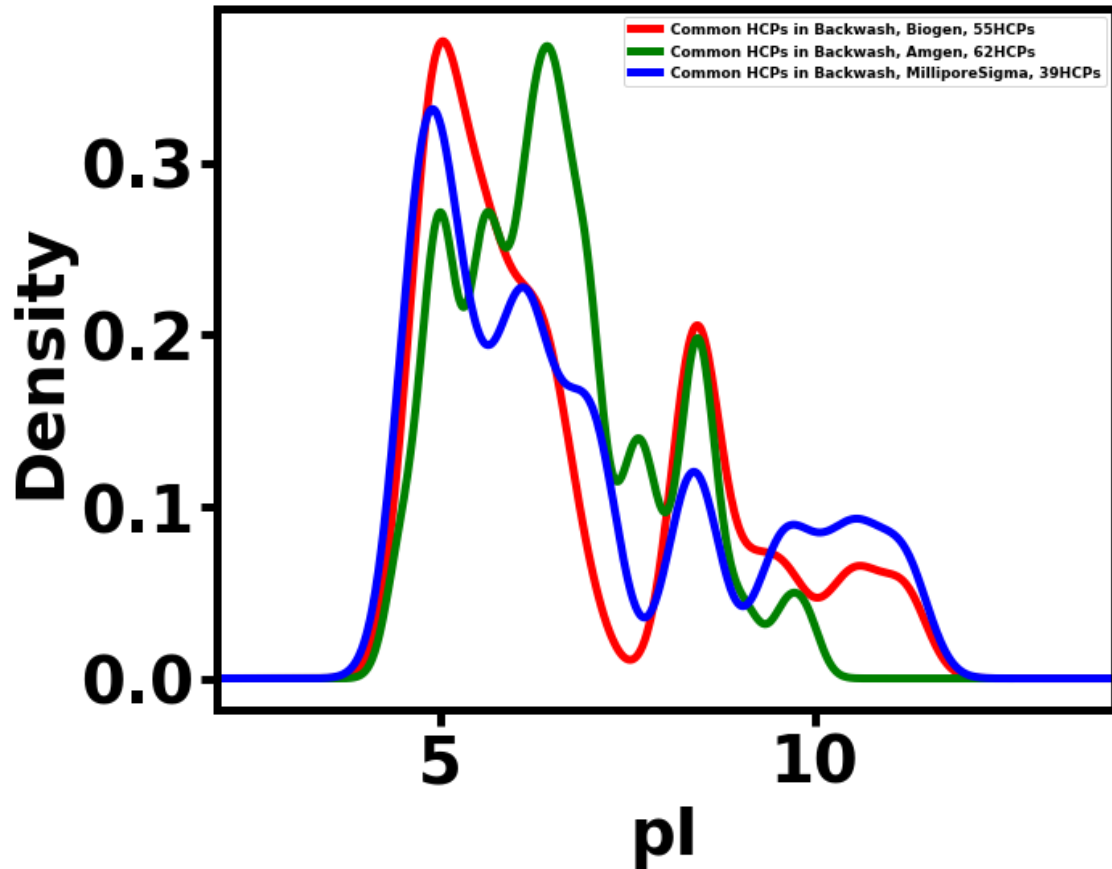Figure 6.8 molecular weight distribution of common HCPs across companies

Figure 6.9 pI distribution of common HCPs across companies

6.3.5   Perfusion cell culture

For all the bioreactors that were performed in the University of Arkansas, the cell reached

peak density around day 10, and then viability started to drop. The cell density and viability of

the perfusion cell culture are shown in Figure 6.10 and Figure 6.11.
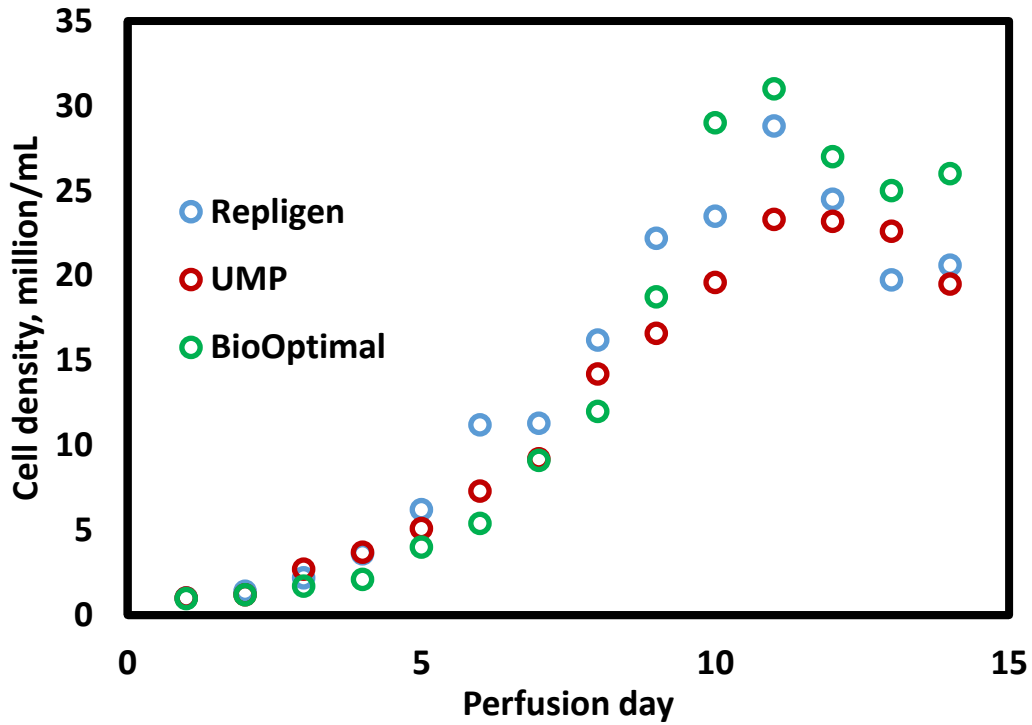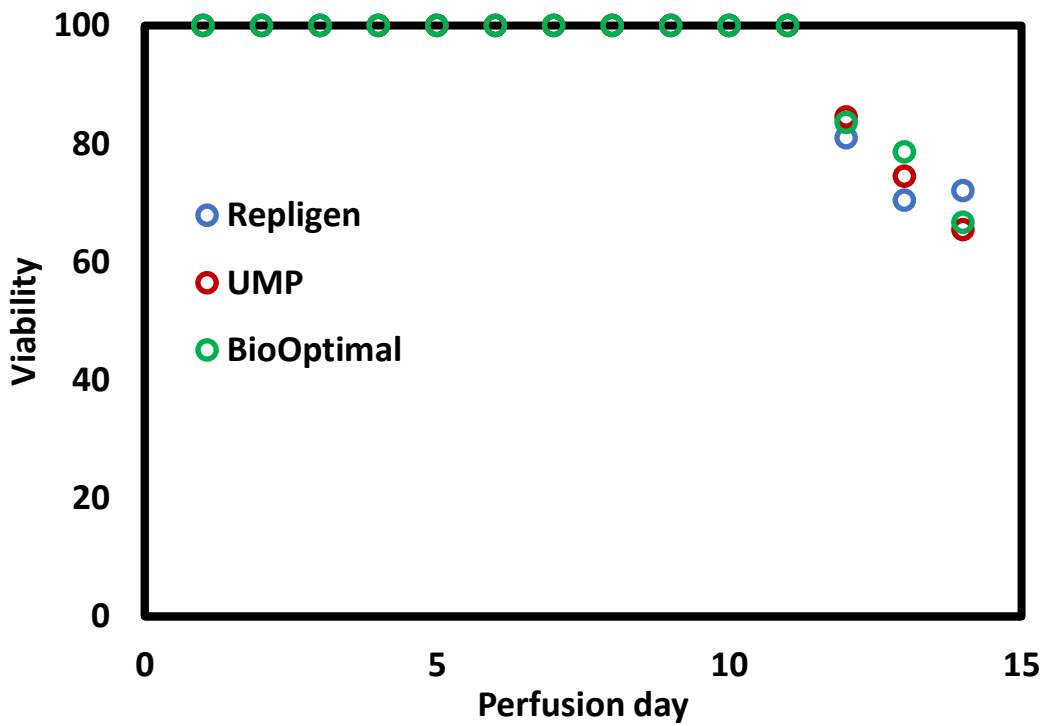
Figure 6.10 Cell density with the perfusion day

Figure 6.11 Viability with the perfusion day

6.3.6　Distribution analysis with different filters

The molecular weight distribution with different filters is shown in Figure 6.12. The main peak for all three filters is below 50 kDa, which is consistent with Biogen and MilliporeSigma distribution. Repligen filter and UMP have the same pore size (0.2 μm). BioOptimal^{TM} MF-SL has a larger pore size (0.4-40 μm). Therefore larger aggregate and protein pass through the membrane, and the protein with low molecular weight are found on the membrane. The distribution of the HCPs in the backwash shows the least peak, which is consistent with the pore size of BioOptimal^{TM} MF-SL, Repligen, and UMP. The result indicates BioOptimal^{TM} MF-SL is not sensitive to high MW fouling.

The distribution of pI shows a more sensitive response to a different filter. The fouling of HCPs involves the electrostatic interaction between HCPs and HCPs with filters. The interactions between HCPs form a larger aggregate, further increasing the fouling extent[13]. Therefore the charges of the membrane cause the fouling in different mechanisms and the distribution of rejected HCPs are also different. From Figure 6.13 The BioOptimal^{TM} MF-SL shows one main peak around pI of 5. However, the UMP shows 2 main peaks. The membrane material of Repligen, Asahi, and Asahi are PES, PVDF, and PSF, respectively. Different materials certainly generate different zeta potential of the membrane surface, and the rejected HCPs are expected to be different[14-16].
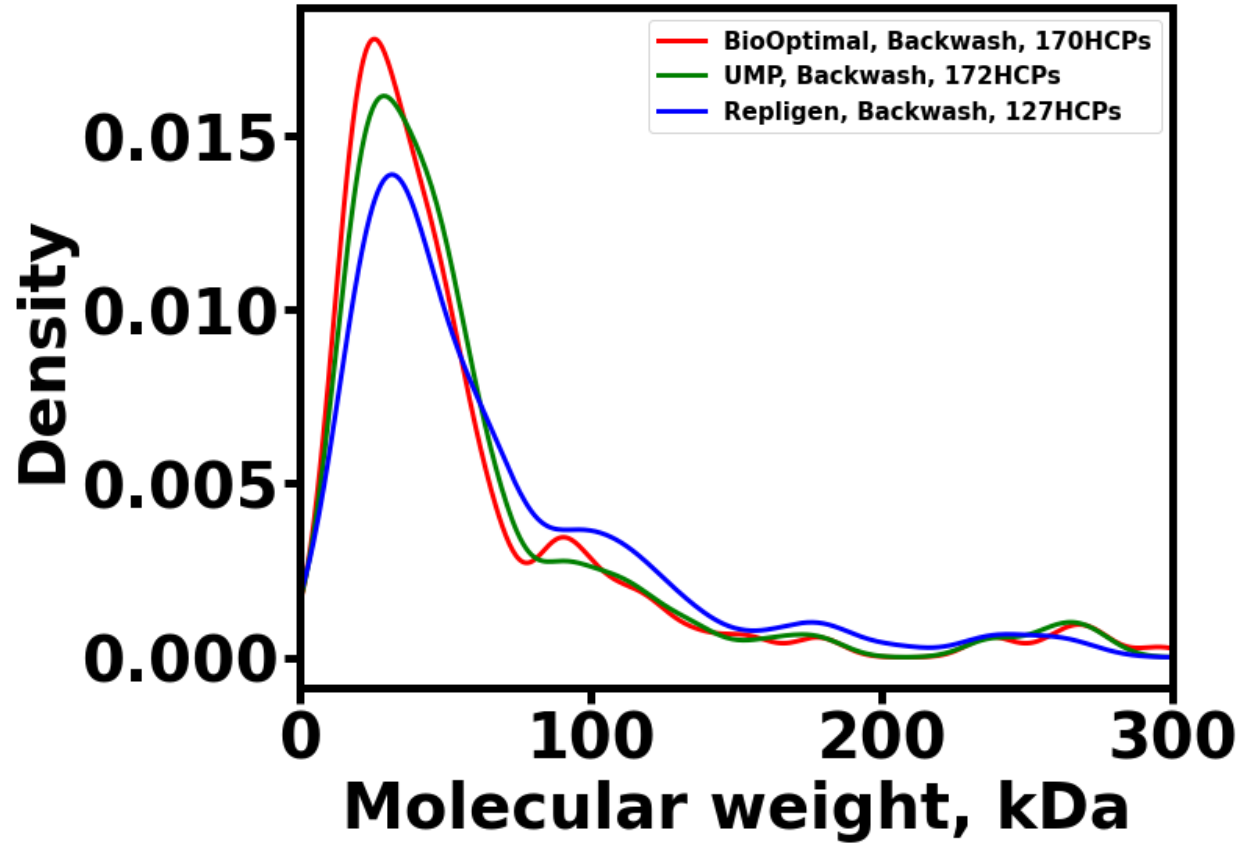
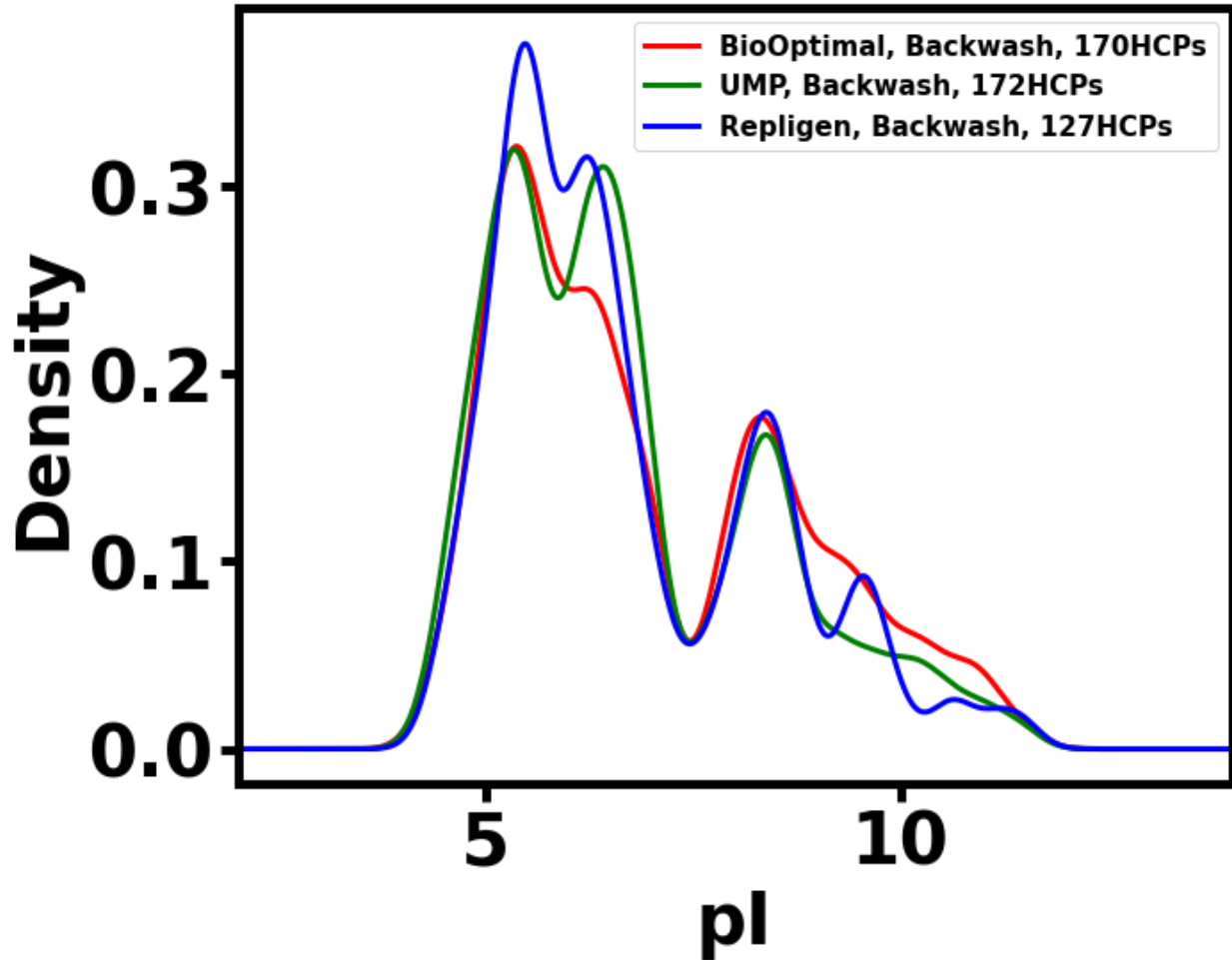Figure 6.12 Molecular weight distribution with different filters

Figure 6.13 pI distribution with different filters

As indicated on page 146, none of the runs are replicates though some uses similar conditions. However it will be interesting to compare the results for perfusion runs conducted in house with those conducted at company sites. The most comparable runs are the in house Repligen filter run and the three Biogen runs that used a Repligen filter as shown in Figures 6.14 and 6.15. The distribution of molecular weight and pI are very similar. Recalling filters with different pore sizes also have a similar distribution. The difference in Figure 6.8 is most like due to the operating conditions. The pI is shown to be a sensitive response to membrane material, and the distribution in the Figure 6.15 is expected to be similar as the same Repligen filters are used.

It can be inferred that the pI distribution of fouling HCP is more closely related to the membrane. It may be also related to the operation parameters because it also shows similarity from the run with MilliporeSigma. The Biogen pI distribution shows the most difference with Amgen since different membranes are used (see Figure 6.7). However, from the comparison using the same membrane, very consistent results were obtained (see Chapter 5). The method of proteomics workflow is also proved to be consistent with MALDI/MS and properties shown from the 2D electrophoresis gel.
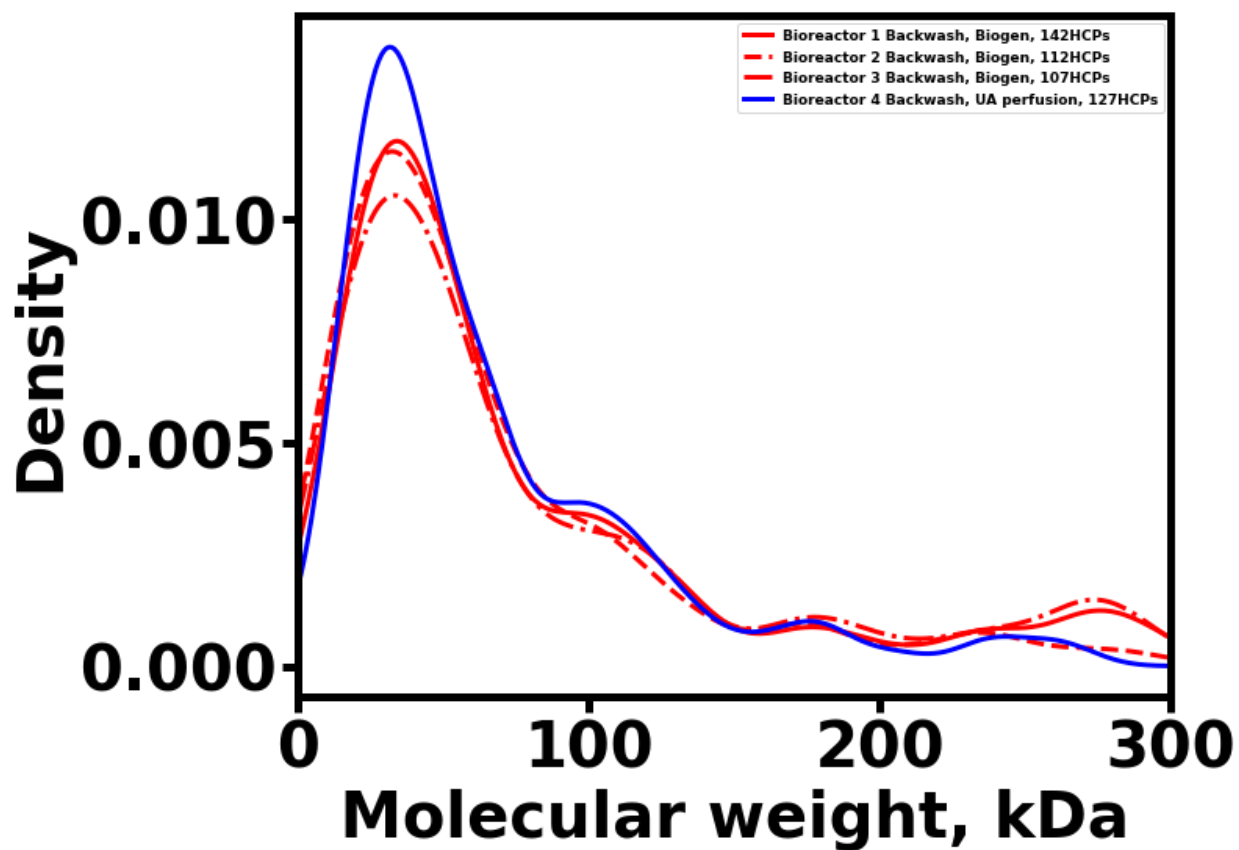

Figure 6.14 Molecular weight distribution between industrial samples and UA perfusion
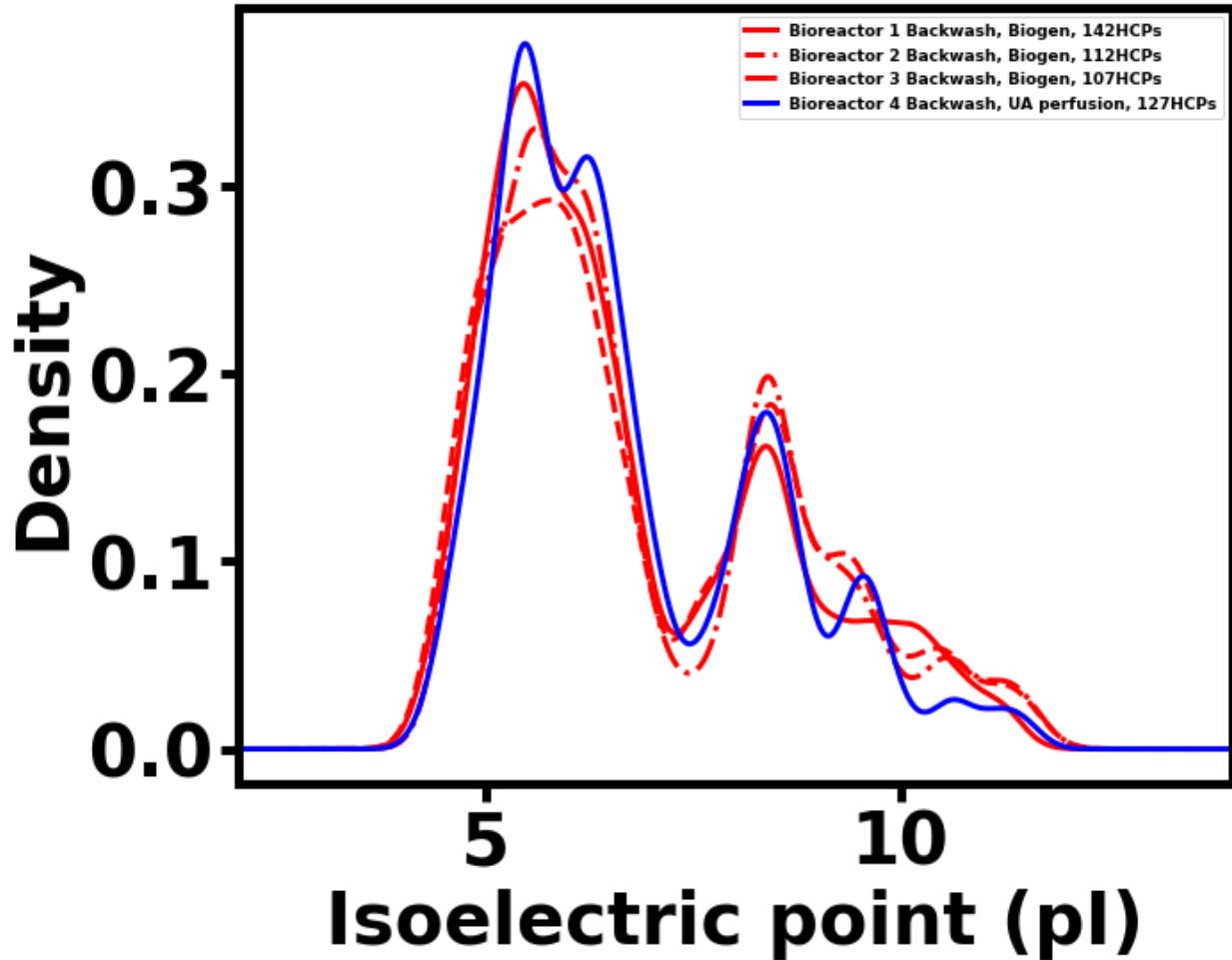
Figure 6.15 pI distribution between industrial samples and UA perfusion

6.4   Conclusion.

Proteomics analysis was applied to characterize the fouling during the perfusion cell

culture process. The perfusion cell cultures are performed in the three biopharmaceutics

companies as well as at the University of Arkansas. The fouling HCPs are identified and

analyzed. The molecular weight and pI distribution of fouling HCPs were observed and

compared across companies. Biogen and MilliporeSigma show a similar trend in molecular

weight distribution of HCPs in the backwash. However, the peak of Amgen is higher than the

other two companies. The pI shows 2 main peaks, and the first peak has a more sensitive

response to different companies. The first peak of pI distribution in Biogen shows a more acidic

trend, while Amgen shows a basic trend. The distribution of MilliporeSigma shows the trend in between. The trend for common HCPs is consistent with distributions of the whole list of identified HCPs

The perfusion cell culture at the University of Arkansas successfully achieved a cell density of around 25 million cells/mL. The proteomics analysis of the used filter indicates that pore size and membrane materials play an important role in the fouling behavior of the filters. The BioOptimal^{TM} MF-SL gives the low peak in molecular weight distribution because it has the largest pore size. This feature reflects BioOptimal^{TM} MF-SL is not sensitive to high MW fouling. The difference in the pI distribution reflects the different materials used to manufacture the filters.

Reference

1. Chu, L. and D.K. Robinson, *Industrial choices for protein production by large-scale cell culture.* Current opinion in biotechnology, 2001. **12**(2): p. 180-187.

2. Bielser, J.-M., et al., *Perfusion mammalian cell culture for recombinant protein manufacturing–A critical review.* Biotechnology advances, 2018. **36**(4): p. 1328-1340.

3. Walther, J., et al., *Perfusion cell culture decreases process and product heterogeneity in a head-to-head comparison with fed-batch.* Biotechnology Journal, 2019. **14**(2): p. 1700733.

4. Wang, S., et al., *Shear contributions to cell culture performance and product recovery in ATF and TFF perfusion systems.* Journal of Biotechnology, 2017. **246**: p. 52-60.

5. Kelly, W., et al., *Understanding and modeling alternating tangential flow filtration for perfusion cell culture.* Biotechnology progress, 2014. **30**(6): p. 1291-1300.

6. Bielser, J.-M., et al., *Perfusion cell culture for the production of conjugated recombinant fusion proteins reduces clipping and quality heterogeneity compared to batch-mode processes.* Journal of biotechnology, 2019. **302**: p. 26-31.

7.   Clincke, M.F., et al., *Very high density of CHO cells in perfusion by ATF or TFF in WAVE bioreactor™. Part I. Effect of the cell density on the process.* Biotechnology progress, 2013. **29**(3): p. 754-767.

8.   Zheng, C., et al., *Improved process robustness, product quality and biological efficacy of an anti-CD52 monoclonal antibody upon pH shift in Chinese hamster ovary cell perfusion culture.* Process Biochemistry, 2018. **65**: p. 123-129.

9.   Clincke, M.F., et al., *Very high density of Chinese hamster ovary cells in perfusion by alternating tangential flow or tangential flow filtration in WAVE bioreactor™—part II: Applications for antibody production and cryopreservation.* Biotechnology progress, 2013. **29**(3): p. 768-777.

10.   Li, Y., *Effective strategies for host cell protein clearance in downstream processing of monoclonal antibodies and Fc-fusion proteins.* Protein Expression and Purification, 2017. **134**: p. 96-103.

11.   Baycin-Hizal, D., et al., *Proteomic analysis of Chinese hamster ovary cells.* Journal of proteome research, 2012. **11**(11): p. 5265-5276.

12.   Pinto, N.D. and M. Brower, *Wide-surface pore microfiltration membrane drastically improves sieving decay in TFF-based perfusion cell culture and streamline chromatography integration for continuous bioprocessing.* Biotechnology and Bioengineering, 2020. **117**(11): p. 3336-3344.

13.   Liu, X., et al., *Identification and characterization of co-purifying CHO host cell proteins in monoclonal antibody purification process.* Journal of Pharmaceutical and Biomedical Analysis, 2019. **174**: p. 500-508.

14.   Möckel, D., et al., *Tangential flow streaming potential measurements: hydrodynamic cell characterization and zeta potentials of carboxylated polysulfone membranes.* Journal of Membrane Science, 1998. **145**(2): p. 211-222.

15.   Al-Amoudi, A., et al., *Cleaning results of new and fouled nanofiltration membrane characterized by zeta potential and permeability.* Separation and purification technology, 2007. **54**(2): p. 234-240.

16.   Breite, D., et al., *The critical zeta potential of polymer membranes: how electrolytes impact membrane fouling.* RSC advances, 2016. **6**(100): p. 98180-98189.

Chapter 7.   Conclusions and future work

Improvements and advances in cell engineering and downstream over the past few decades have been proven by increasing cell density and optimized cell culture. For example, the typical cell density in fed-batch mode could reach 20-30 million per mL with medium enrichment, feeding strategies, temperature shift optimization to accommodate high cell density, and around 200 million per mL in the perfusion cell culture. However, the high cell density challenges the downstream platform, especially the cell clarification step, because it is the first step right after the bioreaction. Cell clarification encounters the highest level and variation of impurities. The membrane separation, among other methods such as centrifugation, expanded bed, and flocculation, is commonly used due to its easy scaling, repeatable clearance, and simple operation.

Even though the membrane is very useful for complex feedstock, it still suffers from permeate flux decline caused by membrane fouling. Membrane fouling also causes negative effects on the product when sieving drops and breakthrough of the impurities. The filtration process can be intensified by developing a novel membrane structure and operation mode. The BioOptimal^{TM} MF-SL launched by Asahi Kasei adopts a unique membrane structure in that the open pores face the feed stream, and the hollow fibers are installed in a tangential flow module. Therefore, BioOptimal^{TM} MF-SL combines the benefits of depth filter and tangential flow filter.

On the one hand, the open pores act as a prefilter that rejects the large aggregates, protecting the dense layer. On the other hand, the tangential flow swipes out the foulants on the membrane surface and suppresses the cake layer's growth. The fouling of BioOptimal^{TM} MF-SL is analyzed using two feed streams: yeast cell and CHO cell. Yeast cells are widely used because yeast can post-translationally modify proteins, grow rapidly, and have a highly versatile DNA

transformation system. CHO cell is the most commonly used mammalian cell line for industrial production of recombinant protein therapeutics because of its long history of research and well adaption to suspension culture. However, with different physical properties, yeast cells foul the membrane in the internal area, while CHO cells deposit more on the external area. As a result. The tangential flow rate effect for CHO cells is much more significant than yeast cells. In addition, the CHO cells are more compressible than yeast cells due to the lack of the cell wall. The determined compressibility is consistent with this hypothesis.

The cell clarification process could be optimized with high viability and a modest shear rate. The cell culture with low viability generates more process-related impurities, such as HCPs, DNA, and aggreges, and less cell diameter. The smaller particle has a dense packing when the cake is formed and fouls the membrane in the internal area. This phenomenon may not be significant in the screen-type filter but play an important role in the depth-like filter.

HCPs are the trickiest impurities in the downstream process because they contain thousands of proteins. The properties of HCPs are similar to the final product and co-purified with it, and a lot of HCPs have an enzymic function that degrades the product during purification. The HCPs are expected to be removed during each step of the downstream unit and even in the cell clarification, where the pore size of the filter is much larger than HCPs. Due to the multiple HCPs clearance principle, the HCPs are mainly adsorbed by the membrane, forming aggregates or interacting with the product. Which HCPs are more likely rejected and how this rejection is related to their properties need to answer. The protein omics study workflow is applied to profile the HCPs during the cell clarification, including the optimization of backwash solution, HCP enrichment, 2D-SDS-PAGE, and LC/MS. The identified HCPs are consistent with the 2D SDS profile. Those abundant HCPs on the membrane show significant differences with

171

"difficult-to-remove" HCPs list from other studies, indicating that the identified HCPs are more easily foul the membrane instead of co-purified with the product. The LC/MS identifies a list of HCPs, and the properties of those HCPs are retrieved from the online database. The HCPs are labeled based on whether the MS spectrum count in the backwash is higher than in the permeate. A deep learning model is trained by 80% of the HCPs dataset and able to predict the label for the rest of 20% HCPs as unknown data with the highest accuracy of 76%

Future work

Viability plays an important factor in filtration. The feed stream properties in different viability can be worth investigating. The determined specific resistance and compressibility can predict the filtration flux using the model. However, the challenge during the determination is the complex composition of the cell culture in different viability. The viability is dynamically changed with cell density. Therefore, specific resistance and compressibility need to be determined not only with real-time cell density but also with real-time cell density. In addition, the viability assay and cell density counting need to be more accurate, for example, using ViCell automatic counter to reduce human handling.

Modeling, including depth filtration, is very interesting to explore. The current model only considers cake filtration. The effect of open pores was essentially reflected by the cake properties instead of the membrane structure. The structure-based modeling needs to be developed. For example, the membrane fouling is modeled by depth and cake filtration in serials. The impact of the model and understanding of the process will be greater. Due to the mechanism of depth filtration being rather complicated, Darcy's and Fick's laws are difficult to apply. Therefore, a simplified depth filtration correlation needs to be proposed. Unlike resistance in

serials model, the depth filtration may fit in resistance in parallel model, where there is a lot of bypass in the porous matrix, and those paths are parallel to each other.

The key properties of HCPs can be more relevant in the future. Protein serves a versatile function in the biological process, including enzymic activity, biosynthetic process, and cell component. The amino acid sequence encrypts its structure and eventually determines its function. Currently, the properties of the HCPs, such as molecular weight, pI, GRAVY are calculated based on the amino acid sequence but not from the experimental value. The experimental value is more related to its 3D structure in real and dynamic conditions. Therefore, those properties may not be accurate enough to represent the HCPs in the real process. A more accurate, relevant, structure-based parameter would help to improve the prediction accuracy of the deep learning model.

The proposed protein omics workflow can be used for perfusion cell culture. The perfusion cell culture differs from the batch mode due to its high cell density, complex flow direction, and longer culture period. Therefore, the fouling of the cell retention device is expected to be different. The HCPs profile in the perfusion cell culture is very interesting to investigate. Due to the time limitation, 16 perfusion runs are analyzed in this work. However, more data can be added to the existing database, and many operations parameters can be incorporated to enrich the HCPs dataset, such as the filter brand, shear rate, cell density, temperature, etc. In addition, the protein omics workflow can be optimized. The in-solution digestion method shows a quick detection, less interface, and higher capacity than in-gel digestion. The LC/MS can also be optimized with higher resolution chromatography equipment.